Gesellschaft für Anlagen- und Reaktorsicherheit (GRS) mbH

Final Report on the Reactor Pressure Vessel Pressurized-Thermal-Shock International Comparative Assessment Study (RPV PTS ICAS)

GRS - 152

Gesellschaft für Anlagen- und Reaktorsicherheit (GRS) mbH

Final Report on the Reactor Pressure Vessel Pressurized-Thermal-Shock International Comparative Assessment Study (RPV PTS ICAS)

Jürgen Sievers
Helmut Schulz
in collaboration with
Richard Bass [1])
Claude Pugh [1])

[1]) Oak Ridge National Laboratory, USA

October 1999

GRS - 152
ISBN 3-931995-14-3

Notice:
This comparitive analyses (round robin) was organized by Gesellschaft für Anlagen- und Reaktorsicherheit (GRS) in cooperation with Oak Ridge National Laboratory (ORNL). The work was supported by the German Minister for Education, Science, Research, and Technology (BMBF) and the U.S. Nuclear Regulatory Commission (NRC). The collaborative aspects of the project were under the auspices of the Organisation for Economic Co-operation and Development (OECD) / Nuclear Energy Agency (NEA) / Committee on the Safety of Nuclear Installations (CSNI) / Principal Working Group (PWG) No. 3 (Integrity of Components and Structures).

The ICAS Project grew out of a strong interest expressed by participants in the previous CSNI/PWG-3 FALSIRE II Project (Fracture Analyses of Large Scale International Reference Experiments) whose final report was issued in 1996 (GRS-130). The ICAS Project brought together an international group of experts on structure mechanics and thermal hydraulics coming from research, utilities and regulatory organizations to perform a comparative evaluation of analysis methodologies employed in the assessment of RPV integrity under prototypical PTS loading conditions.

This report is also published as:
NEA/CSNI/R(99) 3

Keywords:
reactor pressure vessel, integrity assessment, fracture mechanics, thermal shock, finite elements, estimation scheme, probabilistics fracture mechanics, thermal hydraulics, thermal mixing, steam condensation, system code

Abstract

A summary of the recently completed International Comparative Assessment Study of Pressurized-Thermal-Shock in Reactor Pressure Vessels (RPV PTS ICAS) is presented here to record the results in actual and comparative fashions. The ICAS Project brought together an international group of experts from research, utility and regulatory organizations to perform a comparative evaluation of analysis methodologies employed in the assessment of RPV integrity under PTS loading conditions. The Project was sponsored jointly by Gesellschaft für Anlagen- und Reaktorsicherheit (GRS), Köln, Germany, and Oak Ridge National Laboratory (ORNL), USA, with assistance from the Organization for Economic Co-operation and Development (OECD)/Nuclear Energy Agency (NEA)/Committee on the Safety of Nuclear Installations (CSNI)/Principal Working Group (PWG) No. 3 (Integrity of Components and Structures). The Organizing Committee (OC) for the ICAS Project consists of J. Sievers and H. Schulz, GRS, Köln, Germany; R. Bass and C. Pugh (ORNL); A. Miller represented the OECD/NEA/CSNI and provided an important communications link between the OC and the ICAS participants. The ICAS Project grew out of a strong interest expressed by participants in the previous FALSIRE II Project to proceed with further evaluations of analysis methods used in RPV integrity assessment. A Launch Meeting for the ICAS Project was held at GRS-Köln, during June 1996, where an emphasis was placed on identifying the different approaches to RPV integrity assessment being employed within the international nuclear technology community. Also a Problem Statement was drafted that defined a Western type four-loop RPV with cladding on the inner surface. Also, a detailed task matrix was defined that included a set of transient thermal-mechanical loading conditions postulated to result from loss-of-coolant accidents. The primary focus of the analyses was on the behaviour of relatively shallow cracks under these conditions. The assessment activities based on the Problem Statement were divided under three tasks: deterministic fracture mechanics (DFM), probabilistic fracture mechanics (PFM) and thermal-hydraulic mixing (THM). An Intermediate Workshop was held at OECD/NEA-Paris during June 1997, to review progress and discuss preliminary results for each task. Twenty-eight researchers representing 20 organizations in 13 countries participated in that Workshop. A Final Workshop was held at Orlando, Florida, during February 24-27, 1998, to provide a forum for presentation of the full set of solutions that had been submitted by participants. Thirty-four researchers representing 20 organizations in 11 countries participated in

the final workshop. Approximately 145 comparative plots were generated from an electronic data base of results to focus the discussions on the predictive capabilities of the analysis methods applied to the different tasks. Selected plots are presented and discussed in this report. The results show that a best-estimate methodology for RPV integrity assessment can benefit from a reduction of the uncertainties in each phase of the process. Within the DFM task, where account was taken of material properties and boundary conditions, reasonable agreement was obtained in linear-elastic and elastic-plastic analysis results. Linear elastic analyses and J-estimation schemes were shown to provide conservative estimates of peak crack driving force when compared with those obtained using complex three-dimensional (3D) finite element analyses. Predictions of RT_{NDT} generally showed less scatter than that observed in crack driving force calculations due to the fracture toughness curve used for fracture assessment in the transition temperature region. Observed scatter in some analytical results could be traced mainly to a misinterpretation of the thermal expansion coefficient data given for the cladding and base metal. Also, differences in some results could be due to a quality assurance problem related to procedures for approximating the loading data given in the Problem Statement. For the PFM task, linear-elastic solutions were again shown to be conservative with respect to elastic-plastic solutions (by a factor of 2 to 4). Scatter in solutions obtained using the same computer code was generally attributable to differences in input parameters, e.g. standard deviations for the initial value of RT_{NDT}, as well as for nickel and copper content. In the THM task, while there was a high degree of scatter during the early part of the transient, reasonable agreement in results was obtained during the latter part of the transient. Generally, the scatter was due to differences in analytical approaches used by the participants, which included correlation-based engineering methods, system codes and three-dimensional computational fluids dynamics codes. Some of the models used to simulate condensation effects showed a weakness in recognizing the flow regime at the water-stripe discharge in the downcomer. Based on concluding discussions held at the ICAS Workshop, participants drafted a list of proposals for future work concerning further refinement of RPV integrity assessment methodology.

Contents

Executive Summary

This report summarizes the recently completed International Comparative Assessment Study of Pressurized-Thermal-Shock in Reactor Pressure Vessels (ICAS/RPV-PTS). The ICAS Project brought together an international group of experts from research, utility and regulatory organizations to perform a comparative evaluation of analysis methodologies employed in the assessment of RPV integrity under PTS loading conditions. The project was sponsored jointly by Gesellschaft für Anlagen- und Reaktorsicherheit (GRS), Köln, Germany, and Oak Ridge National Laboratory (ORNL), USA, with assistance from the Organization for Economic Co-operation and Development (OECD)/Nuclear Energy Agency (NEA)/Committee on the Safety of Nuclear Installations (CSNI)/Principal Working Group (PWG) No. 3 (Integrity of Components and Structures). The Organizing Committee (OC) for the ICAS Project consists of J. Sievers and H. Schulz, GRS, Köln, Germany; R. Bass and C. Pugh (ORNL); A. Miller represented the OECD/NEA/CSNI and provided an important communications link between the OC and the ICAS participants.

The ICAS Project grew out of a strong interest expressed by participants in the previous FALSIRE II Project to proceed with further evaluations of analysis methods used in RPV integrity assessment. Those assessments represent a multi-step process, involving the selection of transients, thermal-hydraulic calculations, postulation of defects, structural analyses, and fracture assessments based on specified material properties. A Call for Participation was issued jointly by GRS and ORNL in 1996 to an international group of experts to join in a comparative assessment study of RPV integrity under PTS loading, formally designated as the ICAS Project. The activity was originated in PWG No. 3 (Integrity of Components and Structures), with the co-operation of PWG No. 2 (Coolant System Behaviour). Emphasis in the project was placed on comparison of different approaches to RPV integrity assessment (including the determination of loading conditions) employed by the international nuclear technology community.

A Problem Statement for the ICAS Project was drafted following a Launch Meeting held at GRS-Köln, during June 1996 and defined a Western type four-loop RPV with cladding on the inner surface. The RPVs proposed in the Problem Statement incorporate country-specific concerns. A detailed task matrix defined a set of transient thermal-mechanical loading conditions that are postulated to result from

loss-of-coolant accidents. Both asymmetric and axisymmetric cooling conditions were considered, and different cracks (circumferential and longitudinal orientations; infinite and semi-elliptical geometries; through-clad and subclad flaws) were assumed in the near-core weld. The primary focus of the analyses was on the behaviour of relatively shallow cracks under PTS loading conditions due to the postulated emergency cooling transients. Special emphasis was placed on the interdisciplinary aspects of determining RPV loading conditions due to loss-of-coolant accidents. The calculations of fluid temperature and heat transfer to the structure using thermal-hydraulic analysis techniques were studied, with consideration given to models of fluid-fluid mixing and steam condensation.

The Problem Statement was divided into three tasks and a group of analysts addressed each task:

- Deterministic Fracture Mechanics (DFM),
- Probabilistic Fracture Mechanics (PFM),
- Thermal-Hydraulic Mixing (THM).

In the DFM Task Group, an RPV was utilized that is typical of German design (Type 1300 MW). The cladding thickness was proposed to vary in the range of designs used in the U.S., France, Germany and Russia. The postulated loading transients refer to small-break loss-of-coolant accidents (LOCA) due to leaks of different sizes. One transient is appropriate for U.S. nuclear plants, and two other transients are appropriate for German plants. The three transients were specified as follows: axisymmetric small-break LOCA (transient T1), and two asymmetric (plume cooling) loading conditions due to hot leg breaks of 50 and 200 cm^2 (transients T2 and T3, respectively). There were five postulated circumferential and axial surface and subclad cracks. Additional parametric studies were defined for various aspects of the problem, including the influence of clad thickness, clad and weld yield stresses, and crack aspect ratio. Furthermore, different residual stress distributions due to the cladding and the welding process were provided to allow participants to investigate the influence of these stresses on crack loading. Participants were asked to calculate the temperature and stress distributions through the wall and the loading along the postulated crack fronts. Fracture assessment of the postulated cracks required that the maximum allowable transition temperature (RT_{NDT}) be

determined for impending cleavage initiation using maximum, tangent and ninety-percent criteria. The fracture assessments for all cases utilized the fracture toughness curve from the ASME Code, Section XI, Appendix A.

The objectives of the PFM Task Group were to compute the conditional probability of crack initiation and the probability of RPV failure for four subtasks using a PFM methodology. The probability is conditional in the sense that the transient is assumed to occur. Failure is interpreted here as propagation of the flaw through the thickness of the RPV wall. An RPV was proposed which is typical of U.S. construction. The four subtasks investigated conditional probabilities of crack initiation and vessel failure for circumferential and axial welds under two different transients, with a range of inside surface fluences, and a parametric study of the crack aspect ratio.

The objective of the THM Task Group was to compare analytical models that estimate the effects of thermal mixing and steam condensation for the emergency cooling water in the cold leg and the RPV downcomer. The assumed plant type was a 1300 MW four-loop PWR. The internal measurements of the fictitious RPV and the cold legs corresponded to those of the Upper Plenum Test Facility in Mannheim, Germany. The assumed transient was due to a 200 cm^2 leak in a hot leg at time t = 0. Two parametric studies were proposed: the influence of variations of the water level in the downcomer; and influence of variations in the emergency cooling water injection rate per cold leg.

An Intermediate Workshop was held at OECD/NEA-Paris during June 1997 for purposes of reviewing progress and discussing preliminary results for each task. Twenty-eight researchers representing 20 organizations in 13 countries participated in that Workshop. A final ICAS Workshop was held at Orlando, Florida, during February 24-27, 1998. A primary objective of the Orlando Workshop was to provide a forum for presentation of the full set of solutions to the ICAS Problem Statement submitted by participants; 34 researchers representing 20 organizations in 11 countries participated in the Workshop. Representatives of GRS-Köln, were responsible for compiling and updating the electronic data base of analysis results to the ICAS Problem Statement. Staff from ORNL had responsibility for all U.S. arrangements regarding the ICAS Workshop. Final analysis results were provided by 25 organizations in 13 countries. Approximately 145 comparative plots were generated from the electronic data base to provide a focus for discussions about the

predictive capabilities of the analysis methods applied by the participants to the different tasks. In the report selected plots are presented and discussed. As an outcome of the discussions held at the Workshops and of the additional communications by electronic media, the following main conclusions were drawn.

DFM Task Group

Twenty-one organizations from 13 countries participated in the DFM Task Group. According to the task matrix, 104 analyses were performed for the main tasks and 26 for the parametric studies. Because some organizations used more than one method, up to 22 sets of analysis results could be compared in some tasks. Where due account was taken of material properties and boundary conditions, reasonable agreement was obtained in linear-elastic, as well as in more complex elastic-plastic thermal and stress analyses results. To derive consistent solutions, it was observed that particular attention should be paid to the following:

- Adequate representation of the thermal and pressure transients;

- Sufficient mesh refinement and choice of element type in critical regions; particularly within the cladding and across the clad-base interface. Quadratic elements (incorporating mid-side nodes) are recommended.

- Correct definition of material properties. Of particular note was the reference temperature definition for the thermal expansion coefficient (TEC) which is conventionally taken as 20°C.

For analyses incorporating the above factors, crack driving forces computed from elastic analysis and J-estimation schemes were significantly higher than those calculated using 3-D elastic-plastic analyses. This was mainly due to: (i) the over-prediction of stress in the cladding by elastic analyses, (ii) inherent conservatism's within J-estimation schemes such as R6, and (iii) the beneficial influence of the cladding on crack opening for under-clad cracks. Predictions of RT_{NDT} showed less scatter than that observed in crack driving force calculations due to the fracture toughness curve used for fracture assessment in the transition region. Additional parametric studies provided consistent trends regarding the influence of residual stress, cladding thickness and defect aspect ratio on crack driving force. For surface-breaking defects, the presence of residual stresses, increased clad

thickness or decreased defect aspect ratio (a/c) leads to an increase in the crack-driving force. For under-clad defects, different trends were generally observed. Comparison of solutions incorporating plasticity effects with those utilizing linear elastic approaches resulted in discrepancies among the analysis results. The latter discrepancies are similar to those that were observed in the earlier FALSIRE Project. Additional parametric studies showed that the scatter in the linear-elastic and the elastic-plastic DFM results could be traced mainly to a misinterpretation of the thermal expansion coefficient (TEC) data given in the ICAS Problem Statement for the cladding and base metal. Those TEC data were expressed in a conventional form that assumes a reference temperature of 20°C. Most structural analysis computer codes that use mean values of TEC data require conversion of the data, if the stress free reference temperature is different from 20°C. That was not done in several cases. Furthermore, it was noted that differences in some of the analysis results could be a quality assurance problem related to procedures for approximating the loading data given in the Problem Statement.

PFM Task Group

In the PFM Task Group, seven organizations from four countries performed 25 analyses and three parametric studies. The calculated conditional probabilities of crack initiation had the largest scatter, especially for low values of RT_{NDT}, differing by a factor of about 100. For the conditional probability of vessel failure, that factor ranges from approximately 20 to 50. The conditional probabilities for the linear-elastic solutions are larger than those for the elastic-plastic solutions by a factor of about 2 to 4. Some solutions which were produced by different participants using the same computer code showed differences that were apparently due to selection of different input parameters for simulating the margin term in the calculation of RT_{NDT} (i.e., standard deviations for initial value of RT_{NDT}, as well as for nickel and copper content).

THM Task Group

In the THM Task Group, eight organizations from five countries performed seven analyses and 14 parametric studies. The methods used can be grouped into correlation-based approaches, system codes and computational-fluid-dynamics (CFD) codes. In the main task (MIX), the expected plumes/stripes under the cold legs were simulated in some correlation-based models. In these analyses, the temperature difference between the centreline of the plumes under cold legs 2/3 and outside the plumes reached about 30°C. Large scatter in the results can be observed early in the transient when the water level is below the lower nozzle edge of the cold legs and the simulation of condensation effects plays an important role. Some of the models used to simulate condensation effects show a weakness in recognizing the flow-regime at the water-stripe discharge in the downcomer. This effect is more pronounced at heights closer to the lower nozzle edge. The solutions with the lowest temperatures seem to underestimate the condensation effects in the cold legs. The results of the correlation-based models are close together at times when the water level in the downcomer increases again due to low-pressure injection. Comparisons of computed results for heat-transfer coefficient (HTC) show a very large scatter inside the plumes/stripes, with values in the range between zero and about 10,000 W/m^2K. Such a large variation in HTC has important implications for structural mechanics assessments of the vessel. The differences between HTC values inside and outside the plumes produce thermal stresses and, consequently, an increase of the stress-intensity factors for postulated cracks. As a group, the participants computed lower HTC values for the region outside the plumes, but again with very large scatter. These results suggest that a more accurate representation of the HTC may be requir from thermal-hydraulic researchers for input to the thermal/structural/fracture analyses, especially in the range from 1,000 to 8,000 W/m^2K. For the task without condensation effects (PINJ), results from the correlation-based methods show a consistent trend, with differences in the fluid temperatures of less than 50°C and in the HTC values of less than 5,000 W/m^2K. Finally, the concept of symmetric plumes under the cold legs is not supported by the three-dimensional CFD solution.

Future Work

Results from the ICAS Project show that a best-estimate methodology for RPV integrity assessment can benefit from a reduction of the uncertainties in each phase of the process. Based on concluding discussion at the ICAS Workshop, participants proposed a list of future tasks that could contribute to further refinement of RPV integrity assessment methods:

- Selection of consensus reference solutions that could serve as benchmarks for future qualification of analytical methods. These would provide a valuable tool for the qualification of new analysts on the subject of RPV integrity assessment;

- Study of the implications of the observed scatter in the THM task on deterministic fracture mechanics assessments;

- Study of the significance of the heat transfer coefficient on fracture mechanics assessment;

- Assessment of the nozzle region of an RPV;

- Assessment of the significance of residual stresses upon RPV integrity;

- Study of crack arrest of a fast running crack in an RPV;

- Study of micro-mechanical modelling of the crack-tip region;

Furthermore a study of pressure-temperature (P-T) limits, with reference to the methodology for modelling the P-T process was proposed.

Acknowledgement

Gratitude is expressed to the German Minister for Education, Science, Research, and Technology (BMBF) and the U.S. Nuclear Regulatory Commission (NRC) as the Organisation for Economic Co-operation and Development (OECD) / Nuclear Energy Agency (NEA) / Committee on the Safety of Nuclear Installations (CSNI) / Principal Working Group (PWG) No. 3 (Integrity of Components and Structures) for sponsoring our work in support for ICAS. Further, the authors thank each participant listed in Table 2.1 for cooperation in performing analytical work and in making interpretive assessments. Their efforts made ICAS a highly valuable assessment endeavor.

1 Introduction

The International Comparative Assessment Study (ICAS) of Pressurized-Thermal-Shock (PTS) in Reactor Pressure Vessels (RPVs) was organized in 1996 to bring together an international group of experts from research, utility and regulatory organizations in a comparative assessment study of integrity evaluation methods for nuclear RPVs under PTS loading. Final analyses were completed in 1998 and comparative evaluations were recently finished. The Project was sponsored jointly by Gesellschaft für Anlagen- und Reaktorsicherheit (GRS), Köln, Germany, and Oak Ridge National Laboratory (ORNL), USA, with assistance from the Organization for Economic Co-operation and Development (OECD)/Nuclear Energy Agency (NEA)/Committee on the Safety of Nuclear Installations (CSNI)/Principal Working Group (PWG) No. 3 (Integrity of Components and Structures). The Organizing Committee (OC) for the ICAS Project consists of J. Sievers and H. Schulz, GRS, Köln, Germany; R. Bass and C. Pugh (ORNL); A. Miller represented the OECD/NEA/CSNI and provided an important communications link between the OC and the ICAS participants.

This report was prepared by the OC and gives an overview of the results from the ICAS Project. Chapter 2 provides background information, including the organizational aspects and performance steps that culminated in an ICAS Workshop held in Orlando, Florida, during February 1998. A detailed presentation of the ICAS Problem Statement is given in Chapter 3. A summary of analysis techniques and computer codes employed by the participants is included in Chapter 4. A comprehensive assessment and discussion of the analysis results submitted by the participating organizations for each of the Task Group modules in the Problem Statement is presented in Chapter 5. Finally, some conclusions derived from these assessments are given in Chapter 6.

2 Background of the ICAS Project

The ICAS Project grew out of a strong interest expressed by participants in the recently completed Project for Fracture Analyses of Large Scale International Reference Experiments (FALSIRE) [1-2] to proceed with further evaluations of analysis methods used in RPV integrity assessment. The ICAS assessments were designated to include the entire multistep PTS analysis process for a full-scale RPV consistent with a western-designed pressurized water reactor (PWR). This involves the selection of

transients, thermal-hydraulic calculations, postulation of defects, structural analyses, and fracture assessments based on specified material properties. A Call for Participation was issued jointly by GRS and ORNL in 1996 to an international group experts from research, utility and regulatory organizations to join in a comparative assessment study. The project was formally designated as the ICAS Project, and it was originated within NEA/CSNI's PWG No. 3 (Integrity of Components and Structures). Concurrently, PWG No. 2 (Coolant System Behaviour) was informed about this activity. The emphasis of the Project was placed on comparison of the different approaches to RPV integrity assessment, including determination of loading conditions, employed within the international nuclear technology community.

A Problem Statement for the ICAS Project was drafted following a Launch Meeting held at GRS-Köln, during June 1996. The Problem Statement (described in Chapter 3) defined the reference RPV as one from a Western type four-loop PWR with cladding on the inner surface. Country-specific concerns were addressed in the document. A detailed task matrix was established and defined a set of transient thermal-mechanical loading conditions postulated to result from loss-of-coolant accidents. Both asymmetric and axisymmetric cooling conditions were considered, and various types of cracks (circumferential and longitudinal orientations; infinite and semi-elliptical geometries; through-clad and subclad flaws) were assumed to be present in the near-core weld of the RPV. The primary focus of the analyses was on the behaviour of relatively shallow cracks under PTS loading conditions due to emergency cooling transients. Parametric studies were proposed for investigating the effects of cladding thickness, influence of residual stresses, sensitivity to the magnitude of the yield stress, and relative effects of elastic versus elastic-plastic material models. Further, probabilistic fracture mechanics tasks were included to analyze the conditional probability of crack initiation and vessel failure.

Special emphasis was placed on the interdisciplinary aspects of determining RPV loading conditions due to loss-of-coolant accidents. The calculations of fluid temperature and heat transfer to the structure using thermal-hydraulic analysis techniques were studied, with consideration given to models of fluid-fluid mixing and steam condensation.

The Problem Statement was divided into three modules and corresponding Task Groups were formed:

- Deterministic Fracture Mechanics (DFM),
- Probabilistic Fracture Mechanics (PFM), and
- Thermal-Hydraulic Mixing (THM).

The activities of each Task Group were divided into several subtasks. Parametric studies were proposed to investigate the influence of certain parameters on the results of the subtasks. Input for defining the modules (Task Groups) was provided by GRS, Siemens, Electricité de France, and ORNL. The subtasks performed in each Task Group are described in Chapter 3.

An Intermediate Workshop was held at OECD/NEA-Paris during June 1997 for purposes of reviewing progress and discussing preliminary results for each module. Twenty-eight researchers representing 20 organizations in 13 countries participated in that Workshop.

The final Workshop on ICAS was held at Orlando, Florida, during February 24-27, 1998, and its objectives were to:

- provide a forum for presentation of the full set of solutions to the ICAS Problem Statement submitted by participants;
- review and discuss comparisons of these results based on variables defined in the Special Requirements part of the Problem Statement;
- evaluate the overall progress of the analyses and comparative assessments; and
- make recommendations for future work.

Thirty-four researchers from 20 organizations in 11 countries participated in the Workshop. Representatives of GRS-Köln were responsible for compiling and updating an electronic data base of all the analysis provided by the participants. Staff from ORNL had responsibility for all arrangements regarding the ICAS Workshop.

Table 2.1 lists the organizations that participated in the ICAS Project, along with the particular task groups (THM, DFM and PFM) to which each organization made contributions. The Schedule of Events for the ICAS Project is given in Table 2.2.

Following the recommendations of the final Workshop, additional analyses were performed by 11 organizations. The results of those additional analyses were compiled into the data base and are included in this report.

References

[1] Bass, B. R., Pugh, C. E., Keeney, J., Schulz, H., and Sievers, J., “CSNI Project for Fracture Analyses of Large-Scale International Reference Experiments (Project FALSIRE)”, NUREG/CR-5997 (ORNL/TM-12307), Oak Ridge National Laboratory, December 1992, NEA/CSNI/R(94)12, GRS – 108, April 1994

[2] Bass, B. R., Pugh, C. E., Keeney, J., Schulz, H., and Sievers, J., “CSNI Project for Fracture Analyses of Large-Scale International Reference Experiments (FALSIRE II)”, NUREG/CR-6460 (ORNL/TM-13207), Oak Ridge National Laboratory, April 1996, NEA/CSNI/R (96) 1, GRS – 130, November 1996

Table 2.1 Organizations participating in the ICAS Project
(Status November 1998)

Country	**Organization**	**Task Groups**		
		DFM[1]	**PFM[2]**	**THM[3]**
Czech Republic	Nuclear Research Institute (NRI)	X		
France	Electricité de France (EdF)	X		
	Centre d´Etudes Nucleaires de Saclay (CEA)	X	X	
	Framatome	X		
Germany	GRS	X		X
	Siemens AG, KWU	X		X
	IWM Freiburg	X		
	Battelle Ing. Technik			X
Italy	University of Pisa	X		X
India	BARC	X	X	X
Japan	Japan Atomic Energy Research Institute	X	X	
Korea (Republic of)	Korea Institute of Nuclear Safety (KINS)	X		
	KINS+SungKyunKwanUniversity	X		
	KAERI	X	X	
Russian Federation	RRC “Kurchatov Institute”	X		
	CRISM “PROMETEY”	X		
Slovak Republic	VUJE Trnava	X		X
Switzerland	Paul Scherrer Institute (PSI)	X		
Ukraine	State Scientific & Technical Centre	X		
United Kingdom	AEA Technology	X		
	Nuclear Electric Ltd.	X		
United States of America	Oak Ridge National Laboratory	X	X	
	U.S. NRC		X	X
	Electric Power Research Institute (EPRI)		X	
	Brookhaven National Laboratory			X
	Total number of organizations	21	7	8

25 Organizations from 13 countries

[1]**DFM** - deterministic fracture mechanics
[2]**PFM** - probabilistic fracture mechanics
[3]**THM** - thermohydraulic mixing

Table 2.2 Schedule of Events for RPV PTS ICAS

June 1996	Launch meeting to define the objective, the task matrix and other details of ICAS, at GRS Köln
June - August 1996	Call for Participation
December 1996	Distribution of task-specific problem statements to participating analysts
June 1997	Interim Workshop to discuss present state of the analyses , at NEA Paris
November 1997	Submission of structural, fracture mechanics and thermal-hydraulic analysis results for ICAS/PTS by participating organizations
December 1997-January 1998	Compilation of analysis results, construction of comparative plots and organization of the final Workshop
February 1998	Workshop with presentation and discussion of analysis results, at Orlando
May 1998	Submission of additional, and supplemental analysis results
September 1998	Compilation of the additional analysis results and construction of updated comparative plots
August 1998 - June 1999	Preparation and issuance of draft final report

3 ICAS Problem Statement (Task Matrix)

The ICAS problem statement was divided into three task groups (deterministic, probabilistic and thermal-hydraulic) with several main tasks. Additionally, parametric studies were proposed to investigate the influence of certain parameters on the results of the main tasks. Input for these tasks was prepared by Siemens, ORNL, EdF and GRS.

The RPVs described herein incorporate some country-specific concerns. A vessel typical of German design was proposed for the deterministic task group. The cladding thickness was proposed to vary in the range of designs employed in the USA, France, Germany and Russia. The postulated loading transients refer to a small-break loss-of-coolant accident typical for US PWR plants and transients due to leaks with different size typical for German PWR plants. In the Probabilistic Task Group, a vessel typical of U.S. construction was loaded by specific PTS transients. In the thermal-hydraulic task group, a fictitious vessel is proposed with wall thickness typical of a German RPV, but with internal measurements of the Upper Plenum Test Facility (UPTF) vessel in Mannheim (Germany).

3.1 Deterministic Fracture Mechanics (Task Group DFM)

Summary of the DFM Problem Statement

A four-loop RPV was defined with an internal diameter of 5,000 mm, a wall thickness of 243 mm, and a clad thickness of 6 mm, along with detailed information on material properties. Three emergency cooling transients (Tn; n=1-3) due to assumed leaks and five postulated cracks (Cm; m=1-5) were defined for the RPV:

- Transient T1 is due to a small-break loss-of-coolant transient (leak size about 20 cm^2), for which axisymmetric loading conditions are assumed. Time histories of pressure, temperature and heat transfer coefficient in the downcomer for this severe transient were generated from the RELAP-5 code.

- Transients T2 and T3 represent asymmetric loading conditions (plume cooling) due to hot-leg leaks of sizes 50 cm^2 and 200 cm^2, respectively. The cold leg injection is assumed into two neighboring legs which subtend an angle of 45°. One plume,

characterized by its width, is assumed to develop around the centreline between these neighbouring cold legs.

Postulated cracks are positioned in the circumferential weld 2,263 mm below the lower edges of the nozzles. For the transients with asymmetric cooling conditions, the cracks are assumed in the centerline of the plume. The five postulated cracks were defined as:

- Crack 1 is a 360° circumferential surface crack with depth 16 mm, including the clad thickness.

- Cracks 2 and 3 are circumferential and axial semielliptical surface cracks of depth a = 16 mm including clad thickness and aspect ratio a/c = 1/3.

- Cracks 4 and 5 are circumferential and axial semielliptical subclad cracks of depth a = 10 mm and aspect ratio a/c = 1/3.

For the DFM Task Group, Task CmTn denotes the fracture assessment of Crack m subjected to Transient n, where m = 1-5 and n = 1-3.

Additional parametric studies were defined for various aspects of the problem, including the influence of clad thickness, clad and weld yield stresses, and crack aspect ratio. Furthermore, different residual stress distributions due to the cladding and welding processes were provided to allow participants to investigate the influence of these stresses on crack loading.

Detailed special requirements for the DFM analyses were provided to the participants with the objective of comparing the analysis results. These requirements included the following:

- Temperature and stress distributions in the vessel wall for the postulated transients analysed.

- Loading along the crack front for the postulated cracks analysed.

- Fracture assessment of the postulated cracks to determine the maximum allowable transition temperature (RT_{NDT}) that represents impending crack initiation according

to three different criteria: (1) the maximum -, (2) the tangent - and (3) the 90 percent criteria. In the framework of the fracture assessment, the fracture toughness curve from the ASME Code, Section XI, Appendix A, was assumed for all cases.

Detailed Presentation of the Problem Statement

3.1.1 Definition of the RPV Geometry (cylindrical part)

In the near-core region, the proposed four-loop RPV (see Fig. 3.1) has an internal diameter of 5,000 mm, a wall thickness of 243 mm in the base/weld material and a 6 mm cladding thickness. Therefore, the outer diameter is 5,498 mm. Figure 3.1 includes also details of the nozzle geometry and the four support lugs between the nozzles.

A parametric study (**Task PCT**) was proposed to investigate the influence of the cladding thickness by including thickness values of 4 mm and 9 mm.

3.1.2 Material Properties

The base material was assumed to be ferritic steel 22 NiMoCr 37 (German material number 1.6751). The austenitic stainless steel cladding has material number 1.4551. Properties for the respective materials are given in Tables 3.1 and 3.2. The density of the base/weld metal and the cladding was given as 7,800 kg/m^3.

A parametric study **(Task PYS)** was proposed to investigate separately the influence of differences in the yield stress for the cladding and base metal. An alternative value of 250 MPa was considered for the cladding. The base/weld metal yield stress for the given temperature region representing end-of-life conditions was changed to the value of 700 MPa. Furthermore, the differences between results for elastic and elastic-plastic constitutive models were investigated for the parametric cases.

For the fracture assessment, the fracture toughness curve (K_{IC}) was given in accordance with ASME Code (Section XI, Appendix A, 1995), and it reaches a maximum value of 195 MPa:

$$K_{IC}\ [\text{MPa}\sqrt{m}\,] = \min\{36.5 + 3.1 \exp(0.036\,(T - RT_{NDT} + 55.5))\ ;\ 195\}$$

where T and RT_{NDT} are in °C.

3.1.3 Loading conditions

The RPV is loaded by emergency cooling transients (Tn, with n=1,2 and 3) due to assumed leaks. Transient T1 is due to a small-break loss-of-coolant transient (leak size about 20 cm^2). The primary pressure, the averaged fluid temperatures, as well as heat transfer coefficients in the downcomer are presented in Figs. 3.2, 3.3 and 3.4, respectively. The data sets were made available in an electronic form. For transient T1, axisymmetric loading conditions with no change in axial position were assumed.
Transients T2 and T3 are due to hot leg leaks of the size 50 cm^2 and 200 cm^2, respectively. The cold leg injection is made into two neighboring legs which subtend an angle of 45°. The scheme of the injection and the assumptions concerning the loading conditions regarding the plume interaction are presented in Fig. 3.5. Therefore, a single plume was assumed in the centerline of the neighboring cold legs and characterized by the plume width. For transients T2 and T3, data describing internal pressure, fluid temperatures and heat transfer coefficients inside and outside the cooling region were given with respect to different axial positions in the downcomer. Also, the cooling width and the water level were provided in plots and data sets. The following data are depicted in Figs. 3.6-3.11 for T2, and in Figs. 3.12-3.17 for T3:

- absolute internal pressure in the downcomer (Figs. 3.6 for T2 and 3.12 for T3);
- Figures 3.7 and 3.13 show the asymmetric distribution of the fluid temperatures for transients T2 and T3, respectively. Inside the cooling region, the fluid temperatures Ts are given for different axial positions measured from the lower nozzle edge of the cold legs. Outside the cooling region, the fluid temperature Ta is described by the hot water temperature in regions below the water level (plume cooling) and by the saturation temperature in regions above the water level if it falls below the lower nozzle edge of the cold leg (stripe cooling). The water level is presented in Figs. 3.8 and 3.14 for transients T2 and T3, respectively. Negative values indicate the water level is below the lower edge of the nozzle;
- The width of the plume or the stripe was given for different axial positions in Figs. 3.9 and 3.15 for transients T2 and T3, respectively. The water temperature distribution in the plume was assumed of Gaussian type (loading assumption LAG), i.e. the water temperature difference, $\div T(x,y) = T_a - T_S(x,y)$, is given by

$$\div T(x,y) = \div T\,(x,y = 0)\ 1\#\exp(- (2\ y / B_t(x))^2)$$

where

x axial position in the plume

y horizontal coordinate in the plume, symmetry line at y = 0

$\div T$ difference between the fluid temperature outside the plume and the fluid temperature at position (x,y) in the plume.

$B_t(x)$ distance between two points lying symmetric to the symmetry line of the plume for which the maximum temperature difference is decreased to 1/e of the maximum value [see Figs. 3.9 (T2) and 3.15 (T3)].

With increasing distance from the injection nozzle, the width of the plume increased while the width of the stripe decreased.

- The heat transfer coefficients (HTC) ζ_S and ζ_a between RPV wall and fluid inside and outside the cooling region are shown in Figs. 3.10, 3.11 (T2) and 3.16, 3.17 (T3). The HTC distribution inside the plume was assumed of Gaussian type by

  $\zeta_S (x,y) = \zeta_S (x,y = 0) * \exp(- (2\ y / B_t(x))^2)$.

- The HTC values on the symmetry line are given in Figures 3.10 and 3.16 for transients T2 and T3, respectively. The HTC at the outside vessel wall was assumed to be 5 W/m^2 K, which is similar to adiabatic conditions.

Separately, a simplified loading assumption (LAS) was proposed with constant instead of Gaussian temperature and HTC distributions in the plume. In case of stripe cooling, i.e. for the downcomer region between the lower nozzle edge and water level, constant distributions for fluid temperature and HTC in the stripe were assumed for both loading assumptions LAG and LAS.

3.1.4 Postulated cracks

The postulated cracks were positioned in the circumferential weld 2,263 mm below the lower edges of the nozzles. For the transients with asymmetric cooling conditions, the axial cracks were assumed in the centerline of the plume.

- Crack 1 is a 360° circumferential surface crack with depth 16 mm including cladding thickness

- Crack 2 and 3 were circumferential and axial semielliptic surface cracks, respectively, with (a x 2c) of depth a= 16 mm including cladding thickness and aspect ratio a/c = 1/3.

- Crack 4 and 5 were circumferential and axial semielliptic underclad cracks, respectively, with (a x 2c) of depth a= 10 mm and aspect ratio a/c = 1/3.

A parametric study (**Task PCAR**) was proposed to investigate the influence of the aspect ratio, i.e. a/c = 1/2 and 1/1 were also considered.

3.1.5 Residual stresses

The analyses of the main tasks were considered without residual stresses, i.e. stress free temperatures of 288 °C for transient T1 and 284 °C for transients T2 and T3 were proposed.
Additionally, a parametric study **(Task PRS)** was proposed to investigate the influence of residual stress distributions separately and together.

- Distribution 1 was related to residual stresses in the circumferential weld due to the welding process and is characterized by the formula:

  $y(x) = y_{max} \cos\left(2 \phi \frac{x}{x_{max}}\right)$

with

$x > 0$ radial coordinate measured from inner surface of the weld

x_{max} wall thickness

y_{max} = 56 MPa

- Distribution 2 was related to the residual stresses (axial and hoop direction) due to the cladding process after heat treatment and is presented in Fig. 3.18. The given distribution was transferred to the dimensions of the RPV wall, i.e. 243 mm wall thickness and 6 mm cladding thickness.

3.1.6 Special requirements for the analyses

Within the DFM Task Group, analysis results of temperature and stress distributions in the vessel wall were performed according to the given material properties and the postulated transients. Furthermore, the loadings of the postulated cracks were analyzed along the crack front. For each crack, a fracture assessment was performed to determine a maximum allowable transition temperature RT_{NDT} that represents impending crack initiation based on the fracture toughness curve given in Section 3.1.2. The special requirements for the DFM analyses are described in detail in the Appendix A.

3.2 Probabilistic Fracture Mechanics (Task Group PFM)

Summary of the PFM Problem Statement

Objectives of the Probabilistic Fracture Mechanics (PFM) Task Group were to compute the conditional probability of crack initiation and the probability of RPV failure for the following four subtasks using PFM methodology. The probability is conditional in the sense that the different transient loadings were assumed to occur. Failure means propagation of the flaw through the thickness of the RPV wall. The geometry of the RPV was characterised by an internal diameter of 4394 mm and a wall thickness of 219 mm. The cladding thickness was prescribed to be 4.8 mm. The PFM analyses were performed using the Marshall flaw-depth distribution function which evenly spaces 15 initial flaw depths in the first 5.1 cm (2 in.) of the vessel wall. Material properties for the base metal, weld metal, and cladding were as shown in Tables 3.5 and 3.6. The stress-free temperature was assumed to be 288 °C.

The four main tasks, denoted as PFM-n (n = 1-4), were defined as follows:

- **PFM-1:**
  Compute the conditional probability of crack initiation and vessel failure for one axial weld containing one axially oriented infinite-length surface-breaking flaw subjected to a stylised exponentially decaying thermal transient and constant pressure of 6.9 MPa.

- **PFM-2:**
  Compute the conditional probability of crack initiation and vessel failure for one circumferential weld containing one circumferentially oriented continuous 360° surface breaking flaw subjected to the same transient as PFM-1.

- **PFM-3:**
  The same as problem 1 except the loading is due to the postulated small-break LOCA transient T1 defined for the DFM Task Group.

- **PFM-4:**
  The same as problem 2 except the loading is due to the postulated small-break LOCA transient T1 defined for the DFM Task Group.

Analyses for various postulated times in the operating life of the vessel were performed, i.e., the conditional probabilities of crack initiation and vessel failure were determined for a range of mean inside surface fluences that vary from 0.3 to 3.5 x 10^{19} neutrons/cm^2 (E>1.0 MeV).

A parametric study (PFL) was proposed to investigate the influence of cracks with finite length having aspect ratios of a/c = 1/6, 1/3, 1/1.

Detailed Presentation of the Problem Statement

The geometry of the cylindrical part of the RPV was characterized by an internal diameter of 4,394 mm and a wall thickness of the base material of 219 mm. The cladding thickness was assumed to be 4.8 mm.
The PFM analyses were performed using the Marshall flaw-depth distribution function specified in Table 3.3 and which evenly spaces 15 initial flaw depths in the first 5.1 cm (2 in.) of the vessel wall. The interpretation and implementation of the flaw-size cumulative distribution function (see Table 3.3) is as follows:

- For each flaw, select a random number x, such that $0 \leq x \leq 1.0$;
- If x is $\leq$ CDF(1)= 0.418022823, then the flaw depth is 0.3386 cm (0.1333 in.);
- If $CDF(1) \leq x \leq CDF(2)$, then the flaw depth is 0.5758 cm (0.2667 in.);
- In general if $CDF(i) \leq x \leq CDF(i+1)$, then the flaw depth is a(i+1).

In Task PFM-1 and -2, a single region of the RPV beltline containing a single flaw subjected to a simplified stylized thermal-hydraulic boundary condition was considered. In Task PFM-3 and -4, a postulated transient involving complex time histories (transient T1 of Section 3.1.3) was considered. In the Tasks PFM-1 to -4, analyses for various times in the operating life of the vessel were performed, i.e. the conditional probability of crack initiation and vessel failure for the mean values of inside surface fluence, copper, nickel, and RT_{NDTo} provided in Table 3.4 were determined. The material properties of the base metal SA 508 Class 3 and the cladding proposed for the PFM tasks are listed in Tables 3.5 and 3.6. The stress free temperature in the PFM analyses was assumed to be 288 °C.

Task PFM-1:

Compute the conditional probability of crack initiation and vessel failure for one axial weld containing exactly one axially oriented infinite length surface breaking flaw subjected to a simplified stylized transient.

The simplified stylized transient is the one utilized in the US NRC / Electric Power Research Institute (EPRI) co-sponsored PTS benchmarking exercise [1]. Most of the PFM analyses were carried out using the methodology of ORNL which is summarized in [2].

The thermal transient is characterized by a stylized exponentially decaying coolant temperature which follows the formulation:

$$T(t) = T_f + (T_i - T_f) \exp(-ßt)$$

where:

t = time (minutes)

T(t) = coolant temperature at time t

T_i = coolant temperature at time t = 0

T_f= final coolant temperature

ß = exponential decay constant (min^{-1})

The final coolant temperature was 66 °C (150 F), and ß was 0.15 min^{-1}. Additionally, the initial temperature was 288 °C (550 F), the pressure was constant and equal to 6.9 MPa (1 ksi), and the convective heat transfer coefficient was constant and equal to 1700 W/m^2K (300 BTU/hr-ft^2-F). The stress free reference temperature was assumed to be 288 °C (550 F).

Task PFM-2:

Compute the conditional probability of crack initiation and vessel failure for one circumferential weld containing exactly one circumferentially oriented continuous 360 degree surface breaking flaw subjected to the same transient defined in PFM-1. The stress free reference temperature was assumed to be 288 °C (550 F).

Task PFM-3:

The same as PFM-1 except the transient was a postulated small-break loss-of-coolant transient (T1) generated by the RELAP 5 thermal-hydraulics computer code illustrated in Figs. 3.2, 3.3 and 3.4. The RELAP 5 output data for convective heat transfer coefficient time history, fluid-temperature time history and for pressure-time history were made available. The stress-free reference temperature was assumed to be 288°C (550 F).

Task PFM-4:

Compute the conditional probability of crack initiation and vessel failure for one circumferential weld containing exactly one circumferentially oriented continuous 360 degree surface-breaking flaw subjected to the same transient defined in PFM-3. The stress-free reference temperature was assumed to be 288 °C (550 F).

A parametric study **(Task PFL)** was proposed to investigate the influence of cracks with finite length. For that study, semielliptic cracks (2c x a) were proposed with aspect ratio a/c = 1/5, 1/3 and 1/1. Special requirements for the PFM analyses are described in the Appendix A.

3.3 Task Group THM: Thermal-Hydraulic Mixing (Main Task Mix)

Summary of the THM Problem Statement

The objective of the Task Group THM was to compare analytical models that estimate the effects of thermal mixing and steam condensation for the emergency cooling water in the cold leg and the RPV downcomer. The assumed plant type was a 1,300 MW four-loop PWR. The internal measurements of the fictitious RPV, and the cold legs correspond to those of the UPTF in Mannheim, Germany. The internal diameter was 4,870 mm as measured in the test vessel, and the base-metal wall thickness in the cylindrical region was 243 mm with 6 mm cladding, representing the geometry of a real vessel, while the wall thickness of the UPTF test vessel was only 55 mm with 3 mm cladding. Detail drawings of the vessel internals and coolant system were available to participants upon request.

The assumed transient was due to a 200 cm^2 leak in a hot leg at time t = 0 s. A detailed description of the sequence of events related to the emergency cooling water injection during the transient is given in the following section. These include time histories of both the high-pressure and low-pressure injection rates for the emergency cooling water injection, as well as the time histories of the injection temperatures for the cold legs. The hot-leg injection was neglected because of the given primary absolute pressure and the hot-side leak position.

In the first 300 s, the water level of the primary system was assumed to decrease to the level of the RPV nozzles. During this interval, the time histories of the global water temperature in the downcomer and the global HTC at the RPV wall were taken from systems analysis. Time histories of the primary pressure and water level in the downcomer were provided for the full transient. For times after 300 s, the downcomer fluid temperature and the HTC at the RPV wall were calculated by the participants with their analytical models

Two parametric studies were proposed to investigate the influence of variations of the water level in the downcomer (Task PMIX) and the influence of variations in the emergency cooling water injection rate per cold leg (Task PINJ).

Detailed Presentation of the Problem Statement

The assumed plant type was: 1300 MW four-loop-PWR. The assumed transient was due to a 200 cm^2 leak in a hot leg at time t = 0 s. For comparing directly the analytical

results for condensation and for mixing, the time history for the global parameters of (1) absolute pressure in the RPV downcomer, (2) cooling water injection rate, and (3) level in the RPV downcomer, were given.

After the running out of the main cooling pumps and the drop of the primary water level to the lower edge of the main cooling pipe nozzles due to a medium-sized leak in a hot leg of the main cooling pipes, the fluid temperature in the RPV downcomer almost exclusively is determined by the cold cooling water injection and the heat transfer from the walls of the cold legs, the downcomer and the lower plenum. Recent analyses show that the stress in the RPV wall due to primary pressure at medium-sized primary leaks can be much smaller than the stress in the RPV due to fluid temperature decrease. Of course, the time history of the calculated primary pressure and the injection rate is dependent on the analytical models in the transient code (e.g. leak rate and condensation models).

During quantification of the influence of this model dependence on the RPV loading, however, it is to be considered that after a relatively short period of time the leak rate reaches the emergency cooling water injection rate. Thus, the primary pressure level at given leak size focuses only on the employed leak rate model and on the net injection marking line of the post cooling pumps.

Simplifying Assumption

The emergency cooling water injection in the hot legs does not affect the fluid temperature in the RPV downcomer. Therefore, during calculation of the fluid temperature and the HTC in the downcomer, the hot leg injection could be neglected because of the given primary absolute pressure.
To simplify analysis methods, the stripes of colder water that form below the cold legs with ECC-water injection due to a decreased downcomer water level were assumed to flow down the RPV-wall, independent of the ECC-water injection rate per leg. Detachment from the RPV-wall and downflow along the core barrel at higher injection rates was not taken into account. This assumption, which is not in agreement with the UPTF data, was chosen to enable an easy comparison of the calculated water stripe temperatures. If a multidimensional code was used, this assumption should have been ignored and the differences should have been demonstrated.

3.3.1 Geometry

The internal measurements of the fictitious RPV and the cold legs corresponded to the internal measurements of the UPTF test vessel (see Figs. 3.19-3.20). The internal diameter of the UPTF test vessel was 4,870 mm. In the cylindrical part of the fictitious RPV, the wall thickness of the base material (22NiMoCr37, Material No. 1.6751) was 243 mm. The thickness of the austenitic cladding (Material No. 1.4551) was 6 mm everywhere. Therefore, the external diameter of the fictitious RPV was of 4,870mm + 2 (6+243)mm = 5,368 mm. The RPV external diameter in the cylindrical part was assumed constant between the nozzles of the main cooling lines and the lower plenum. The wall thickness of the 2,075-mm tall lower plenum was 150 mm (without cladding).
The internal diameter of the main cooling line was of 750 mm with a wall thickness of 50 mm, the internal diameter of the injection nozzle was 222.5 mm. The pump housing also had a wall thickness of 50 mm. The cold legs as well as the pump shells were from austenitic material No. 1.4541. The measurements of the relevant RPV internals could be taken directly from the UPTF drawings.

3.3.2 Emergency cooling water injection
Lateral injection in the cold leg

The centerline of the injection nozzle forms an angle of 60° with the centerline of the main cooling line and both are in a horizontal plane (lateral injection). The length of the cold leg is 9.52 m and the distance between the injection nozzle and the RPV inlet is 5.796 m.

Two of the four cold-injecting high-pressure (HP) pumps are considered as non-available; the remaining two HP pumps take in water from the storage tanks with a temperature of 15°C and inject in two neighbouring cold legs. The HP injection starts 100 s after beginning of the incident and ends when the available water volume is used up (2800 s).

The four accumulators which inject into the cold legs are available, but they are turned off 500 s after the beginning of the incident. At that moment, the primary pressure is still beyond the pressure of 26 bar at which the accumulators can start to inject. Therefore, they do not inject. As a consequence, no nitrogen saturated water can get from the accumulators into the cold legs.

All four low-pressure (LP) injection pumps are available. Every LP pump injects into both the cold and the hot legs of the main cooling lines. Injection is possible below the pressure level of 10.4 bar.

At 300 s after beginning of the incident, the bends of the pumps are filled with water as a result of the inflow of water from the steam generator pipes. After this period of time, the bends of the pumps remain filled with fluid but, as a result of the stagnation and the pressure decrease, steam bubbles appear for the time interval 300 s to 700 s in the bends of the pumps.

The height of the lower edge of the main coolant pump diffusor is on the same level as the overflow edge in the UPTF pump simulator, 690 mm above the lower edge of the cold leg. The stroke of the UPTF pumps simulator is 120 mm, corresponding to a pressure loss value of 14.6 bar at streaming through the standing main coolant pumps in the ordinary stream direction (relating to the internal diameter of the main coolant line of 750 mm).

Rate of emergency cooling water injection

The beginning of the incident is at time t = 0. The time history of the HP injection rate (M_{HP}) for each cold leg is given as follows:

Time [s]	0.	99.	100.	200.	400.	600.	800.	2800.	2801.	5000.
M_{HP} [kg/s]	0.	0.	31.6	34.4	43.7	60.7	68.6	68.6		

The time history of the LP injection rate (M_{LP}) for each cold leg is given as follows:

Time [s]	0.	750.	800.	5000.
M_{LP} [kg/s]	0.	0.	60.	60.

Injection in:

Cold leg 1 = M_{LP}
Cold leg 2 = M_{HP}+ M_{LP}
Cold leg 3 = M_{HP}+ M_{LP}
Cold leg 4 = M_{LP}
Angle between cold leg 1 and 4: 45°
Angle between cold leg 2 and 3: 45°

Temperature of emergency cooling water injection

The minimum water temperature in the storage tanks is 15°C. The water taken in from the storage tanks or from the reactor sump for the LP pumps runs through coolers. The back-feed operation where the LP pumps get water from the reactor sump starts 2800 s after beginning of the incident because no further water is available from the storage tanks. The minimum injection temperature is 4.7°C when the water comes from the storage tanks and 12.5°C when the water comes from the reactor sump. The output of each LP pump is 120 kg/s (60 kg/s into cold leg and 60 kg/s into hot leg). The injection temperatures result from the ideal mixing of HP and LP water in the injection leg with these data.

The time history of the injection temperature is given as follows.
Cold leg 1 as well as cold leg 4:

Time [s]	0.	750.	2800.	2801.	5000.
T [°C]	4.7	4.7	4.7	12.5	12.5

Cold leg 2 as well as cold leg 3:

Time [s]	0.	100.	750.	800.	2800.	2801.	5000.
T [°C]	15.	15.	15.	10.2	10.2	12.5	12.5

3.3.3 Global thermal hydraulic parameters

In the first 300 s after beginning of the incident, the water level of the primary system decreases to the level of the RPV nozzles. For this phase, the relevant thermal-hydraulic parameters, e.g., fluid temperature and HTC in the downcomer, were taken from the system analysis. For the time after 300 s, the downcomer fluid temperature and the HTC between RPV wall and fluid were calculated by the participants with their analytical models.

Time history of the primary pressure in the RPV downcomer

The time history of the primary pressure is given as follows:

Time [s]	0.	0.5	2.0	5.0	10.	300.	625.	700.	800.	5000.
Pressure [bar]	160.	140.	110.	100.	85.	75.	25.	10.	8.9	8.9

After 720 s, the primary pressure was determined by the equality of the emergency cooling water injection rate and the leak rate.

Time history of the global water temperature in the RPV downcomer in the first 300s

The time history of the global water temperature is given as follows:

Time [s]	0.	50.	120.	170.	300.
T_{water} [°C]	297.	297.	293.	288.	261.

Time history of the global heat transfer coefficient between RPV wall and fluid in the first 300 s

The global HTC ζ (in kW/m^2K) in the downcomer is given as follows:

Time [s]	0.	10.	30.	40.	50.	60.	73.	110.	165.	300.
ζ [kW/m^2K]	19.	19.	11.	9.	3.	1.4	0.8	3.	5.	5.

Time history of the water level in the RPV downcomer

Height position H = 0 corresponds to the cold leg lower nozzle edge (which is 375 mm below the centerline of the cold leg). A negative H value means the water level falls below the nozzle edge. H = 2 m indicates a completely water-filled RPV downcomer.

The time history of the water level is given as follows:

Time [s]	0.	200.	300.	400.	800.	900.	5000.
H [m]	1.525	1.5	0.	-1.5	-1.5	1.525	1.525

In a real plant, the water level reduction below the lower nozzle edge of the cold leg is not so deep. This time history was chosen to make it possible for participants to apply and compare models for condensation at water stripes.
Additionally, a parametric study was proposed to investigate the influence of the results on variations of the minimum water level **(Task PMIX)**. For that study, values of -2.5 m and 0 m were considered at 400 – 800 s. In addition, for a minimum water level of 0.5 m, the following time history of the downcomer water level was taken into account:

Time [s]	0.	200.	300.	400.	800.	900.	5000.
H [m]	1.525	1.5	0.5	0.5	0.5	1.525	1.525

Furthermore, a parametric study was proposed to investigate the influence of variations in the emergency cooling water injection rate per cold leg in a water filled sytem. For that study, only 20 percent of the specified cold side HP and LP injection rates was assumed together with a downcomer water level of 1.525 m throughout the transient **(Task PINJ)**. Task PINJ was the only task which allows a direct comparison of the fluid-fluid mixing results, because the downcomer global water temperature was not modified by condensation phenomena. Special requirements for the THM analyses are described in the Appendix A.

3.4 Task Matrix

The tasks of RPV ICAS are summarized in Table 3.7.

References

[1] ”Documentation of Probabilistic Fracture Mechanics Codes used for Reactor Pressure Vessels Subjected to Pressurized Thermal Shock Loading”, EPRI TR-105001, 1995

[2] Dickson T. L., “An Overview of FAVOR: A Fracture Analysis Code for Nuclear Reactor Pressure Vessels“, Transactions of the 13th International Conference on Structural Mechanics in Reactor Technology (SMiRT 13), Volume IV, pp 701-706, Porto Alegre, Brazil, 1995

Table 3.1 Material properties of base metal (22 NiMoCr 37) and weld metal

Temperature [°C]	20	100	200	300	350
Modulus of elasticity E [MPa]	206000	199000	190000	181000	172000
Poisson's ratio τ	0.3	0.3	0.3	0.3	0.3
Thermal conductivity [W/m K]	44.4	44.4	43.2	41.8	39.4
Specific heat capacity Cp [J/g K]	0.45	0.49	0.52	0.56	0.61
Mean thermal expansion coef. $\zeta * 10^6$ [1/K]	10.3	11.1	12.1	12.9	13.5
Yield strength R_{p02} [MPa]	450	431	412	392	--
Tangent modulus E_T [MPa]	2000	2000	2000	2000	2000

Table 3.2 Material properties of the austenitic cladding

Temperature [°C]	20	100	200	300	400
Modulus of elasticity E [MPa]	200 000	194 000	186 000	179 000	172 000
Poisson's ratio τ	0.3	0.3	0.3	0.3	0.3
Thermal conductivity [W/m K]	16.0	16.0	17.0	17.0	18.0
Specific heat capacity Cp [J/g K]	0.5	0.5	0.54	0.54	0.59
Mean thermal expansion coef. $\zeta * 10^6$ [1/K]	15.0	16.0	17.0	19.0	21.0
Yield strength R_{p02} [MPa]	320	320	320	320	--
Tangent modulus E_T [MPa]	2000	2000	2000	2000	2000

Table 3.3 Flaw distribution proposed for PFM task group

Flaw number	flaw depth (a) [inches]*	Cumulative distribution function CDF(a)
1	0.1333	0.41802823
2	0.2667	0.66130886
3	0.4000	0.80289131
4	0.5333	0.88528831
5	0.6667	0.93324103
6	0.8000	0.96114817
7	0.9333	0.97738933
8	1.0667	0.98684123
9	1.2000	0.99234197
10	1.3333	0.99554324
11	1.4667	0.99740629
12	1.6000	0.99849054
13	1.7333	0.99912153
14	1.8667	0.99948876
15	2.0000	1.00000000

* 1 inch = 25.4 mm

Table 3.4 Embrittlement-related parameters for Tasks PFM 1-4

Mean fluence*	Mean $RT_{NDT}(F)$ **
0.3	166
0.5	195
1.0	237
1.5	262
2.0	278
2.5	291
3.0	300
3.5	308

* Neutron fluences are expressed in 10^{19} neutrons / cm^2 (E > 1.0 MeV) at the inside vessel surface

** Calculated by U.S. NRC RG 1.99 Rev 2, using values of mean copper and nickel of 0.30 percent and 0.75 percent, respectively, and a mean value of RT_{NDTo} = 20 F.

[T(F) = 1.8 T (°C) + 32]

Table 3.5 Material properties of base metal (SA 508 Class 3) and weld metal

Temperature [°C]	20	100	200	300
Modulus of elasticity E [MPa]	204 000	200 000	193 000	185 000
Poisson's ratio τ	0.3	0.3	0.3	0.3
Thermal conductivity [W/m °C]	37.7	39.9	40.5	39.5
Density * Specific Heat capacity ψ# Cp [10^6 J/m^3 °C]	3.488	3.775	4.087	4.423
Mean thermal expansion coef. ζ * 10^6 [1/ K]	11.22	11.79	12.47	13.08
Yield strength R_{p02} [MPa]	350	350	350	350
Tangent modulus E_T [MPa]	2000	2000	2000	2000

Table 3.6 Material properties of the cladding (types 309L - 308L stainless steel)

Temperature [°C]	20	100	200	300
Modulus of elasticity E [MPa]	197 000	191 500	184 000	176 500
Poisson's ratio τ	0.3	0.3	0.3	0.3
Thermal conductivity ς [W/m °C]	14.0	15.2	16.6	17.9
Density * Specific Heat capacity ψ* C_p [10^6 J/m^3 °C]	3.559	3.907	4.160	4.293
Mean thermal expansion coef. ζ * 10^6 [1/ K]	15.54	16	16.60	17.10
Yield strength R_{p02} [MPa]	350	350	350	350
Tangent modulus E_T [MPa]	2000	2000	2000	2000

Table 3.7 Task Matrix of RPV PTS ICAS

Task Group		Task		Parametric Study	
DFM	Deterministic Structure and Fracture Mechanics	CmTn	Fracture Assessment of crack Cm loaded by transient Tn (m=1-5; n=1-3) For the asymmetric loading transients T2 and T3 different loading conditions were assumed (LAG, LAS).	PCT PCAR PYS PRS	Influence of the cladding thickness Influence of the cracks aspect ratio Influence of cladding and weld yield stress as well as elastic and elastoplastic approaches Influence of residual stresses
PFM	Probabilistic Fracture Mechanics	PFMn	Conditional probability of crack initiation and vessel failure for two assumed crack orientations loaded by two transients (n=1-4)	PFL	Influence of cracks with finite length (semielliptic, different aspect ratio)
THM	Thermohydraulic Mixing	MIXn	Distribution of the fluid temperature and heat transfer coefficient (HTC) in the downcomer due to fluid-fluid-mixing and steam condensation for a medium size leak	PMIX PINJ	Influence of different minimum water levels Influence of reduced emergency cooling water injection rate

4 Computer Codes and Analysis Techniques

Organisations that provided analysis results for the various ICAS tasks are identified only by an alpha-numeric code in the tables and comparative plots included in Chapters 4 and 5. This identification approach preserves anonymity of the contributing organisations regarding analysis results and continues a policy that was adopted in the previous FALSIRE projects.

Task Group DFM

The distribution of solutions contributed by the participating organisations among the DFM tasks is given in Table 4.1. The computer codes and approaches employed by the participants are summarized in Table 4.2. The latter approaches are subdivided into structural and fracture mechanic categories.

Task Group PFM

The distribution of solutions contributed by the participating organisations among the PFM tasks is given in Table 4.3. The computer codes and approaches employed by the participants are summarized in Table 4.4.

Task Group THM

The distribution of solutions contributed by the participating organisations among the THM tasks is given in Table 4.5. The computer codes and approaches employed by the participants are summarized in Table 4.6.

Table 4.1 Participants in RPV ICAS benchmark analyses , DFM[1]-Task Group

	DFM-Tasks			
Code	**T1**	**T2**	**T3**	**Param. Study**
A1	C1-C5	C1-C5		
A2	C5			
A3	C2, C3		C4	
A4	C1, C2, C4	C2, C4	C2	PCT
A5		C4	C4	
A6	C1, C2, C4	C4		PCAR
A8	C1,C2,C3			PYS,PCAR
A9	C1-C5 (1,2)	C1-C5 (1)	C1-C5 (1)	PCT,PCAR,PRS
A10	C2,C3			
A11	C1-C5			PRS,PCAR
A12	C1,C2,C3			PCAR,PRS
A13	C2, C4	C2, C4		
A14	C1			PCT, PYS, PRS
A15	C2-C5	C2-C5	C2-C5	
A17	C1			PCT,PYS,PRS
A18	C1-C5			PCT,PCAR,PRS
A19	C1- C5			PRS
A20	C1,C2,C3	C1,C2,C3		
A24	C4			PRS
A25	C1-C5			PCT,PCAR
A26	C1 – C5			PCT, PCAR

[1]**DFM** - deterministic fracture mechanics

21 organizations from 13 countries performed 104 analyses and 26 parametric studies

Table 4.2 Computer codes and approaches in RPV ICAS benchmark analyses , DFM[1]-Task Group.

Code	Computer codes, approaches	Computer codes, approaches
	STRUCTURAL ANALYSIS	**FRACTURE ANALYSIS**
A1	COSMOS/M 1.75, 3D, FE-code, elastic	Estimation scheme
A2	ASTER, 3D, Fe-code, elastic-plastic	ASTER, VCE
A3	CASTEM 2000, 3D, FE-code, elastic-plastic	CASTEM 2000, VCE
A4	ADINA 6.1.6, 3D, FE-code, elastic-plastic	ADINA 6.1.6, VCE
A5	ABAQUS 5.6, 3D, FE-code, elastic-plastic	ABAQUS 5.6, EDIA
A6	ADINA 6.1.6, 3D, FE-code, elastic-plastic	Weight function
A8	Analytical, axisymmetric, elastic-plastic	Estimation scheme
A9_1	WELT3D, VENUS, CSMOS/M, 3D, FE-code, elastic	R6
A9_2	2D axisymmetric, FE-code, elastic	Influence functions
A10	ADINA_T, ADINA 7.1, 3D, FE-code, elastic-plastic	ADINA 7.1, VCE
A11	Analytical method	ASME
A12	ABAQUS, 2D axisymmetric, FE-code, elastic-plastic	Estimation scheme
A13	TEMPO1, UZOR1, 3D, FE-code, elastic-plastic	UZOR1, EDIA
A14	2D axisymmetric, FE-code, elastic-plastic	FE-code, J-integral
A15	PMD II, 3D, FE-code, elastic	Influence function
A17	ADINA, 2D axisymmetric, FE-code, elastic-plastic	ADINA, VCE
A18	Analytical, axisymmetric, elastic	Influence function
A19	ABAQUS, 2D axisymmetric, FE-code, elastic-plastic	Weight function R6, R6 app.4
A20	FAVOR, FE	FAVOR, Influence coefficient
A24	ABAQUS, 3D, FE-code, elastic-plastic	ABAQUS, EDIA
A25	ABAQUS, 3D, FE-code	ABAQUS, EDIA
A26	CALORI, TADA Handbook, analytical, elastic	CALORI, TADA Handbook, Influence functions

[1]**DFM** - deterministic fracture mechanics
VCE - Virtual Crack Extension
EDIA - Equivalent Domain Integral Approach

Table 4.3 Participants in RPV ICAS benchmark analyses , PFM[1]-Task Group

	PFM-Tasks				
Code	**PFM1**	**PFM2**	**PFM3**	**PFM4**	**PFL**
A3	X				
A9_1, _2	X	X	X	X	
A10	X	X	X	X	X
A12	X	X	X	X	
A20	X	X	X	X	X
A21	X	X	X	X	
A22	X	X	X	X	X

[1]**PFM** - probabilistic fracture mechanics

7 organizations from 4 countries performed 25 analyses and 3 parametric studies

Table 4.4 Computer codes and approaches in RPV ICAS benchmark analyses , PFM-Task Group

Code	**Computer codes, approaches**
A3	Quadrature rules & CASTEM 2000
A9_1	Monte Carlo , PARISH
A9_2	Monte Carlo
A10	Monte Carlo, PASCAL
A12	Monte Carlo & ANSYS
A20	Monte Carlo, FAVOR
A21	Monte Carlo, FAVOR
A22	Monte Carlo, FAVOR

Table 4.5 Participants in RPV ICAS benchmark analyses , THM Task Group

	THM-Tasks		
Code	**MIX**	**PMIX**	**PINJ**
A4_1, _2	X	X	X
A5	X	X	X
A7	X		
A8	X	X	
A9	X	X	X
A15		X	X
A21	X	X	X
A23	X	X	X

[1]**THM - thermohydraulic mixing**

8 organizations from 5 countries performed 7 analyses and 13 parametric studies

Table 4.6 Computer codes and approaches in RPV ICAS benchmark analyses , THM[1]-Task Group.

Code	Computer codes, approaches
A4_1	correlation mainly based on large scale experiments at UPTF and HDR
A4_2	CFD code CFX-TASCflow
A5	correlation mainly based on large scale experiments at UPTF and HDR
A7	correlation mainly based on large scale experiments at UPTF and HDR
A8	system code RELAP5 mod3.2
A9	code TFSPTS based on REMIX
A15	code MIXEBO based on REMIX/NEWMIX
A21	system code TRAC-P
A23	physically based zonal approach

[1]**THM** - thermohydraulic mixing

5 Discussion of Analysis Results and Comparative Assessments

As part of the detailed comparison of analysis results a number of discrepancies were noted regarding the analytical methods and the input parameters referenced. These discrepancies serve to increase the scatter in results above what might otherwise have been expected, and highlight the need for careful quality assurance and good engineering judgement in undertaking structural integrity assessments. Where due diligence has been paid to select the analysis methodology and to correctly represent the geometry, material properties and boundary conditions in the analyses, there is generally good agreement between results.

5.1 Comparison of Analysis Results - Task Group DFM

In the DFM Task Group, 21 organizations from 13 countries participated. According to the task matrix included in the problem statements, 104 analyses were performed for the main tasks and 26 parametric studies (see Table 4.1). Comparative plots of the DFM results of the participating organizations are presented in this chapter. For tasks CmTn, m = 1-5, n = 1-3, in the DFM module, analysis results were compared for selected variables defined in the Special Requirements (see Appendix A). Based on the information given in Section 3.1, the time histories of fluid temperature, internal pressure and HTC for transients T1, T2 and T3 are depicted in Figs. 5.1.1 through 5.1.3 in a comparative manner, respectively. Some organizations provided updated

results after the final Workshop (February 1998). In the comparative plots, these results are labelled with the index ‘new’.

Transient T1

- The plots of temperature distributions in the wall show that 15 of the 20 computed distributions agree very well. Discrepancies are indicated in five calculations. At time 2400 s, the scatter in temperature at the inner wall ranged from 160 - 190 °C (see Fig. 5.1.4). In some cases either an over-simplified representation of the thermal transient, inadequate mesh refinement close to the inner surface of the vessel or poor choice of element type may have led to erroneous results.

- The plots of axial stresses across the wall (without crack) at time t = 3600 s (Figs. 5.1.5 and 5.1.6) indicate that within the cladding and 10 mm into the base material, elastic solutions lie significantly above the elastic-plastic solutions, 425 to 645 MPa compared with 305 to 345 MPa respectively. While a significant amount of scatter in results is observed, a careful study of the methodologies used to derive these solutions indicates that consistent results are obtained when particular attention is paid to the following:

  - Adequate representation of the pressure transient,

  - Sufficient mesh refinement and choice of element type in critical regions; particularly within the cladding and across the clad-base metal interface. Quadratic elements (incorporating mid-side nodes) are recommended,

  - Correct definition of material properties. Of particular note were the cladding yield stress and the reference temperature definition for the thermal expansion coefficient (TEC).

  With respect to this latter point, within the ICAS problem statement, TEC values were given as usual according to the reference temperature of 20°C. In some codes, the input of these values is transferred correctly to a different stress-free reference temperature. On the other hand, some codes require the user to transfer the TEC values to a different reference temperature. A study undertaken by NRI indicated that incorrect TEC input data produces an underestimation of the elastic axial stress in the cladding of approximately 22 percent. This would result in a non-conservative

prediction of crack driving force. Participants A12 (nonlinear) and A20 (nonlinear) have clearly used the cladding yield stress appropriate to the PFM task (350MPa) rather than that specified for the DFM task (320MPa). Some analysts provided updated analysis results in cases where misinterpretation of the data given in the ICAS problem statements had originally been made. Since the stresses are dominated by the thermal component of the loading, a study by AEA showed that in considered cases the presence of the cold-leg nozzle has only a small influence on the stresses in the belt-line weld.

Case T1C1

- A comparison of the calculated crack-mouth-opening displacement (CMOD) is shown in Fig. 5.1.7. A related study by GRS indicated that the incorrect use of the TEC in an elastic-plastic calculation produced an underestimation of the CMOD by about 18 percent.

- The range of calculated SIF versus crack-tip temperature is given in Fig. 5.1.8. In general, elastic analyses and J-estimation schemes provide higher predictions of SIF when compared to the more complex 3D FEA. The maximum predicted SIFs range from 65 to 95 MPa· m. For elastic-plastic calculations this range is reduced to 65 to 80 MPa· m (see Fig. 5.1.9). The GRS study demonstrated that an incorrect TEC reference temperature of 288°C rather than 20°C leads to a reduction in predicted maximum SIF of approximately 15 percent. The treatment and interpretation of the TEC input to the codes appears to be a major contributor to the scatter in the analysis results. The mentioned scatter in the temperature calculations (see Fig. 5.1.4), especially near the inner surface where the cracks are located effects a scatter of the load paths which ends with lowest temperatures in the range of 35 to 55°C.

- The objective of the analyses was to derive maximum allowable RT_{NDT} temperatures for the defects under consideration. The derived values thus provide an indication of the severity of the defect and loading conditions. Comparisons of critical RT_{NDT} values indicate that 13 out of 17 analysts calculated values in the range 120 to 140°C based on the maximum criterion, while the tangent and 90-percent criteria gave values of 70 to 95°C (see Fig. 5.1.10). The predicted scatter of

the calculated maximum allowable RT_{NDT} values is less than that observed in the calculation of maximum SIF. This arises due to the shape of the fracture toughness curve in the transition region sampled by the predicted loading paths.

Case T1C2

- The seven calculated curves of CMOD time history include elastic as well as elastic-plastic solutions (see Fig. 5.1.11). A scatter of about 20 percent in the region where the maximum value is observed.

- Similar to results for Case T1C1, elastic and elastic-plastic calculations of SIF versus temperature at the deepest point exhibited a scatter of about 40 percent near the maximum level (see Fig. 5.1.12). The scatter is reduced to about 27 percent for the plastic calculations, which are generally below the elastic analysis and estimation scheme results (see Fig. 5.1.13). The maximum criterion provided estimates of critical RT_{NDT} in the range of 100-160°C (see Fig. 5.1.14). Within that scatter the position of individual analyses is different from the position in the scatter of the maximum SIFs due to the shape of the fracture toughness curve used for the determination of maximum allowable RT_{NDT} (see formula in chapter 3.1.2).

- More significant uncertainties in the analysis results were observed in SIF versus crack-tip temperature at the near clad-base material interface location. This arose from local errors in numerical solutions at the material interface due to inadequate mesh refinement and the assumptions made regarding the most appropriate location to establish the SIF. For the 12 results from estimation schemes (7) and finite element methods (5), the scatter is about 80 percent in the region of the maximum. The scatter for the four elastic-plastic FE solutions is significantly reduced to about 20 percent.

Case T1C3

- This through-clad defect is of the same dimension as defect C2, but it is oriented axially, rather than circumferentially. Since the PTS loading is dominated by the thermal component, it is almost equi-biaxial, and the predicted stresses, SIFs and calculated RT_{NDT} are similar to those estimated for defect C2. Scatter in the results is also similar to those for Case T1C2.

Case T1C4

- The scatter in SIF versus crack-tip temperature at the deepest point of the underclad crack produced by the three elastic-plastic FE results ranges about 20 percent, and that of the 11 ES results ranges about 60 percent. Most of the ES methodologies are found to be very conservative. However, the ES results are not consistent with an elastic FE calculation, in which case they could be non-conservative.

Case T1C5

- The scatter in SIF versus crack-tip temperature at the deepest point of the underclad crack produced by the two elastic-plastic FE results ranges about 30 percent and that of the nine ES results ranges about 40 percent.

The objective of the work was to derive maximum allowable values of RT_{NDT} for the five defects. The value of maximum allowable RT_{NDT} is an indicator of the severity of the defect and PTS transient. Critical RT_{NDT} values calculated for all of the main T1 tasks are summarised in Table 5.1.1. These results show that scatter in the critical values of RT_{NDT} is relatively modest when compared with the scatter in SIF. This modest degree of scatter arises from the shape of the fracture toughness curve in the transition region used for assessment of the loading paths. The predicted values of maximum allowable RT_{NDT} for the through-clad semielliptical defects C2 and C3 are broadly similar and generally higher than those for C1. Where calculated, the values of RT_{NDT} for the sub-clad defects C4 and C5 are higher than those for defects C1 to C3.

Transient T2

- The temperature distribution through the wall inside and outside the cooling region at time 1,500 s indicate very good agreement for the seven submitted solutions, i.e., scatter within four percent (see Figs. 5.1.15 and 5.1.16). In contrast, the temperature results of transient T1 show larger scatter (see Fig. 5.1.4). The main difference in the tasks is that for transient T1 many more data values were provided so that data selection was necessary. Therefore, some of the T1 analyses could have experienced a quality assurance problem, especially concerning the approximation of the fluid temperature and HTC data.

- Hoop and axial stresses through the wall (without crack) at time t = 1000 s exhibited scatter of about 20 percent in the base/weld material near the interface to the cladding. Differences between elastic and elastic-plastic solutions are observed only in the cladding.

Case T2C1

- Calculations of SIF versus crack-tip temperature exhibited approximately 20 percent scatter.

Case T2C2

- Time histories of CMOD were in good agreement for the three submitted solutions (see Fig. 5.1.17).

- Plots of SIF versus crack-tip temperature show load paths with two maxima. Two of the three plastic solutions (A4 and A20) agree well (see Fig. 5.1.18). The elastic solution of A20 overestimates the first maximum of SIF by about 17 percent. The lower temperature limit in Fig. 5.1.18 shows low scatter due to the good coincidence in the temperature results. Consequently, the critical values of RT_{NDT} for three different criteria exhibited the scatter given in Fig. 5.1.19.

Case T2C3

- The three elastic and two elastic-plastic calculations of SIF versus crack-tip temperature at the deepest point exhibited a scatter of about 20 percent in the first maximum of the SIF, which can be traced to the consideration of plasticity effects.

Case T2C4

- The SIF versus crack-tip temperature curves for the underclad crack are very flat at low levels of K_I. Therefore, the determination of critical values of RT_{NDT} is very sensitive to the scatter in SIF level. These values are very different if determined from maximum or tangent criteria.

Critical RT_{NDT} values calculated for all of the main T2 tasks are given in Table 5.1.2. These show a similar trend to those derived for transient T1, with defect C5 providing the highest values of RT_{NDT} and C1 the lowest. A greater difference in RT_{NDT} for defects C2 and C3 is observed for transient T2 when compared to T1. This arises due to the orientation of the defects within the cooling plume.

Transient T3

- Temperature distributions through the wall inside and outside the cooling region for the five sets of results agree very well (see Fig. 5.1.20 and 5.1.21).

Case T3C4

- The comparison of the calculated CMOD values is shown in Fig. 5.1.22. The curves for SIF versus crack-tip temperature are shown in Fig. 5.1.23. The main reason for the discrepancies between A5 and the other curves seems to be the different treatment of the TEC input values in the various codes as already described in the section devoted to transient T1. A parametric study performed by GRS showed that incorrect use of the TEC in an elastic-plastic calculation can lead to an underestimation of the maximum SIF by about 20 percent.

- The critical values of RT_{NDT} calculated for three different criteria are compared in Fig. 5.1.24 and Table 5.1.3. The observation made regarding predicted maximum allowable RT_{NDT} values for transients T1 and T2 are supported by these results.

Critical RT_{NDT} values calculated for all of the main T3 tasks are given in Table 5.1.3.

Parametric Study on Residual Stresses (PRS)

- Nine participants did studies on residual stresses for transient T1. The results show consistent trends indicating that residual stresses due to cladding, as well as welding, enhance the maximum SIFs at the deepest points of the considered cracks. For the surface crack C1, the increase in K_I^{max} is about 50 to 100 percent, for C3 about 50 percent and for the underclad crack C4 there is no significant effect (see Fig. 5.1.25).

Parametric Study on Clad Thickness (PCT)

- For the surface cracks C1, C2 and C3 in Task T1, the maximum SIF at the deepest point of the flaw increased with increasing clad thickness, while for the underclad crack C4 the trend is opposite (see Fig. 5.1.26).

Parametric Study on Crack Aspect Ratio (PCAR)

- Seven participants did studies on crack aspect ratio for transient T1. The results show consistent trends. For the semielliptic surface cracks C2 and C3 as well as the underclad cracks C4 and C5, the maximum SIF at the deepest points increased with decreasing crack aspect ratio a/c = 1/1, 1/2, 1/3 (see Fig. 5.1.27).

Table 5.1.1 DFM-Tasks T1: Evaluation of the maximum allowable RT_{NDT} for the cracks C1,C2,C3,C4 and C5 (deepest point) based on tangent, ninety-percent, and maximum criteria on the K-T diagram.

	C1			C2			C3			C4			C5		
PARTICIPANT	tang.	90%	max	tang.	90%	max	tang.	90%	max	tang.	90%	max	tang.	90%	max
A1, new	79	79	121	94	94	141	91	93	140	154	-	184	140	141	170
A2													190	-	215
A3 (elastic)				80		130	110		155						
A3 (plastic)				98		145	150		180						
A4	83	84	123	97	97	135				unlim	unlim	unlim			
A6	78	80	130												
A6 (ep1)			130												
A6 (ep2)	83														
A8 (elastic), new	75	77	124	85	86	137	83	89	133						
A8 (plastic), new	83	84	134	92	93	142	90	99	141						
A9_1, new	80,4	82,1	126,5	89,35	95,9	122,3	125	127	150	unlim	unlim	unlim	unlim	unlim	unlim
A9_2, new	68	76	87	85	88	98	83	86	127	160	-	186	145	155	167
A10				104		141	104		138						
A11	66		95	86		111	81		111	unlim		unlim	200		203
A12	68	69	136	91	93	153	110	116	158						
A13				108	118	152				unlim	unlim	unlim			
A14		69	126												
A15				111		159	106		152	unlim		unlim	unlim		unlim
A17	90,5	98,3	137,5												
A18 (meth. 1)	87,1			104,5			101,5			unlim			249,6		
A18 (meth. 2)	82,9			101,6			97,9								
A19 (elastic)	82	90	136	96	102	145	93	99,5	143	153	158,5	185	143	145,5	170
A19 (R6 J)	78	86	133	90	98	142	88	95,5	140	140	142	175	132,5	137,5	165
A19 (R6 ap.4)	86	93,5	137	99	105	147	95	104	142	140	142	174	131	137	163
A20 (elastic)	73,6			81,4			79,4								
A20 (plastic)	81,9			92,3			89								
A25	64,7		109,2	101,7		152,3	99,6		144,6				unlim		unlim
A26	70		110	80		120	80		120	160		190	135		175

Table 5.1.2 DFM-Tasks T2: Evaluation of the maximum allowable RT_{NDT} for the cracks C1,C2,C3,C4 and C5 (deepest point) based on tangent, ninety-percent, and maximum criteria on the K-T diagram.

	C1			C2			C3			C4			C5		
PARTICIPANT	tang.	90%	max	tang.	90%	max	tang.	90%	max	tang.	90%	max	tang.	90%	max
A1, new	21	31	103	36	43	112	52	61	127	65	68	136	92	129	155
A4, new				39	52	115				190	190	190			
A5										74	84	131			
A6										150	165	195			
A9_1, new	29,7	36,4	60,1	35,5	41,2	108,6	50	52	120	114		168,8	165		185
A13				81,6	128	149				196	197	203			
A15				55		124	77		130	161		174	207		218
A20 (elastic)	24			30,7			50,4								
A20 (plastic)	34,4			38,3			60,9								

Table 5.1.3 DFM-Tasks T3: Evaluation of the maximum allowable RT_{NDT} for the cracks C1,C2,C3,C4 and C5 (deepest point) based on tangent, ninety-percent, and maximum criteria on the K-T diagram.

	C1			C2			C3			C4			C5		
PARTICIPANT	tang.	90%	max	tang.	90%	max	tang.	90%	max	tang.	90%	max	tang.	90%	max
A4, new				46	49	55									
A3, new										76		84			
A5										63	65	68			
A9_1, new	38,2	38,1	48,8	41,4	42,1	51,3	50	57	65	83,4		92	92	100	103
A15				44		46	59		64	80		80	154		154

5.2 Comparison of Analysis Results - Task Group PFM

In the PFM Task Group, seven organizations from four countries participated. According to the task matrix included in the problem statements, 25 analyses were performed for the main tasks and three parametric studies (see Table 4.3). For tasks PFM-n, n = 1-4, in the PFM module, analysis results were compared for conditional probabilities of initiation and vessel failure versus mean surface RT_{NDT} (see Figs. 5.2.1 – 5.2.8). The approaches employed by the participants in generating solutions to these tasks are noted in Table 4.4. After the final Workshop, one organization provided updated results and one organization joined the task group. In the comparative plots these results are labelled with the index 'new'.

- For all tasks, significant differences were observed between the A20 and A22 solutions, although both organizations utilized the same computer code. The latter result is illustrated for task PFM-1 in the plot of the conditional probability of crack initiation versus mean surface RT_{NDT} given in Fig. 5.2.1. The differences in these solutions were apparently due to selection of different input parameters. It was determined that A20 used the procedures given in USNRC Regulatory Guide 199, Rev. 2 for simulating the margin term in the calculation of RT_{NDT}, while A22 used numbers (i.e., standard deviations for initial value of RT_{NDT} as well as for nickel and copper content) obtained from another source.

- Participant A20 determined that the conditional probabilities of the elastic solutions are larger than the values of the plastic solutions by a factor of 2 to 4.

- The elastic-plastic results of A3 shown in Fig 5.2.1 are close to the elastic results of A20.

- The calculated conditional probabilities of crack initiation, especially for low values of RT_{NDT}, have the largest scatter, i.e. about a factor of 100. For the conditional probability of vessel failure, this factor ranges from 20 to 50.

- For task PFM-4, the level of conditional probability of vessel failure is much smaller than in task PFM-1. ORNL reported that the relatively low probabilities computed for the PFM-4 task necessitated that a large number of vessels (at least 100 million!) be analyzed in order to get convergent results.

5.3 Comparison of Analysis Results - Task Group THM

In the THM Task Group, eight organizations from five countries participated. According to the task matrix included in the ICAS problem statements, seven analyses were performed for the main task and 14 for parametric studies (see Table 4.5). For the Tasks MIX and PINJ in the THM module, analysis results of eight organizations with approaches summarized in Table 4.6 were compared for selected variables defined in the Special Requirements (see Appendix A). Some organizations provided updated results after the final Workshop. In the comparative plots, these results are labelled with the index 'new'.

Task MIX, global downcomer temperature outside of plumes

- The six sets of results show similar trends with maximum discrepancies concerning the global cooling in the downcomer in the range of about 40°C (see Fig. 5.3.1). This uniform result can be traced back mainly to the data describing the system pressure. The time history of the pressure was given for this task, and as partly saturation conditions in the downcomer were reached, global temperatures followed partly the saturation temperature.

Task MIX, downcomer temperatures inside the plumes/stripes

- Figures 5.3.2 – 5.3.5 show the fluid temperatures in the centrelines of the plumes at a location 1 and 2 m below the cold legs 1/4 and 2/3 calculated by the participants. Large scatter in the results can be observed below cold legs 2/3 in the time interval 400 to 800 s when the water level is 1.5 m below the lower nozzle edge of the cold legs and the simulation of the condensation effects plays an important role (see Figs 5.3.4 and 5.3.5). Some of the models used to simulate the condensation effects are affected by the mesh sizes of the analysis models. The condensation effects are more pronounced at heights closer to the lower nozzle edge. It seems that the solutions with the lowest temperatures in that time interval underestimate the condensation effects in the cold legs.

- At times greater than 800 s, when the water level in the downcomer increases again due to low-pressure injection, the results of the correlation-based models (A4_1, A5, A23) are close together. Significant differences could be observed in the period that is influenced by the condensation effects.

- Figure 5.3.6 shows the azimutal temperature distribution in the downcomer at the location 2 m below the lower nozzle edge, at time t = 900 s after start of the transient. The expected plumes under the cold legs are simulated only in A5 and A4_1. In these analyses, the temperature difference between the centerline of the plumes under CL 2/3 and outside the plumes reaches about 30 °C.

Task MIX, heat transfer coefficients (HTC) inside and outside the plumes/stripes

The HTC is a function of almost all system variables like pressure, fluid temperature and velocity, wall temperature and conductivity, etc.. The HTC is defined as a local quantity and is computed in some models as an average quantity. Therefore the computed values may be affected by the mesh sizes of the analysis models. The comparison of the HTC results of the analyses shows a significant degree of scatter, with values in the range between zero and about 10,000 W/m^2K. This variation in HTC may have relevance for structure mechanics analyses (see Figs. 5.3.7 to 5.3.10). It is recommended that this aspect be addressed in future work.

- As a group, the participants determined lower HTC values, mostly far below 7,000 W/m^2K for the region outside the plumes (see Fig.5.3.7). For structure mechanics analyses, the region below 7000 W/m^2K is sensitive. Differences between the HTC values inside and outside the plumes may produce additional thermal stresses which are likely to influence the stress intensity factors.

- When the water level is lowered (between 400 s and 800 s), condensation and thermal mixing determine the fluid temperature, as well as the HTC value. The scatter in the calculated HTC values is very pronounced in that time interval.

- The system codes RELAP5 (A 8) and TRAC-P (A21) have problems with the estimation of the condensation. These codes determine non-uniform trends which may be affected by the used mesh sizes.

- The behaviour of the correlation-based models (A 4_1, A 5) is similar except during the phase with condensation. During that phase, they differ in the value by a factor of 2, but they are similar in trend (see Fig. 5.3.9). In contrast to the model used in A 5, the model used in A 4_1 assumes reduced condensation. It tries to consider uncertainties, which can result from a nitrogen release in a reactor coolant system. By this means, the water-jet enters into the water pool with a lower temperature

than in model used in A 5. As a consequence, the entrained water plume sinks comparatively faster and induces a higher HTC value. After finishing of the operating mode with lowered water level, the differences conditioned by condensation are compensated. The trend produced by both models is equal.

- For times greater than 900 s, A 23 gives the highest values which stay stable for this operating mode. All other models give results in opposition to this, i.e., a decrease of the HTC values (see Fig. 5.3.9).

- During the phase with lowered water level and also after this phase, the HTC values determined by A 4_1 and A 23 outside the plumes are nearly constant at a level of about 1,500 W/m^{2}K. After the downcomer is refilled, a decrease of the HTC values is determined by the other participants (see Fig. 5.3.7).

Task PINJ, downcomer temperatures inside the plumes

- For this task without condensation effects, Figures 5.3.11 and 5.3.12 show that the results of the correlation-based methods (A4_1, A 5, A 15 and A 23) give a consistent trend, with differences in the fluid temperature of less than 50 °C.
- In the CFD application (A 4_2), the slope of the temperature decrease in the plumes under cold legs 1/4 is comparable with the other results, but it starts at a later time (see Fig. 5.3.12). The concept of symmetric plumes under the cold legs is not supported by the three-dimensional solution.
- Lowest temperatures are calculated by the approaches of A 9 and A 21.

Task PINJ, heat transfer coefficient inside the plumes

Figure 5.3.13 shows the calculated HTC values under cold legs 2/3.

- The correlation-based methods (A4_1, A 5 and A 15) show a consistent trend with differences in the HTC values of up to 5,000 W/m^{2}K.
- Solutions A23 and A4_2 show nearly constant HTC values during the transient, while A9 and A21 show rapid decreases to a level lower than 1,000 W/m^{2}K.

6 Summary and Conclusions

Final analysis results for the ICAS Project were provided by 25 organizations in 13 countries (see Table 2.1). The analysis results submitted by the participants were compiled in a data base, and about 145 comparative plots were generated as a basis for discussions about the predictive capabilities of the analysis methods applied by the participants to the different tasks. In the report selected plots are presented and discussed. As an outcome of the discussions held on the Workshops and the additional communications by phone and electronic media, the following main conclusions were drawn:

DFM Task Group

In the DFM Task Group, 21 organizations from 13 countries participated. According to the task matrix, 104 analyses were performed for the main tasks and 26 parametric studies. Some organizations used various methods. Therefore, in some tasks up to 22 sets of analysis results could be compared.

As part of the detailed comparison of analysis results, a number of discrepancies were noted regarding input parameters referenced (user effect). These discrepancies served to increase the scatter in results above that which might otherwise have been expected, and highlight the need for careful quality assurance and good engineering judgement in undertaking structural integrity assessments. Where due account was taken of material properties and boundary conditions, reasonable agreement was obtained in linear-elastic as well as in more complex elastic-plastic thermal and stress analyses results. The influence of the cold-leg nozzle on the through-thickness stresses and therefore on the crack loading at the position of the near core weld was negligible. To derive consistent solutions, it was observed that particular attention should be paid to: (i) adequate representation of the thermal and pressure transients, (ii) sufficient mesh refinement and choice of element type in critical regions; particularly within the cladding and across the clad-base interface, (iii) quadratic elements (incorporating mid-side nodes) are recommended, (iv) correct representation of material properties. Of particular note was the reference temperature definition for the thermal expansion coefficient (TEC) and the differences concerning use of the TEC input. Most of the codes which use mean TEC as input need a conversion of the data, if the stress-free reference temperature is different from 20°C.

Crack driving forces derived from 3-D elastic-plastic analyses were generally significantly lower than those calculated using elastic analysis and J-estimation schemes. Predictions of maximum allowable RT_{NDT} showed less scatter than that observed in crack driving force calculations. The latter result was due to the shape of the fracture toughness curve used for fracture assessment in the transition region. Additional parametric studies provided consistent trends regarding the influence of residual stress, cladding thickness and crack aspect ratio (a/c) on crack driving force. For surface-breaking defects, the presence of residual stresses, increased clad thickness or decreased crack aspect ratio (a/c) leads to an increase in the crack-driving force. For under-clad defects, different trends were generally observed.

PFM Task Group

In the PFM Task Group, seven organizations from four countries performed 25 analyses and three parametric studies.The calculated conditional probabilities of crack initiation, especially for small values of RT_{NDT}, have the largest scatter, i.e., about a factor of 100. For the conditional probability of vessel failure, this factor ranges from 20 to 50. The conditional probabilities of elastic solutions are larger than the values for plastic solutions by a factor of 2 to 4.

Some solutions which were produced with the same computer code showed differences that were apparently due to selection of different input parameters for simulating the margin term in the calculation of RT_{NDT} (i.e., standard deviations for initial value of RT_{NDT} as well as for nickel and copper content).

THM Task Group

In the THM Task Group, eight organizations from five countries performed seven analyses and 14 parametric studies. The methods used can be grouped into correlation-based approaches, system codes and CFD codes. It should be noted that system codes are the only qualified tools in the area of system thermal-hydraulics.

In the main task (MIX), the expected plumes / stripes under the cold legs are simulated in some correlation-based models. In these analyses, the temperature difference between the centerline of the plumes under CL 2/3 and outside the plumes is about 30°C. Large scatter in the results were observed early in the transient when the water level is below the lower nozzle edge of the cold legs and simulation of the

condensation effects play an important role. Some of the models used to simulate the condensation effects are affected by the mesh sizes of the analysis models. The condensation effects are more pronounced at heights closer to the lower nozzle edge. The solutions with the lowest temperatures seem to underestimate the condensation effects in the cold legs. The results of the correlation-based models are more closely grouped at times when the water level in the downcomer increases again due to low-pressure injection. Furthermore it should be noted that the flow regimes at the water-stripe discharge in the downcomer are not universally identified and characterized.

Comparison of the HTC results shows a significant degree of scatter inside the plumes/stripes, with values in the range between zero and about 10,000 W/m^2K. This scatter may have important implications for structure mechanics analyses. The differences between the HTC values inside and outside the plumes may produce additional thermal stresses and, consequently, a likely increase of the stress intensity factors for postulated cracks. As a group, the participants determined lower HTC values for the region outside the plumes, but again with significant scatter. Therefore, a more accurate representation of the HTC, especially in the range of about 1,000 to 8,000 W/m^2K, is needed from thermal-hydraulic researchers for input to the thermal/structural/fracture analyses.

For the task without condensation effects (PINJ), the results of the correlation-based methods show a consistent trend, with differences in the fluid temperature of less than 50 °C and in the HTC values of up to 5,000 W/m^2K. The concept of symmetric plumes under the cold legs is not supported by the three-dimensional CFD solution.

Future Work

Based on concluding discussions at the ICAS Workshop, participants proposed a list of future tasks that could contribute to further refinement of RPV integrity assessment methods:

- Selection of consensus reference solutions that could serve as benchmarks for future qualification of analytical methods. These would provide a valuable tool for the qualification of new analysts on the subject of RPV integrity assessment;

- Study of the implications of the observed scatter in the THM task on deterministic fracture mechanics assessments;
- Assessment of the nozzle region of an RPV;
- Assessment of the significance of residual stresses upon RPV integrity;
- Study of crack arrest of a fast running crack in an RPV;
- Study of micro-mechanical modelling of the crack-tip region;

Furthermore, a study of pressure-temperature (P-T) limits, with reference to the methodology for modelling the P-T process was proposed.

A bibliography of recent ICAS-related publications is given in the following section.

Bibliography: Recent ICAS-Related Publications

Cappariello A., D'Auria F., Vigni P., "On the Use of Thermalhydraulic Codes to Evaluate PTS Situations", 16th Conf. of Italian Society of Heat Transport - Siena (I), June 18-19, 1998.

Cappariello A., D'Auria F., Galassi G.M., "Application of the Relap5/mod3.2 to the Analysis of the Reactor Pressure Vessel PTS - International Comparative Assessment Study", University of Pisa Report, DCMN - NT 320(97), Pisa (I), 1997.

Dickson T. L., B. R. Bass, “Solutions to Reactor Pressure Vessel Pressurized Thermal Shock International Comparative Assessment Study“, Oak Ridge National Laboratory, ORNL/NRC/LTR-98/5, 1998.

Jhung M. J., Y. W. Park, "Deterministic Structural and Fracture Mechanics Analyses of Reactor Pressure Vessel for Pressurized Thermal Shock," KINS/AR-656, Korea Institute of Nuclear Safety, February 1999.

Jhung M. J., Y. W. Park, "Deterministic Structural and Fracture Mechanics Analyses of Reactor Pressure Vessel for Pressurized Thermal Shock," Structural Engineering and Mechanics, Vol.8, No.1, 1999.

Jung J. W., Y. S. Bang, K. W. Seul,H. J. Kim, J. I. Lee, “Thermal Hydraulic Mixing Analysis on Presuurized Thermal Shock International Comparative Assessment Study“, KINS/AR-593, 1998.

Kato D., Y. Li and K. Shibata, “Development of a PV Reliability Analysis Code Based on Probabilistic Fracture Methodology Part(2) Analysis Methodology Verification and Sensitivity Analysis“, 1998 Fall Meeting of the Atomic Energy Society of Japan, 1998.

Keim E., A. Schöpper, S. Fricke, "Fracture Mechanics Assessment of Surface and Sub-Surface Cracks in the RPV Under Non-symmetric PTS Loading", IAEA Specialists Meeting on Methodology for Pressurized Thermal Shock Evaluation,Esztergom, Hungary, 1997.

Li Y., D. Kato, K. Shibata, “Sensitivity Analysis of Failure Probability on PTS Benchmark Problems of Pressure Vessel using a Probabilistic Fracture Mechanics Analysis Code”, 7th ICONE, paper 7266, Tokyo, 1999.

Niffenegger M., K.Reichlin, "The Proper Use of Thermal Expansion Coefficients in Finite Element Calculations", PSI TM-49-98-15, 1998.

OECD/NEA/CSNI PWG 3, “Summary Record of the Intermediate Workshop on PWG 3 International Comparative Assessment Study on Reactor Pressure Vessel Pressurized Thermal Shock (RPV PTS ICAS) in Paris”, NEA/SEN/SIN/WG3(97)9, 1997.

OECD/NEA/CSNI PWG 3, “Summary Record of the Workshop on PWG 3 International Comparative Assessment Study on Reactor Pressure Vessel Pressurized Thermal Shock (RPV PTS ICAS) in Orlando”, NEA/SEN/SIN/WG3(98)11, 1998.

Schimpfke T. and J. Sievers, “Reactor Pressure Vessel - International Comparative Assessment Study: Analyses on Deterministic Fracture Mechanics (DFM) Tasks - Technical Note”, GRS Technical Note, December 1997.

Schimpfke T., J. Sievers, “Vergleichsanalysen zur bruchmechanischen Bewertung unterstellter Risse in einem Reaktordruckbehälter mit internationaler Beteiligung (RPV-PTS-ICAS)”, 24. MPA Seminar, Stuttgart, 1998.

Sherry A., T. Richardson, R. Sillitoe and F. Trusty, “Analysis of Benchmark PTS Problem: Comparison of R6 and 3D-Finite Element Results”, ASME Pressure Vessel and Piping Conference, Boston, 1999.

Shibata K., D. Kato and Y. Li, “Development of a PV Reliability Analysis Code Based on Probabilistic Fracture Methodology Part (1) Outline of the Code“, 1998 Fall Meeting of the Atomic Energy Society of Japan, 1998.

Shibata, K., D. Kato and Y. Li, “Development of PFM Code for Evaluating Reliability of Pressure Components subjected to transient Loading“, to be presented at SMIRT-15, Seoul, 1999.

Sievers J., T. Schimpfke, “Verifikation bruchmechanischer Methoden durch Vergleichsanalysen mit internationaler Beteiligung (FALSIRE, NESC, RPV PTS ICAS)”, 21. GRS-Fachgespräch, München, 1997.

Sievers J., R. Bass, A. G. Miller, “Activities of the OECD Nuclear Energy Agency in the Area of RPV PTS Fracture Mechanics Analysis”, paper G2-A2-FR of SMIRT – 15, Seoul, 1999.

Appendix A: Special Requirements Concerning Comparative Analyses

∉ Task Group DFM (Main Tasks CmTn, m=1-5,n=1-3, parametric studies PCT, PCAR, PYS, PRS)

In the framework of the deterministic task group, analyses of the temperature and stress distribution in the vessel wall should be performed according to the material properties and the postulated transients (**Tn, n=1-3**) given in the problem statements. Furthermore the crack loading of the postulated cracks (**Cm, m=1-5**) should be analyzed along the crack front. For each crack, a fracture assessment should be performed concerning crack initiation based on the fracture toughness curve given in chapter 1.2 of the problem statement, in the sense that a maximum allowable RT_{NDT} should be determined. Detailed results are required for:

- Temperature distribution in the wall at the position of the cracks for the times given in Table A.1. In the case of asymmetric loading conditions (transient T2 and T3) temperature distributions should be given also outside the cooling region (180° distance from the crack)
- Time history of crack mouth opening displacement (CMOD). For the surface cracks, CMOD should be evaluated at the half length position on the inner surface. For the underclad cracks, CMOD should be evaluated at the position of half length and half depth.
- Axial, hoop and effective stresses across the wall thickness should be evaluated at the position of the cracks but without influence of the cracks for the times in Table A.1.
- Stress intensity factor versus crack tip temperature (KT-Diagram) at the deepest point and at the interface between cladding and weld material.
- Evaluation of the maximum allowable RT_{NDT} based on tangent, 90 percent and maximum criterion in the KT-Diagram.
- Constraint / stress triaxiality parameters on the ligament of the cracks deepest point and the crack position at the interface between cladding and weld material for the times in Table A.1; the parameters Q and h (definitions see [2] of references in chapter 2) are recommended and should be evaluated on the ligament in a range of about 10 mm from the crack tip position.

Table A.1: Requested solution times for transients T1,T2,T3

Task (m=1-5)	Requested solution times
CmT1	0[1], 300, 1200, 2400, 3600, 6000, 9000, 12000 s
CmT2	0[1], 500, 1000, 1500, 2500, 3500, 5000 s
CmT3	0[1], 400, 800, 1200, 1600, 2000, 3000 s

[1] only mechanical loading

– In the framework of parametric studies, the influence of changes in the cladding thickness (**PCT**), in the cracks aspect ratio (**PCAR**), in the cladding/weld yield stress, as well as in consideration of plasticity effects (**PYS**), and in assumptions about residual stresses (**PRS**), on the results of the main tasks should be demonstrated especially in the KT-Diagram.

∉ **Task Group PFM (Main Tasks PFn, n=1-4, Parametric Study PFL)**

- **PFM1:** Conditional probability of crack initiation P(I|E) and vessel failure P(F|E) versus mean surface RT_{NDT} for axially oriented infinite length surface breaking flaw subjected to simplified stylized transient described in problem statement.
- **PFM2:** Conditional probability of crack initiation P(I|E) and vessel failure P(F|E) versus mean surface RT_{NDT} for circumferentially oriented continuous 360 degree surface breaking flaw subjected to simplified stylized transient described in problem statement.
- **PFM3:** same as PFM1 except the transient is a complex transient as described in the problem statement.
- **PFM4:** same as PFM2 except the transient is the same complex transient specified for PFM3 as described in the problem statement.

PFL: Conditional probability of crack initiation P(I|E) and vessel failure P(F|E) versus mean surface RT_{NDT} for semi-elliptic surface breaking flaws having aspect ratios a/c = 0.2, 0.33, and 1.0. Results for finite-length flaws should be compared with those for infinite length flaws obtained in PFMn.

The PFM analyses to determine P(I|E) and P(F|E) for each of the above cases should be performed at various levels of embrittlement representative of various times in the operating life of the vessel as represented in Table 3.4 of the problem statements.

∉ Task Group THM (Main Tasks MIX)

The task **THM** comprises the main task named **MIX** and the parametric studies **PMIX** and **PINJ**. The main task **MIX** requires the prediction of the following parameters inside the downcomer region for the transient period from 0 s to 2000 s:

- The time history of the global downcomer temperature outside the plume region is required.
- If a multidimensional code is used as the predictive tool, the global downcomer temperature outside the plume may be vertically resolved. Temperature values at four elevations (0 m, 1 m, 2 m and 3 m below the lower edge of the cold leg) in the downcomer may be presented by the participant instead of one global temperature value.
- The time history of the temperature in the centre of the plume (stripe, respectively) at four elevations below the lower edge of the cold leg in the downcomer (0 m, 1 m, 2 m and 3 m) is required. These plume (stripe, respectively) temperatures are to be calculated for the plumes developing below the cold legs 2 and 3. And from 800 s transient time onward temperatures are to be evaluated for the developing plumes below the cold legs 1 and 4.
- The time history of the heat transfer coefficient inside the plume at four elevations
  (0 m, 1 m, 2 m and 3 m below the lower edge of the cold legs 2 and 3) as well as the global heat transfer coefficient outside the plume are required.
- If a multidimensional code is used as the predictive tool, the global heat transfer coefficient outside the plume may be vertically resolved. Heat transfer coefficients at four elevations (0 m, 1 m, 2 m and 3 m below the lower edge of the cold leg) in the downcomer may be presented by the participant instead of one global heat transfer coefficient.
- The time history of the plume width (stripe width, respectively) at four elevations
  (0 m, 1 m, 2 m and 3 m below the lower edge of the cold leg 2 and 3) is required. The plume width requested here is defined by the distance between two points lying symmetric to the symmetry line of the plume for which the

temperature difference between the fluid temperature outside the plume and in the centre of the plume is decreased to 1/e (see Chapter 3.1.3 of the problem statement). In case of the utilization of a multidimensional code, an adequate procedure has to be taken for identifying the plume width.

- The azimuthal temperature distribution in the downcomer for the transient time of 900 s and at an elevation of 2 m below the lower edge of the cold leg is required.
- The azimuthal heat transfer distribution in the downcomer for the transient time of 900 s and at an elevation of 2 m below the lower edge of the cold leg is required.

In the parametric study **PMIX,** the influence of variations of the minimum water level in the downcomer on the results of the main task is investigated. The different assumptions concerning the minimum water level are -2.5 m, 0. m and +0.5 m (related to the lower edge of the cold leg) respectively. The same set of parameters which has been requested under the task **MIX** is requested for the task **PMIX**. Only the azimuthal distributions can be omitted for this task.

In the parametric study **PINJ,** a transient with a reduced emergency core cooling injection rate in combination with a completely water filled downcomer volume is considered. The flow rate is reduced to 20 percent. The same set of parameters which has been requested under the task **PMIX** is requested for the task **PINJ**. But the transient time to be covered by the prediction for the task **PINJ** reaches from 0 s to 4000 s.

Appendix B: Availability of Data

The following data sets were made available to the ICAS participants in the Task groups DFM and PFM.

Table B.1: Data sets for TaskgGroup DFM and PFM

Data set name	Type of data	Content of the data set
psiem1.xls	MS-EXCEL	loading conditions for the transients T2 and T3 with 50 cm^2 and 200 cm^2 leak (Task Group DFM)
prob_dat.txt	ASCII	loading conditions for small-break LOCA transient T1 (Task Groups DFM and PFM)
Probsub.txt	ASCII	subroutines useful for PFM analyses

For the participants in the Task Group THM a special data set of about 100 pages with details about the vessel internals, the cold legs and pump shells including the volume calculation was made available on request.

Furthermore, data of figures in chapter 5 of the report can be made available to ICAS participants on request to one of the authors of the report.

Appendix C: List of Tables

Appendix D: List of Figures

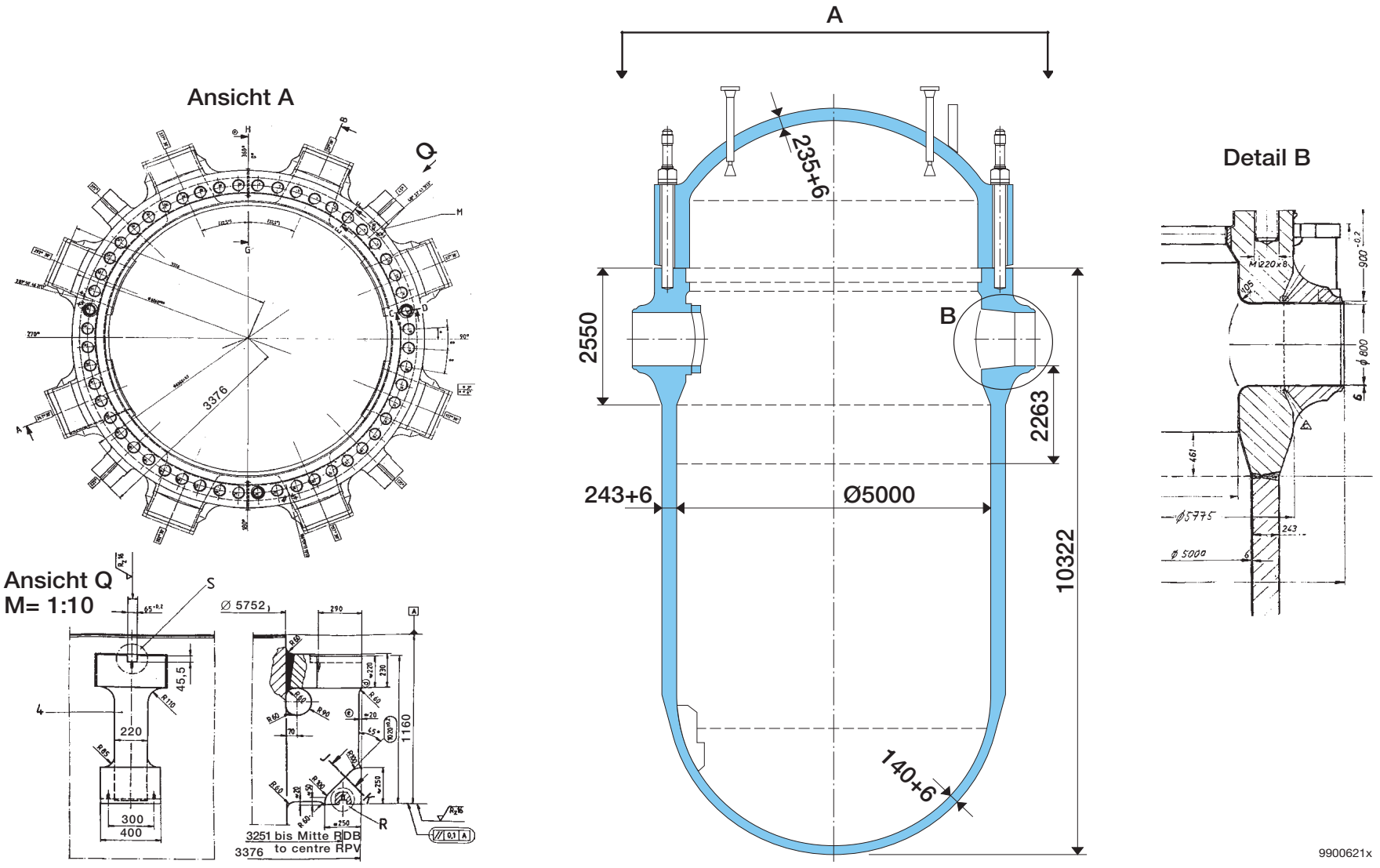

Figure 3.1 Geometry of the RPV (4 loop PWR 1300 MW)

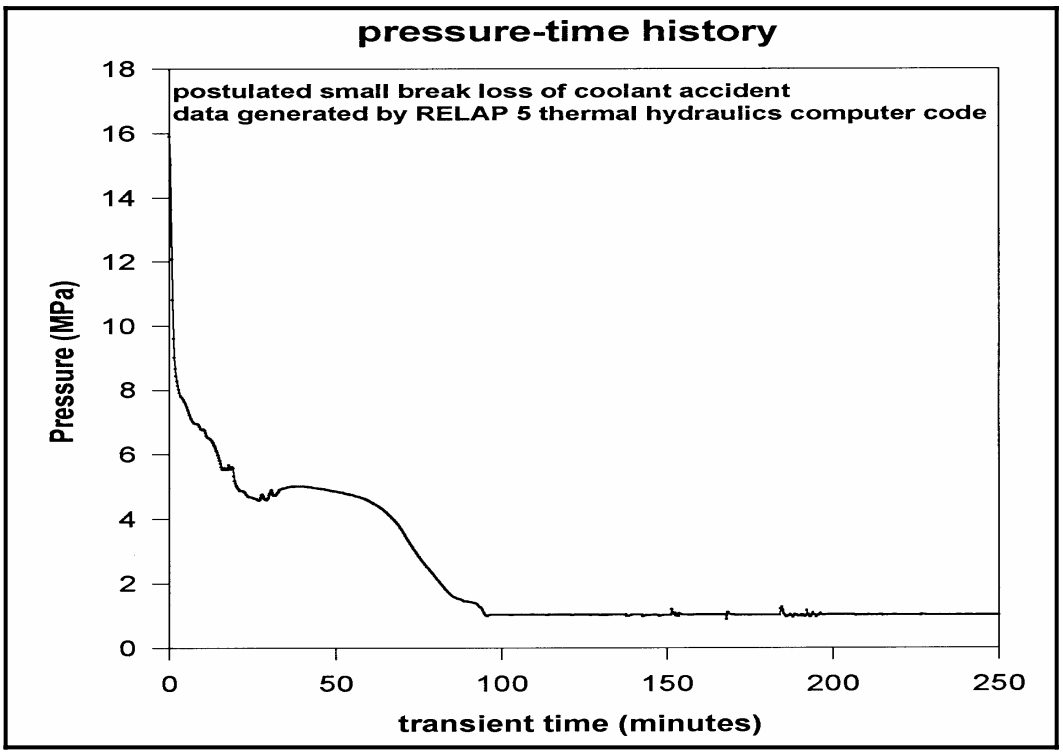

Figure 3.2 Pressure in the primary system (transient T1)

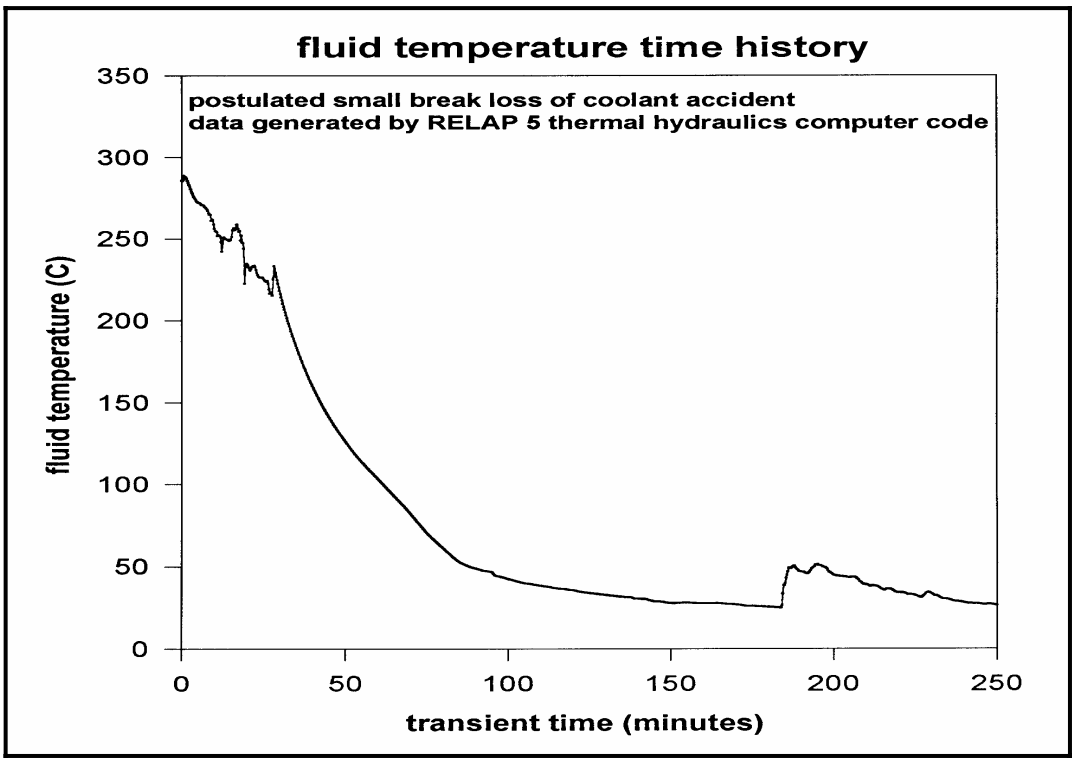

Figure 3.3 Averaged fluid temperatures in the RPV downcomer near the inside RPV wall (transient T1)

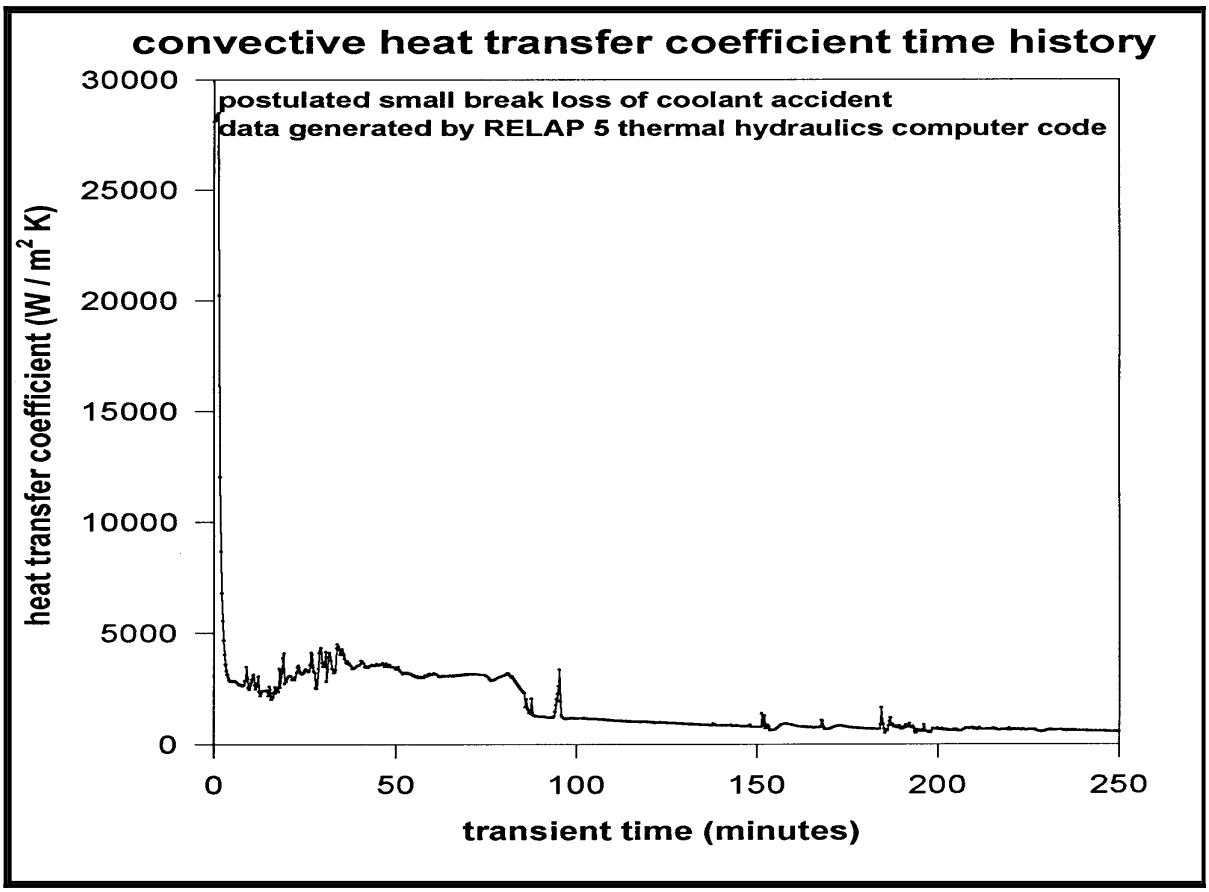

Figure 3.4 Averaged heat transfer coefficient between the fluid in the downcomer and the inside RPV wall (transient T1)

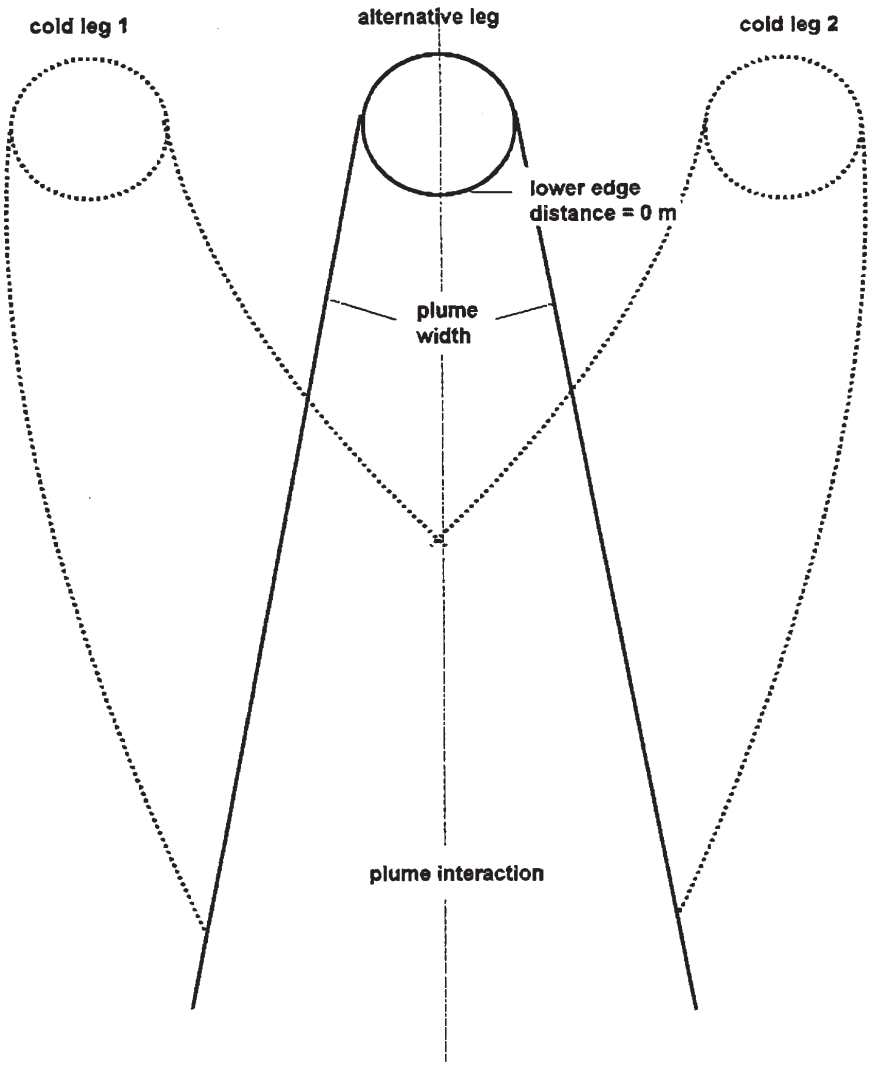

circumferential weld near core mid-height (distance = 2.263 m)

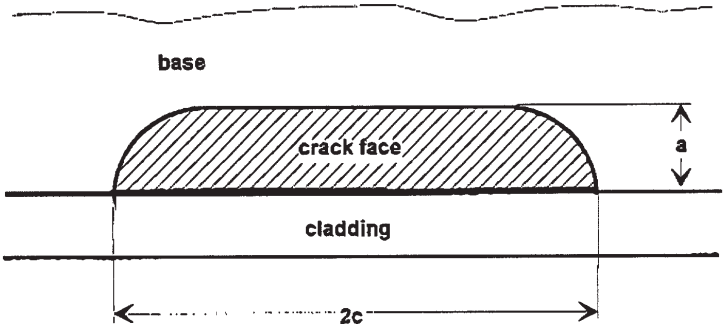

99006x19

Figure 3.5 Scheme of injection throuth two neighboured nozzles

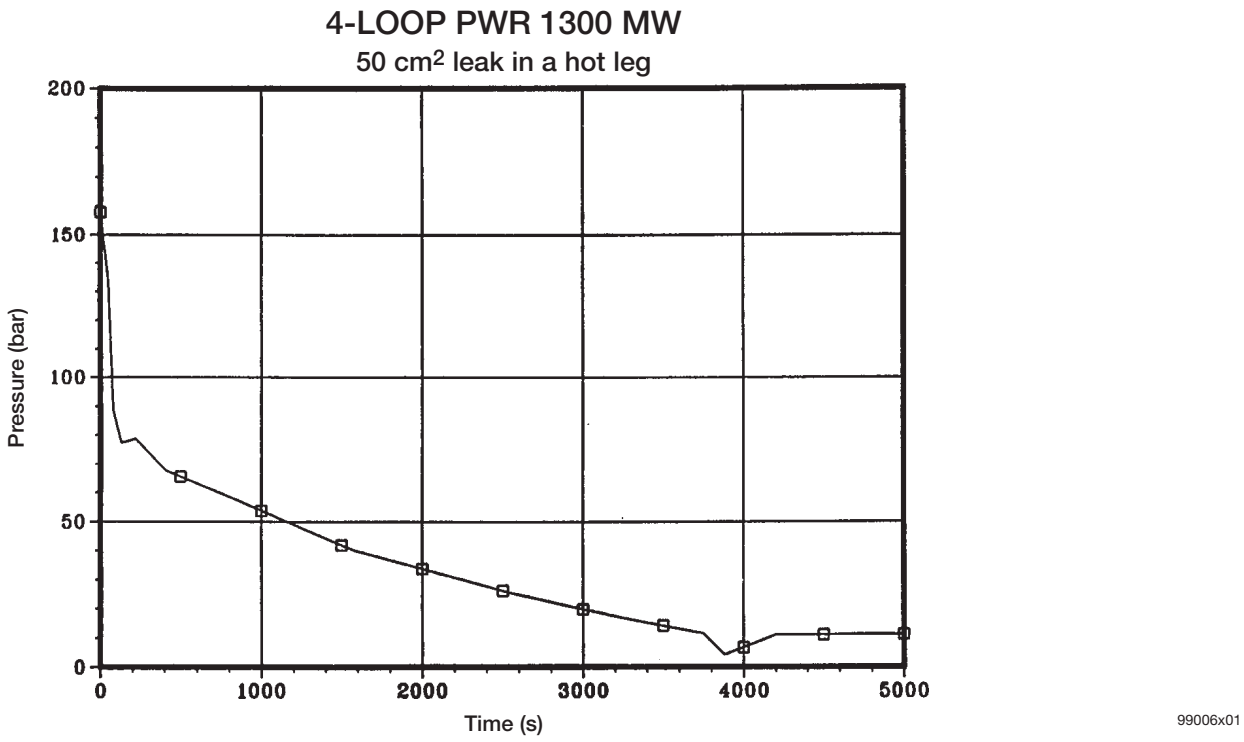

Figure 3.6 Pressure in the primary circuit (transient T2)

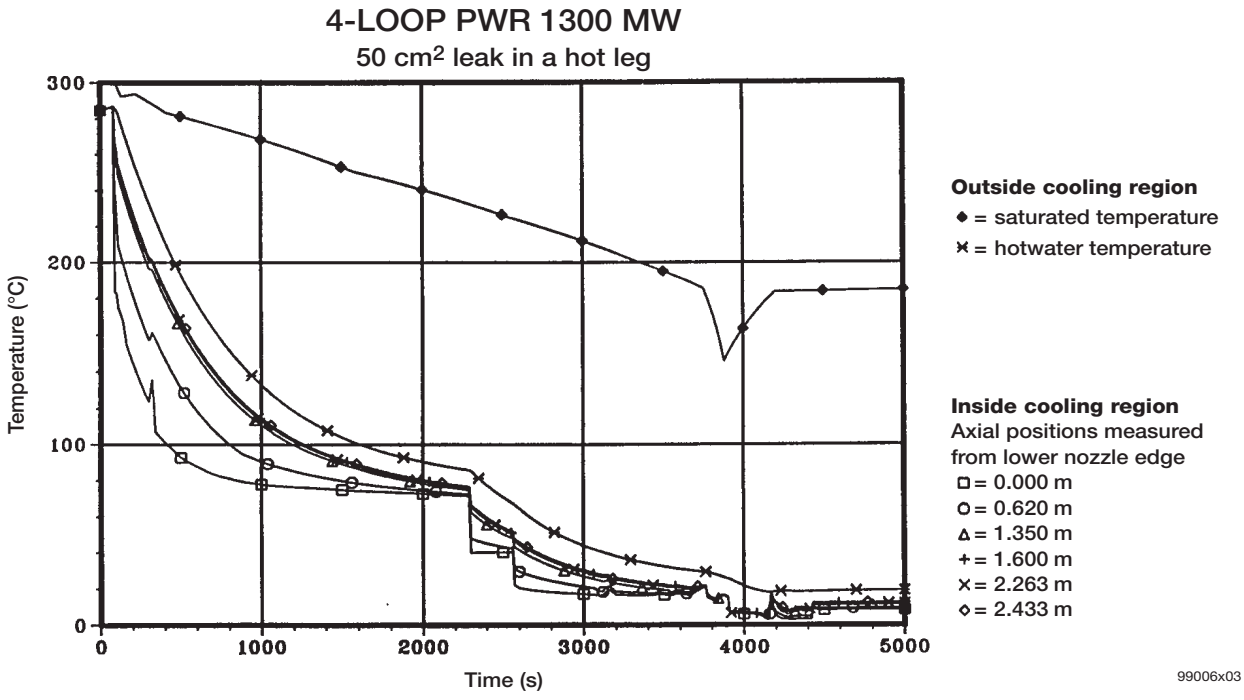

Figure 3.7 Fluid temperatures in the RPV downcomer near the inside RPV wall (transient T2)

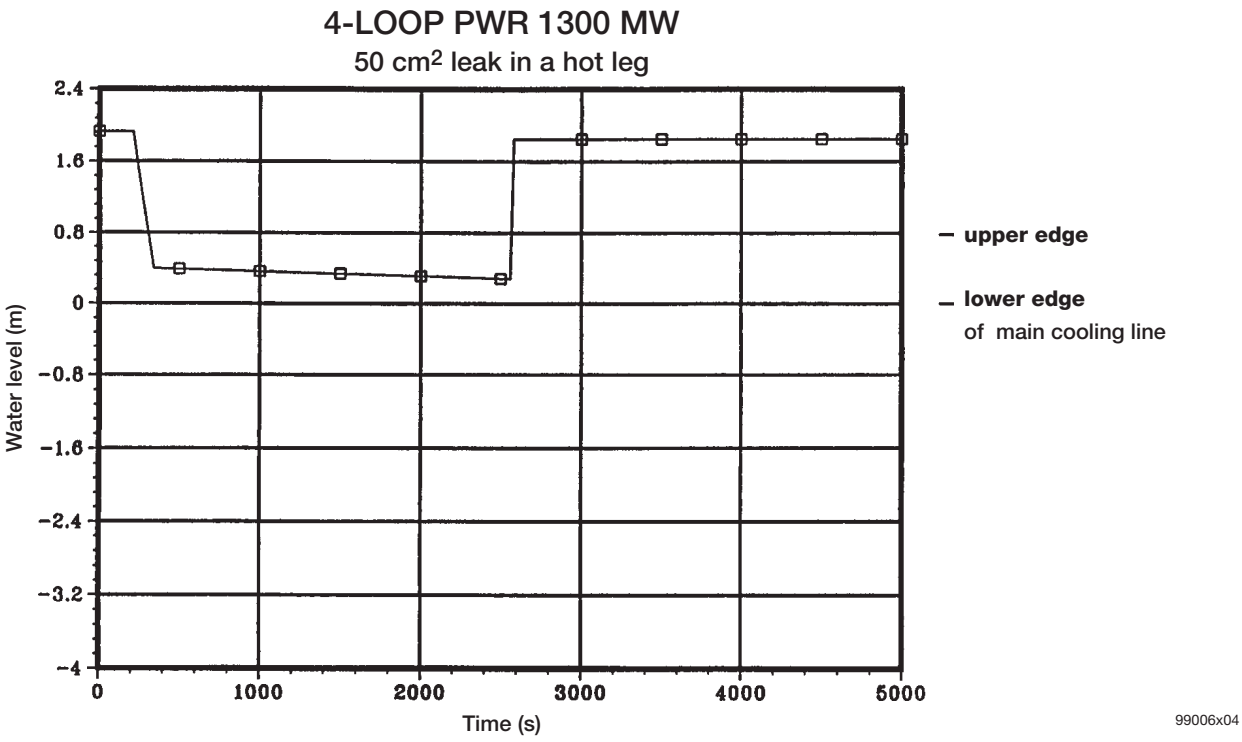

Figure 3.8 Water level in the RPV-downcomer (transient T2)

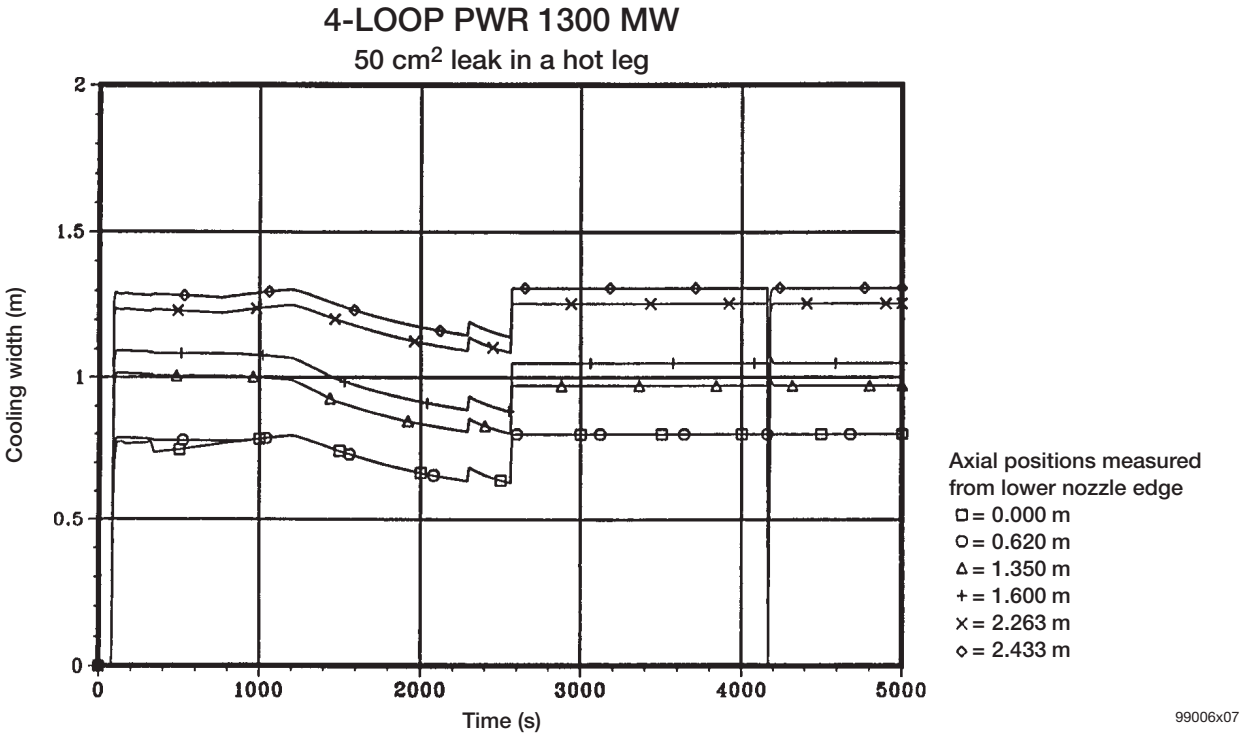

Figure 3.9 Cooling width in the RPV downcomer (transient T2)

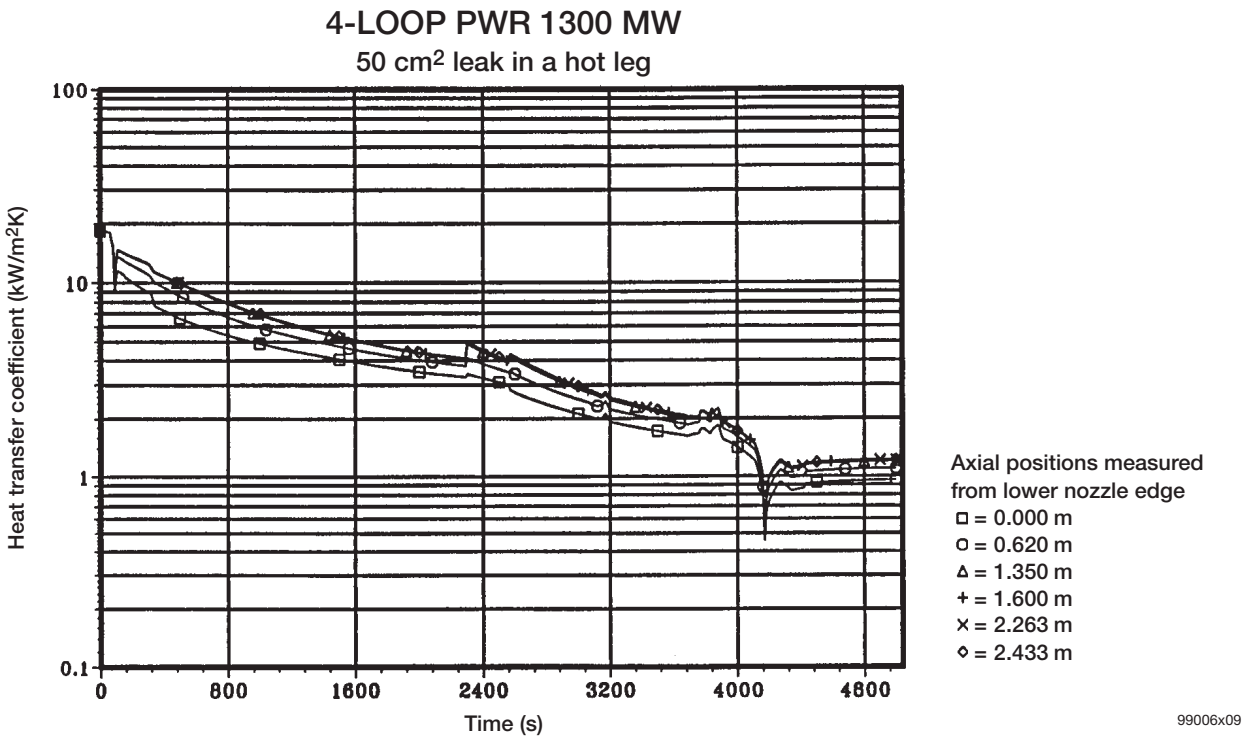

Figure 3.10 Heat transfer coefficient inside the cooling region (transient T2)

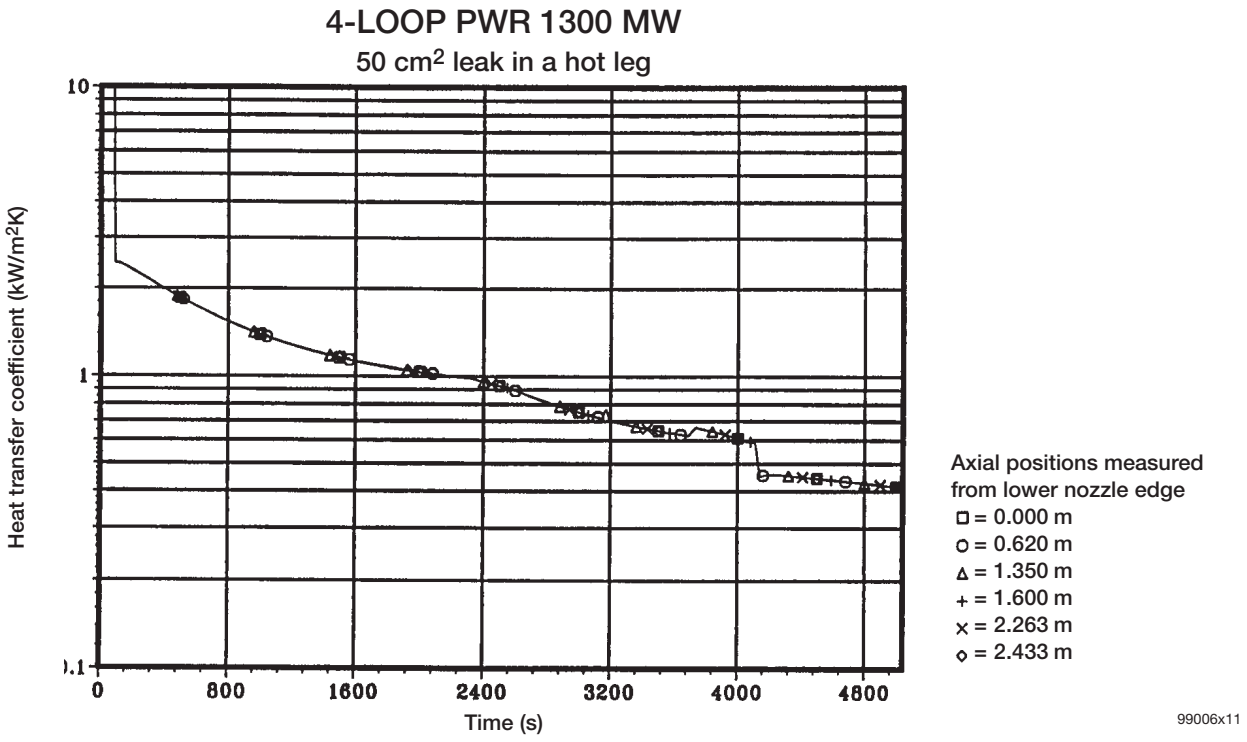

Figure 3.11 Heat transfer coefficient outside the cooling region (transient T2)

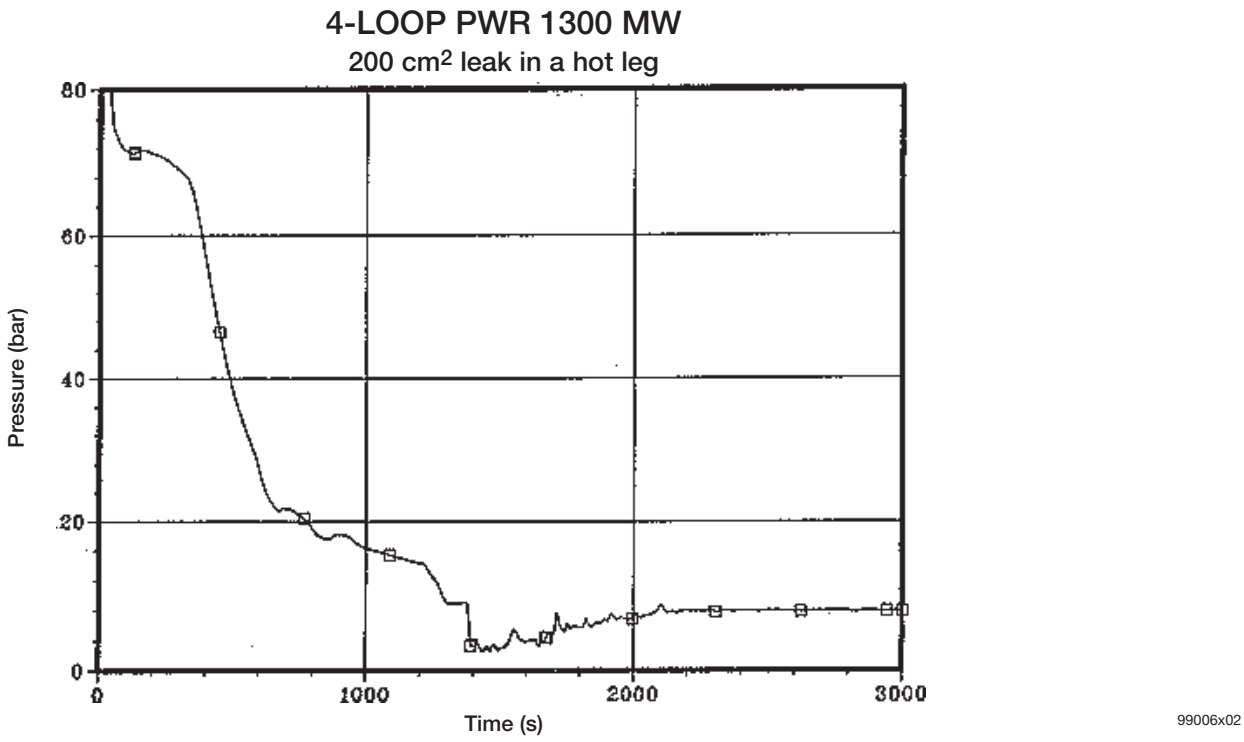

Figure 3.12 Pressure in the primary circuit (transient T3)

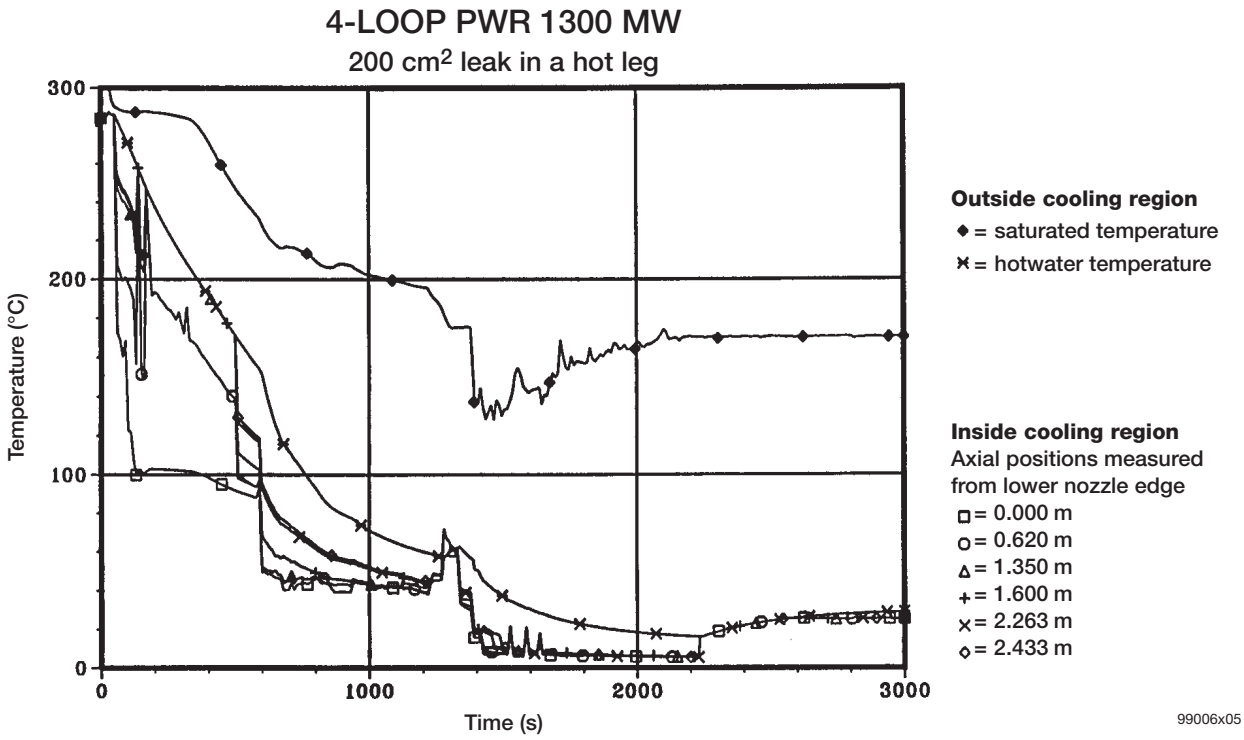

Figure 3.13 Fluid temperatures in the RPV downcomer near the inside RPV wall (transient T3)

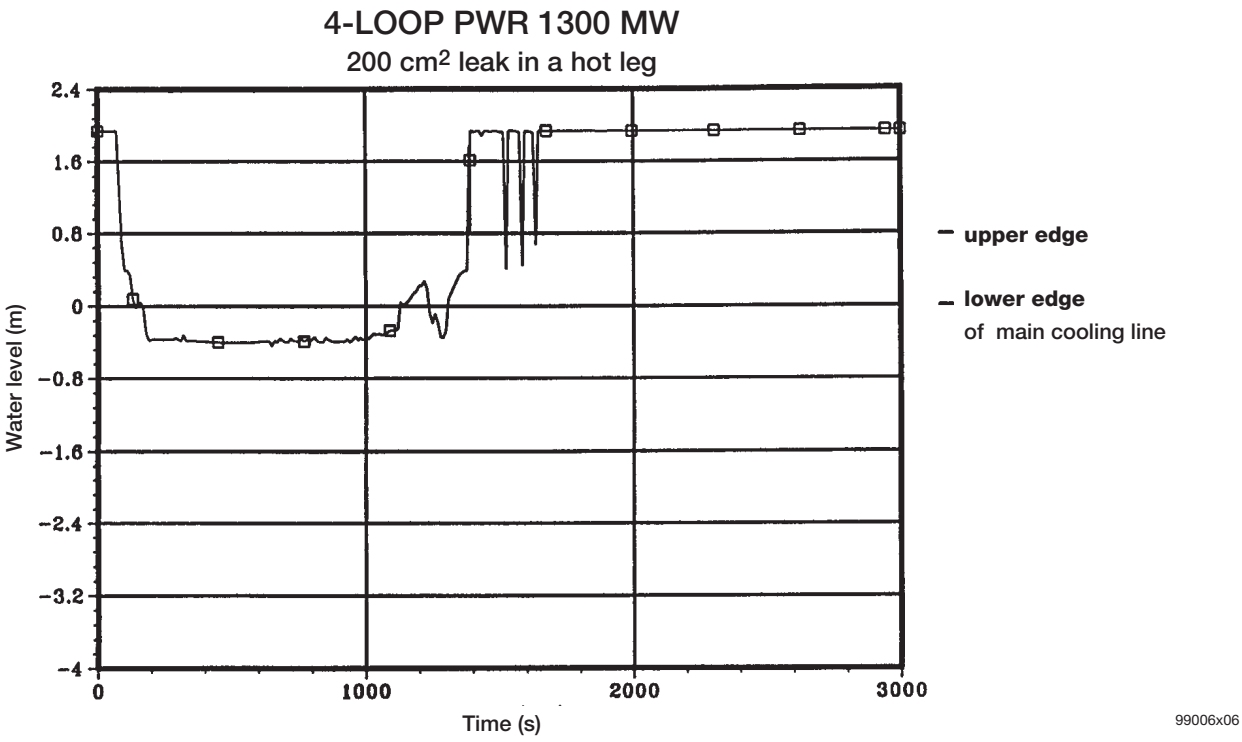

Figure 3.14 Water level in the RPV-downcomer (transient T3)

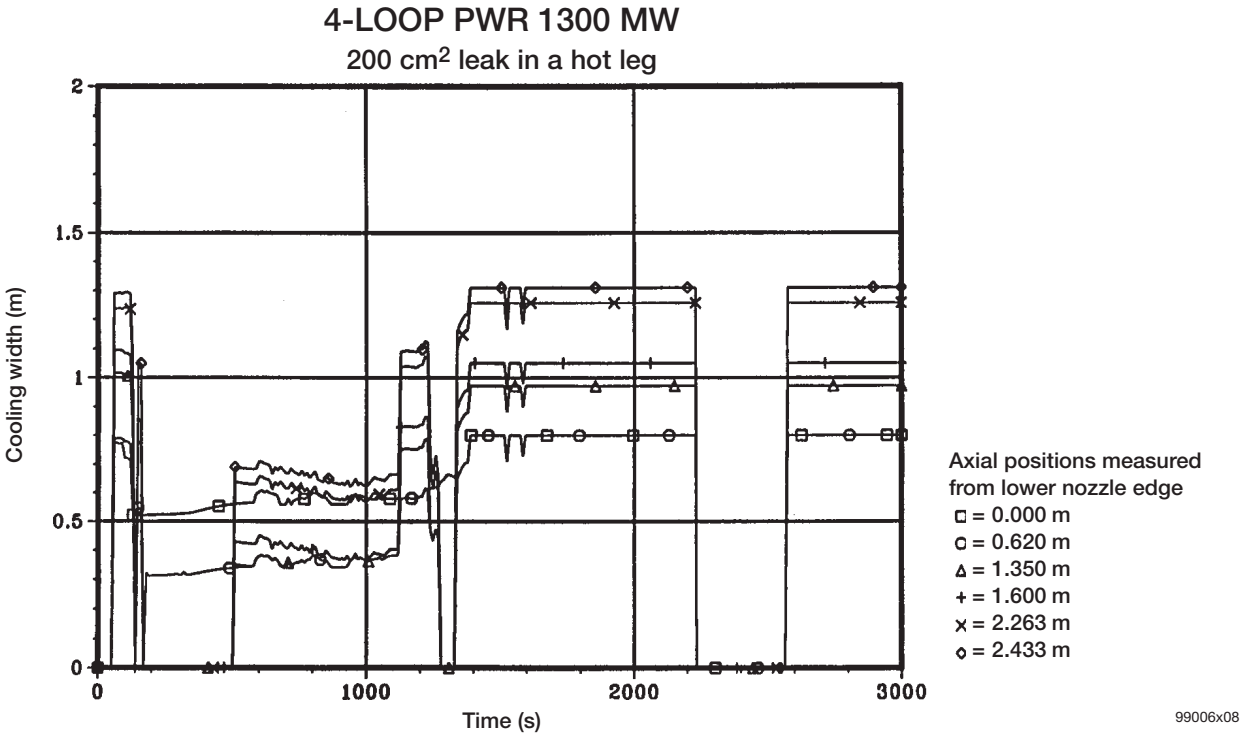

Figure 3.15 Cooling width in the RPV downcomer (transient T3)

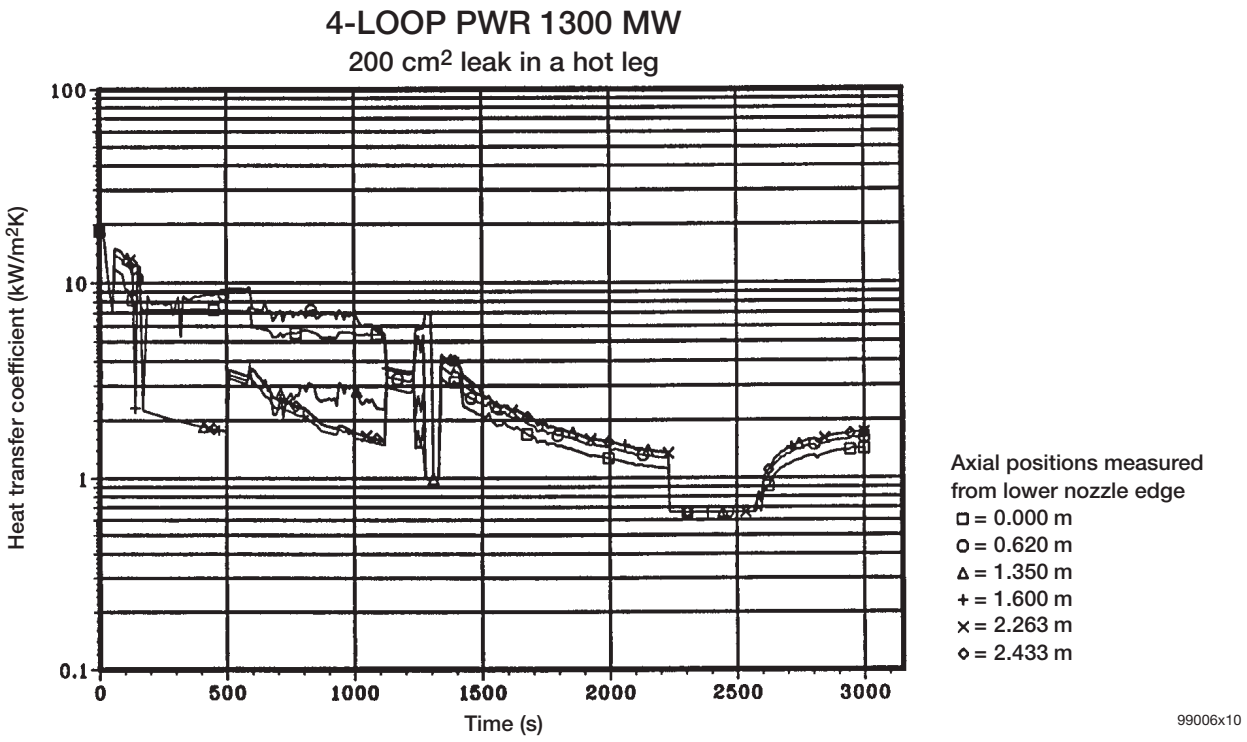

Figure 3.16 Heat transfer coefficient inside the cooling region (transient T3)

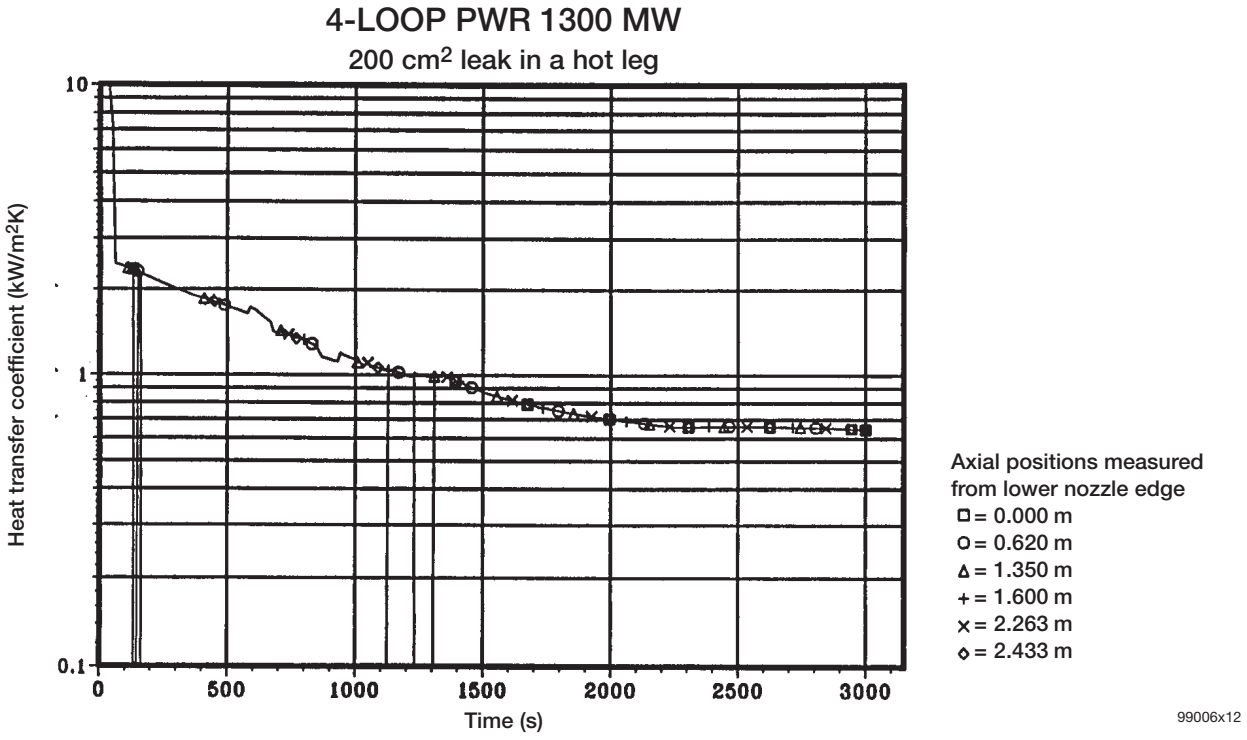

Figure 3.17 Heat transfer coefficient outside the cooling region (transient T3)

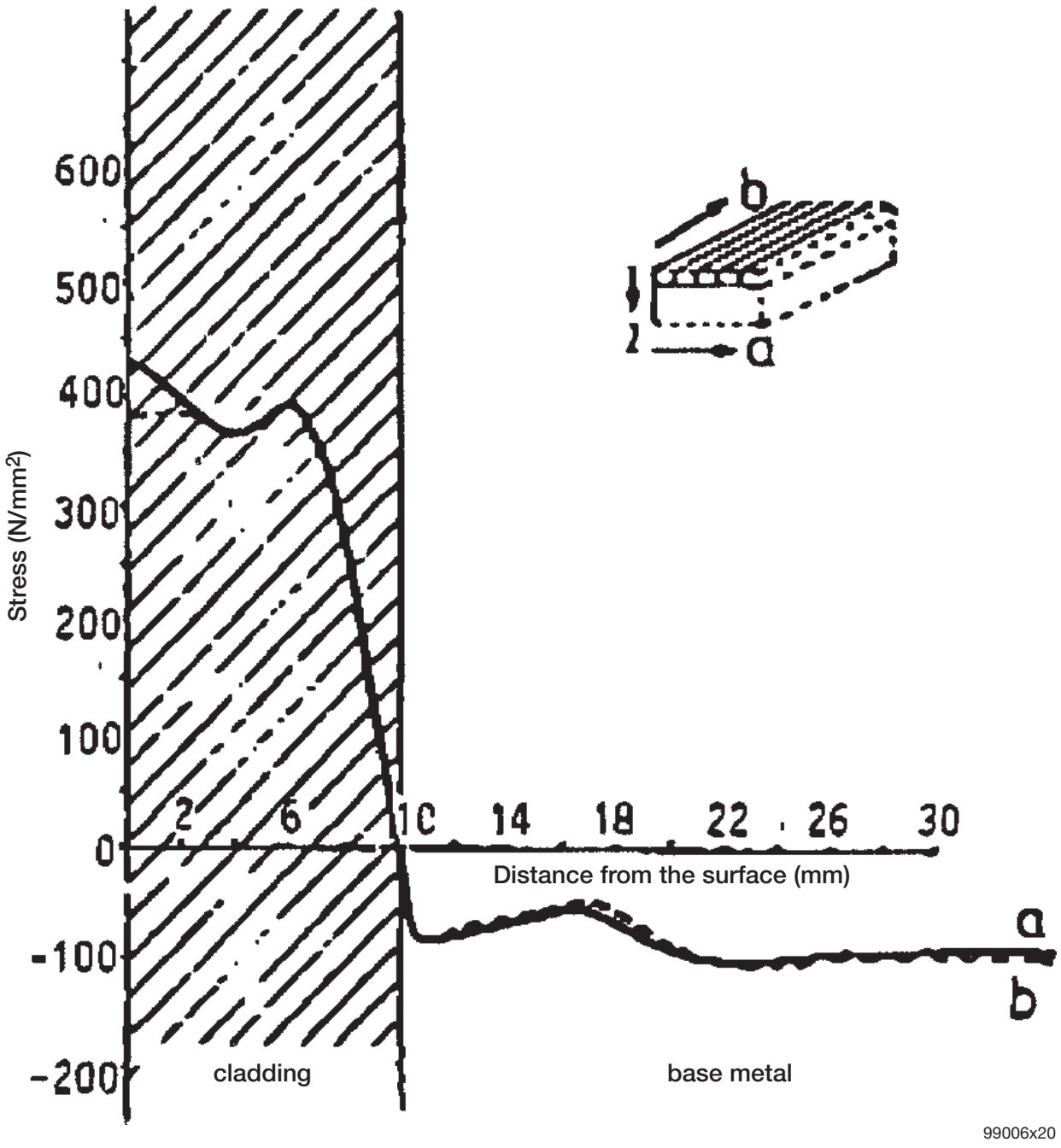

Figure 3.18 Typical distribution of residual stresses due to cladding after heat treatment (12 h at 610 °C)

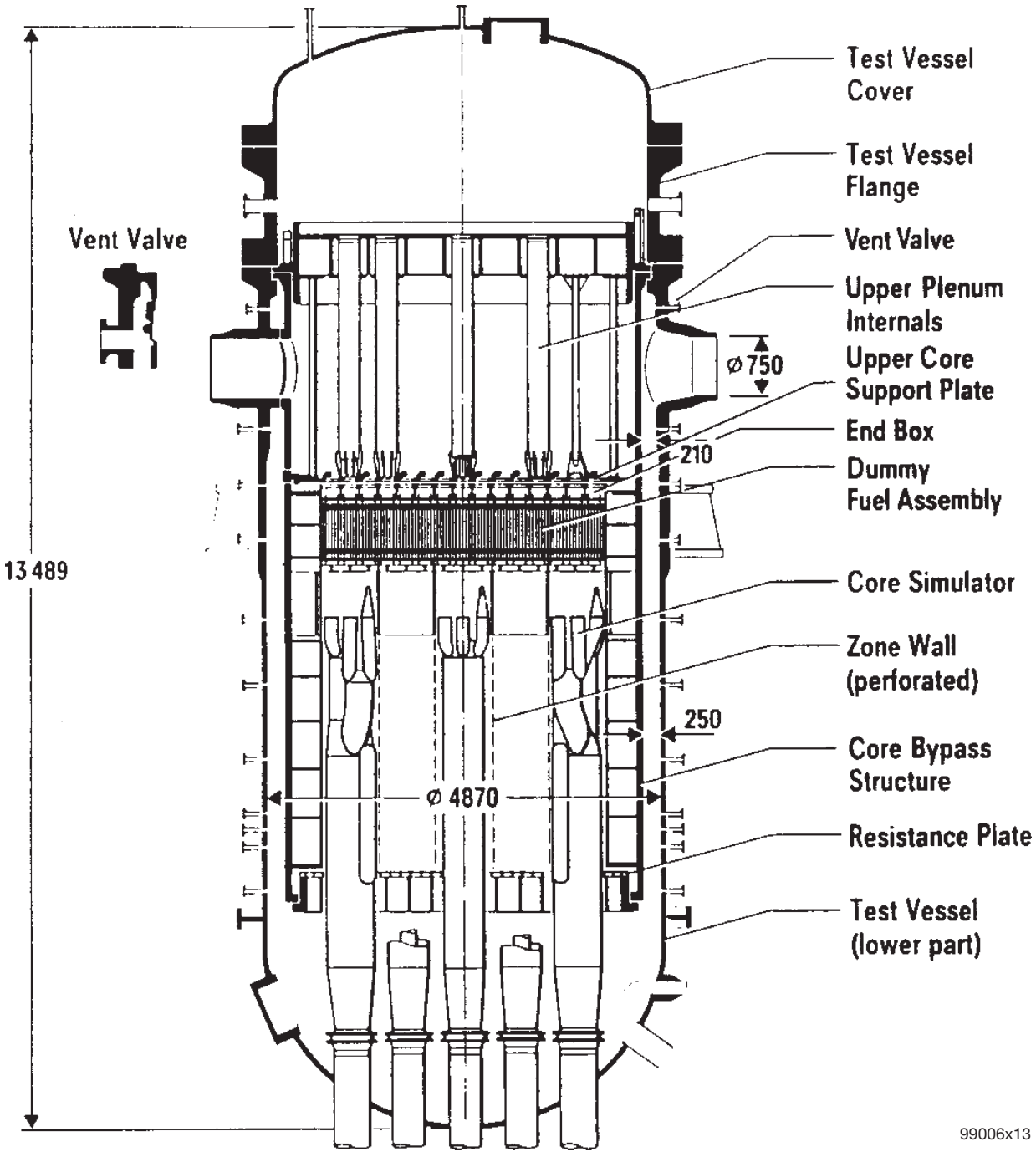

Figure 3.19 UPTF test vessel and its internals, to be used for the geometry of the RPV internals, not to be used concerning the RPV-wall thickness

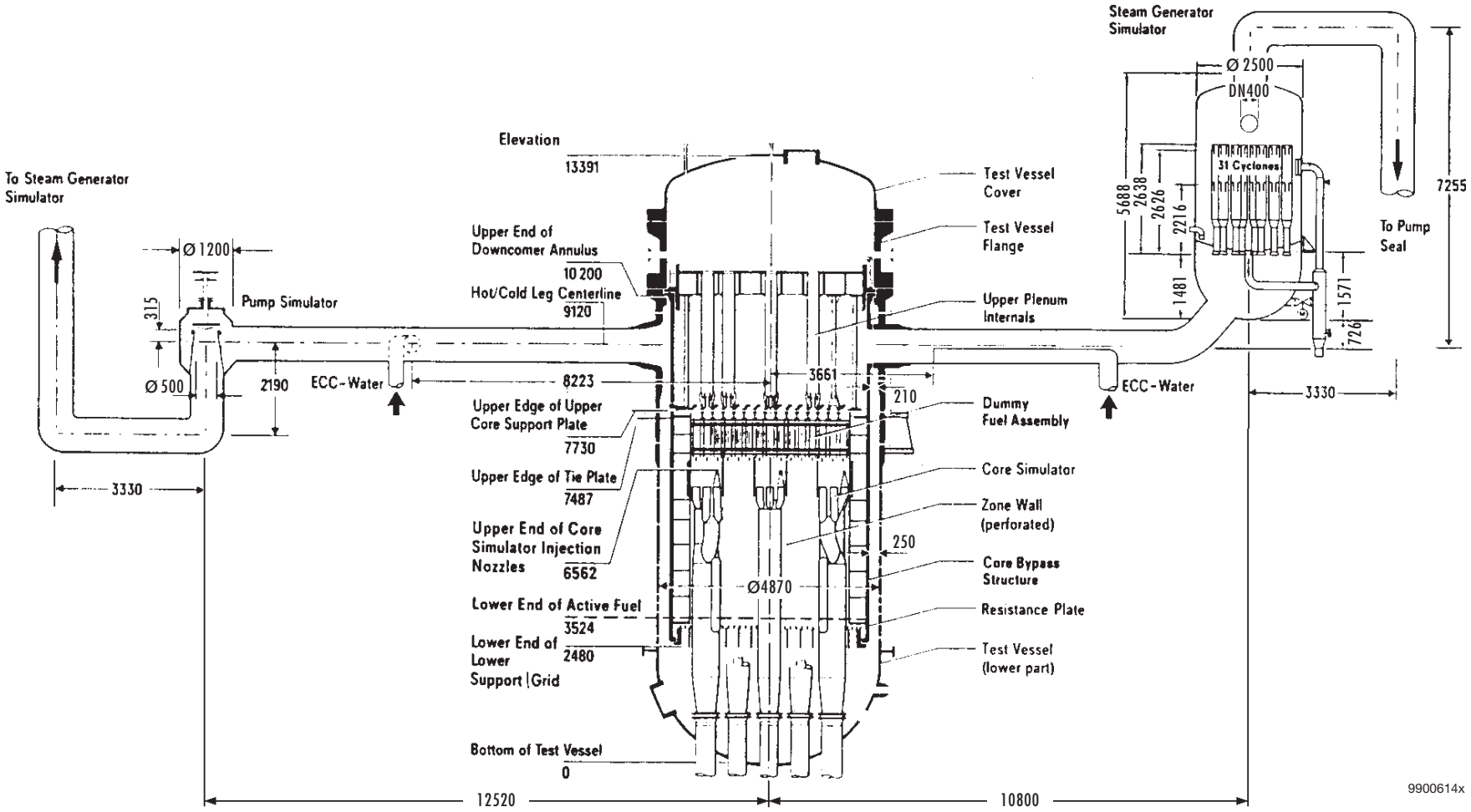

Figure 3.20 Major dimensions of the UPTF –primary system

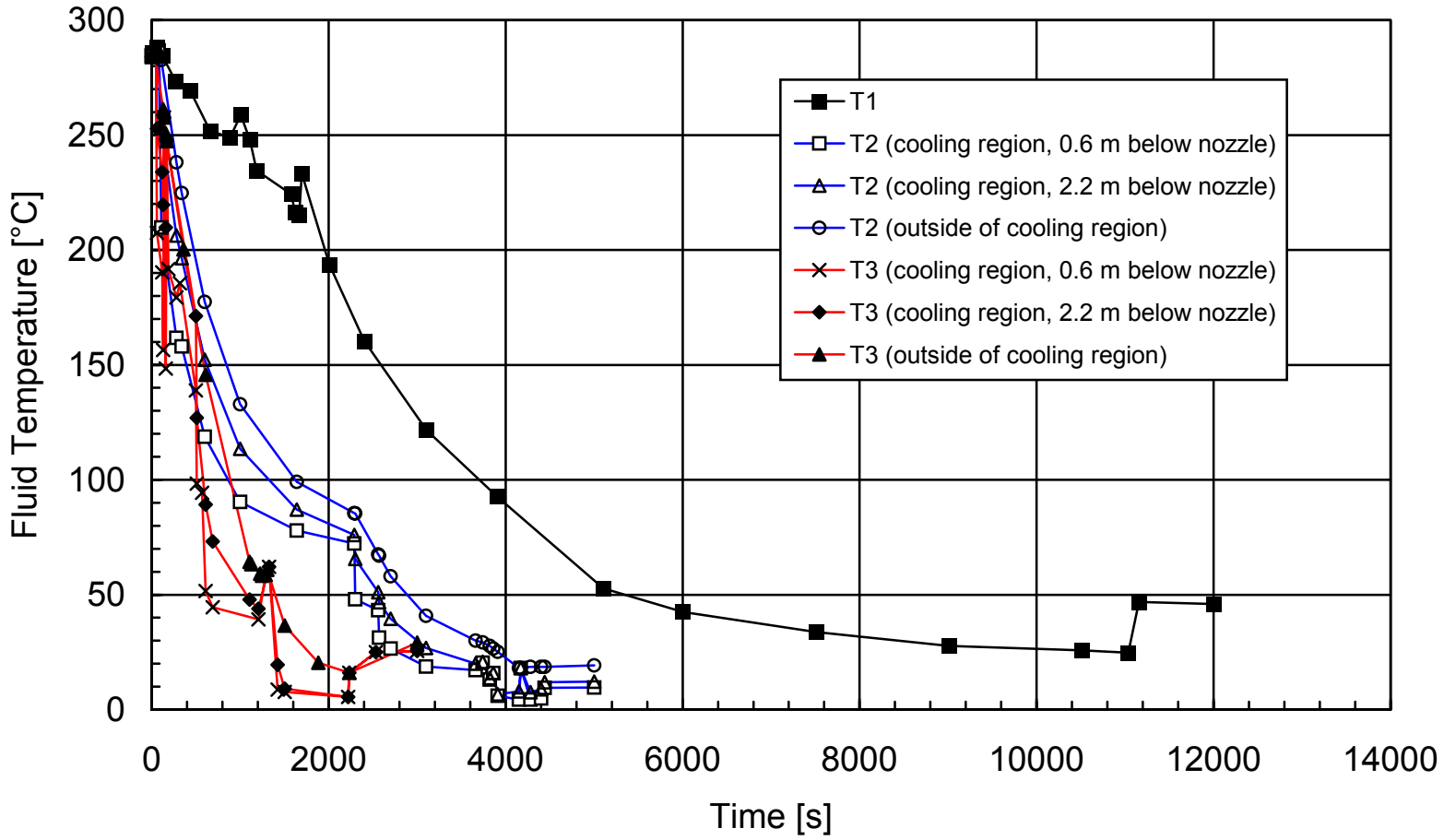

Figure 5.1.1 Time history of fluid temperatures for LOCA transients T1, T2 and T3.

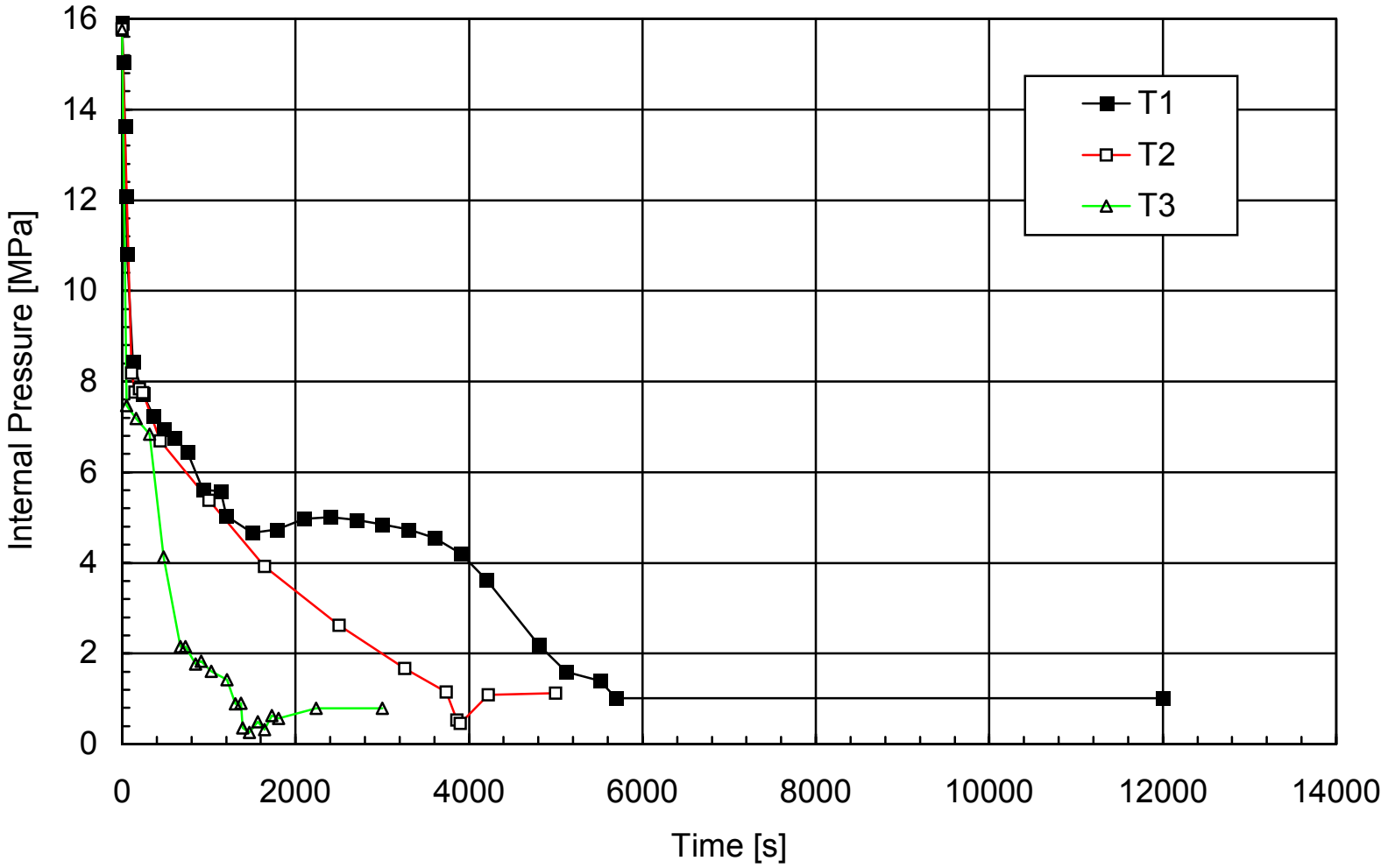

Figure 5.1.2 Time history of internal pressure for LOCA transients T1, T2 and T3.

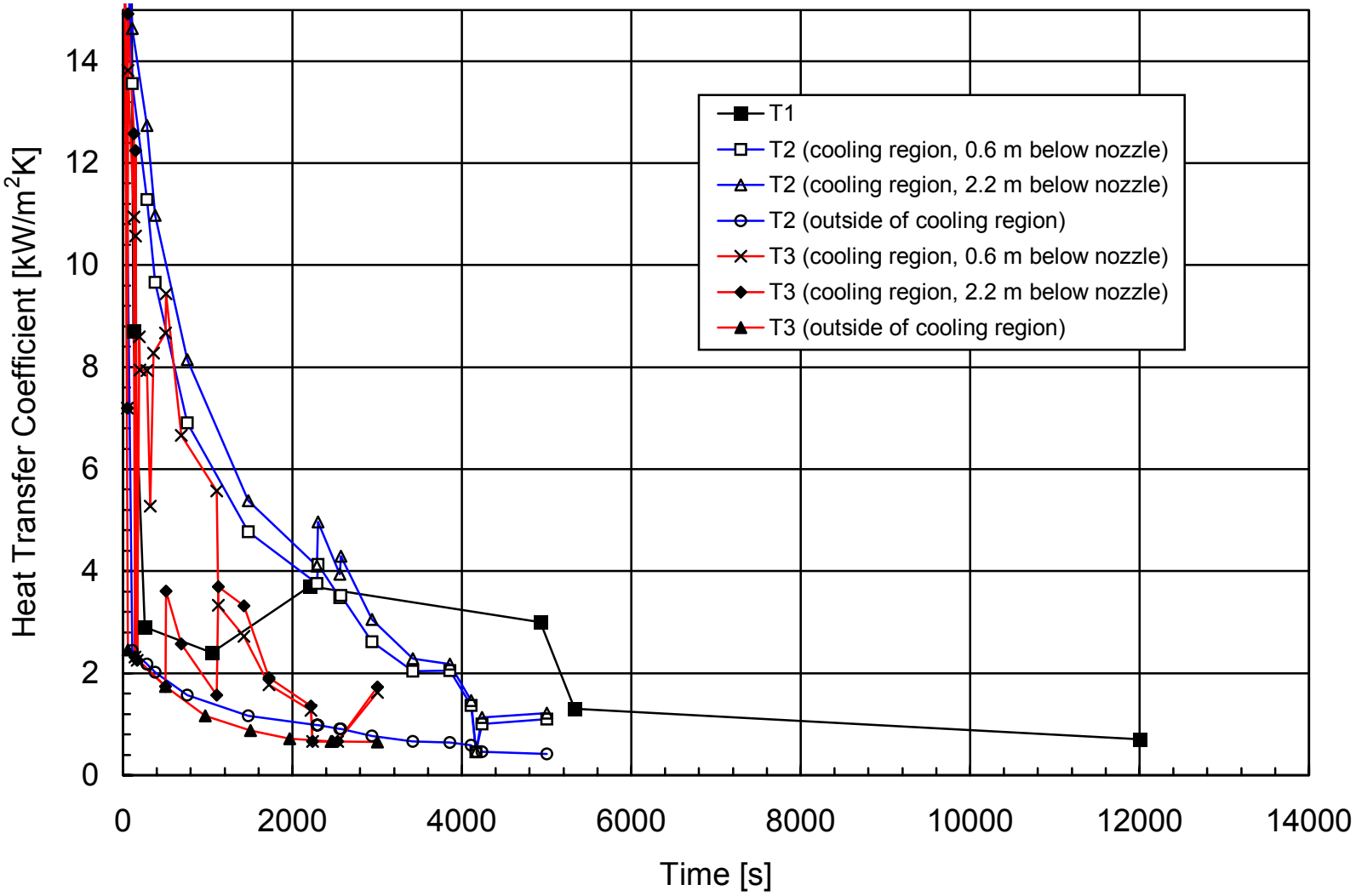

Figure 5.1.3 Time history of heat transfer coefficients for LOCA transients T1, T2 and T3.

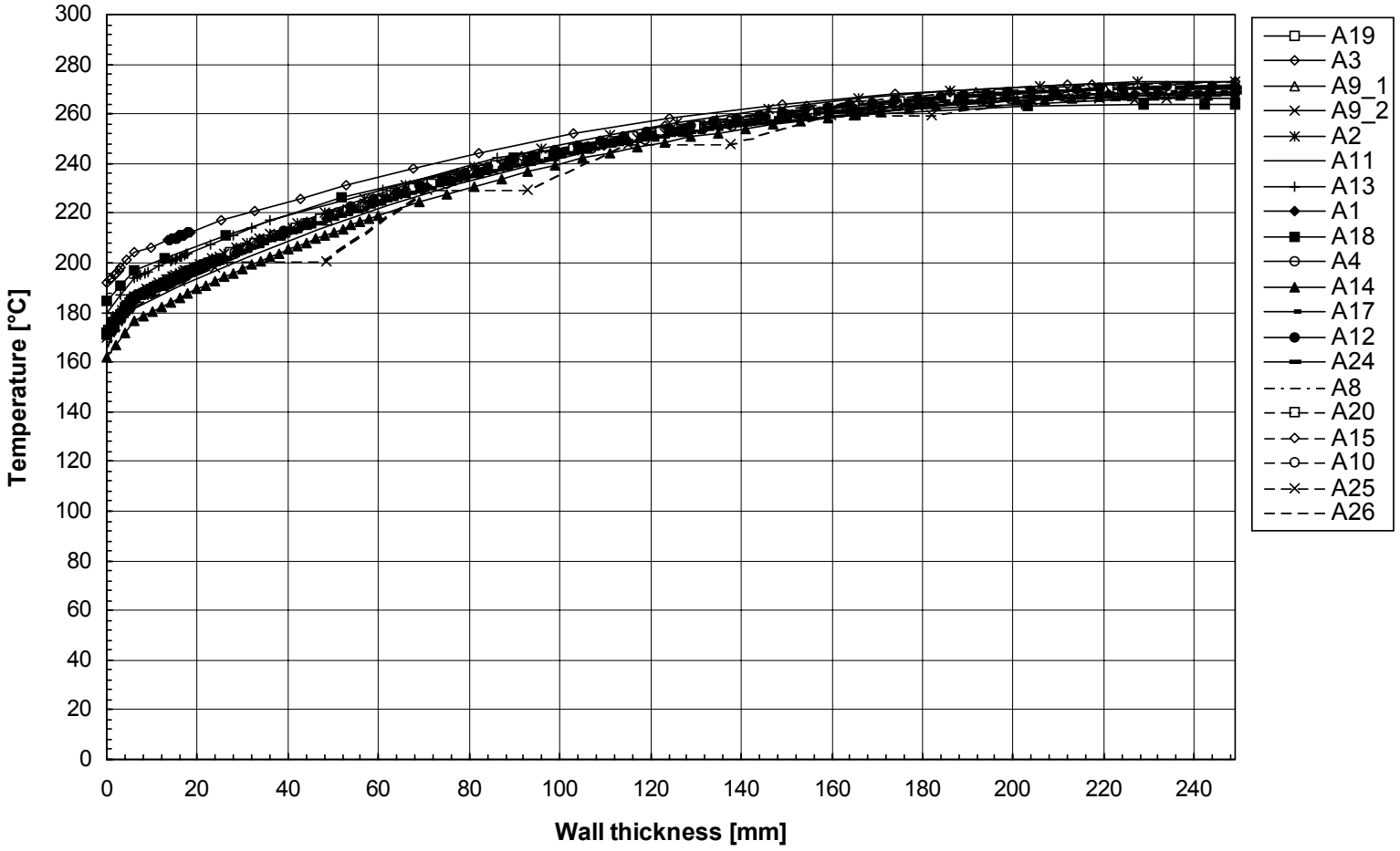

Figure 5.1.4 Task T1: Temperature distribution in the wall at time 2400 s.

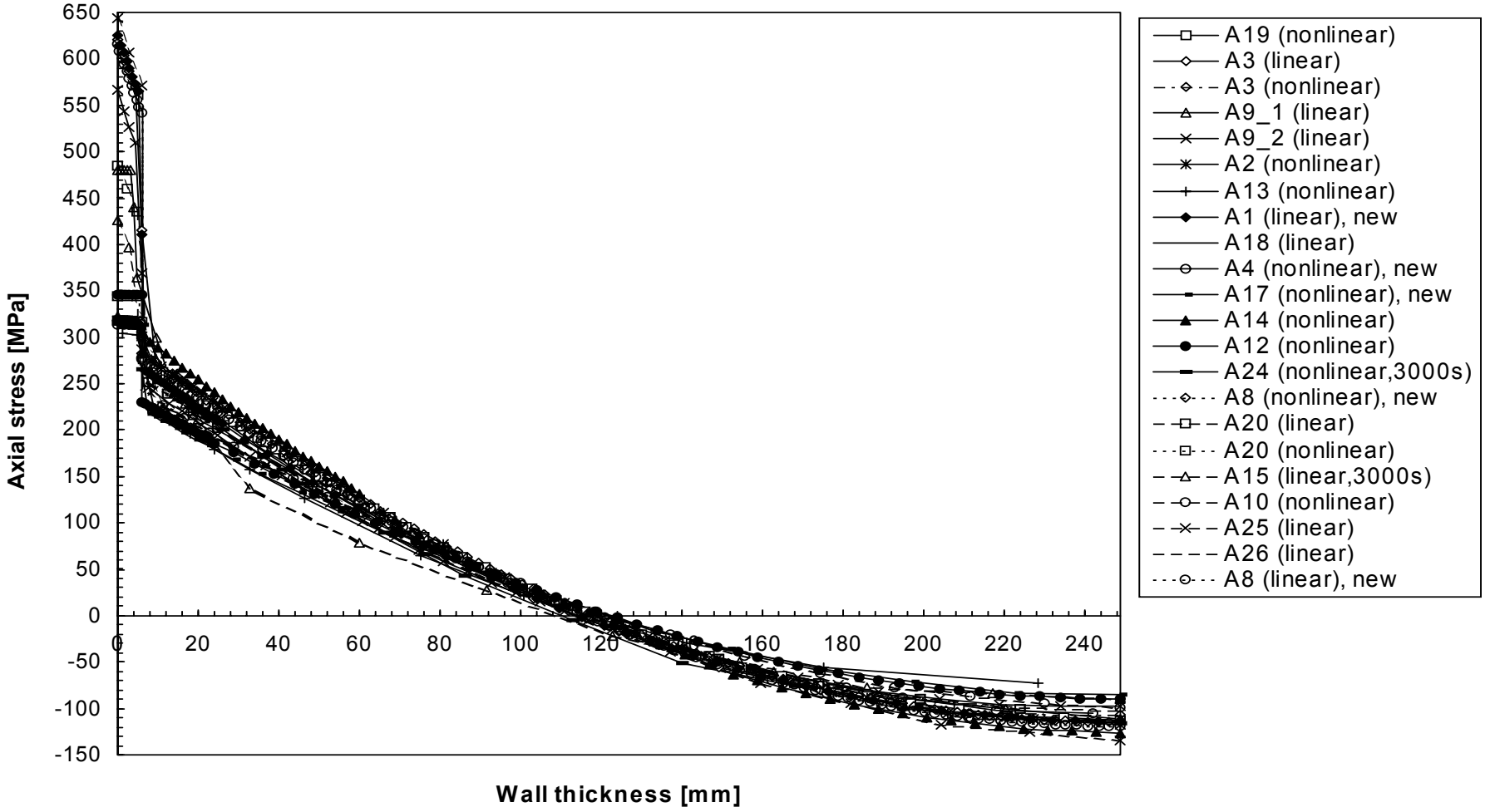

Figure 5.1.5 Task T1: Axial stress across the wall without cracks at time 3600 s.

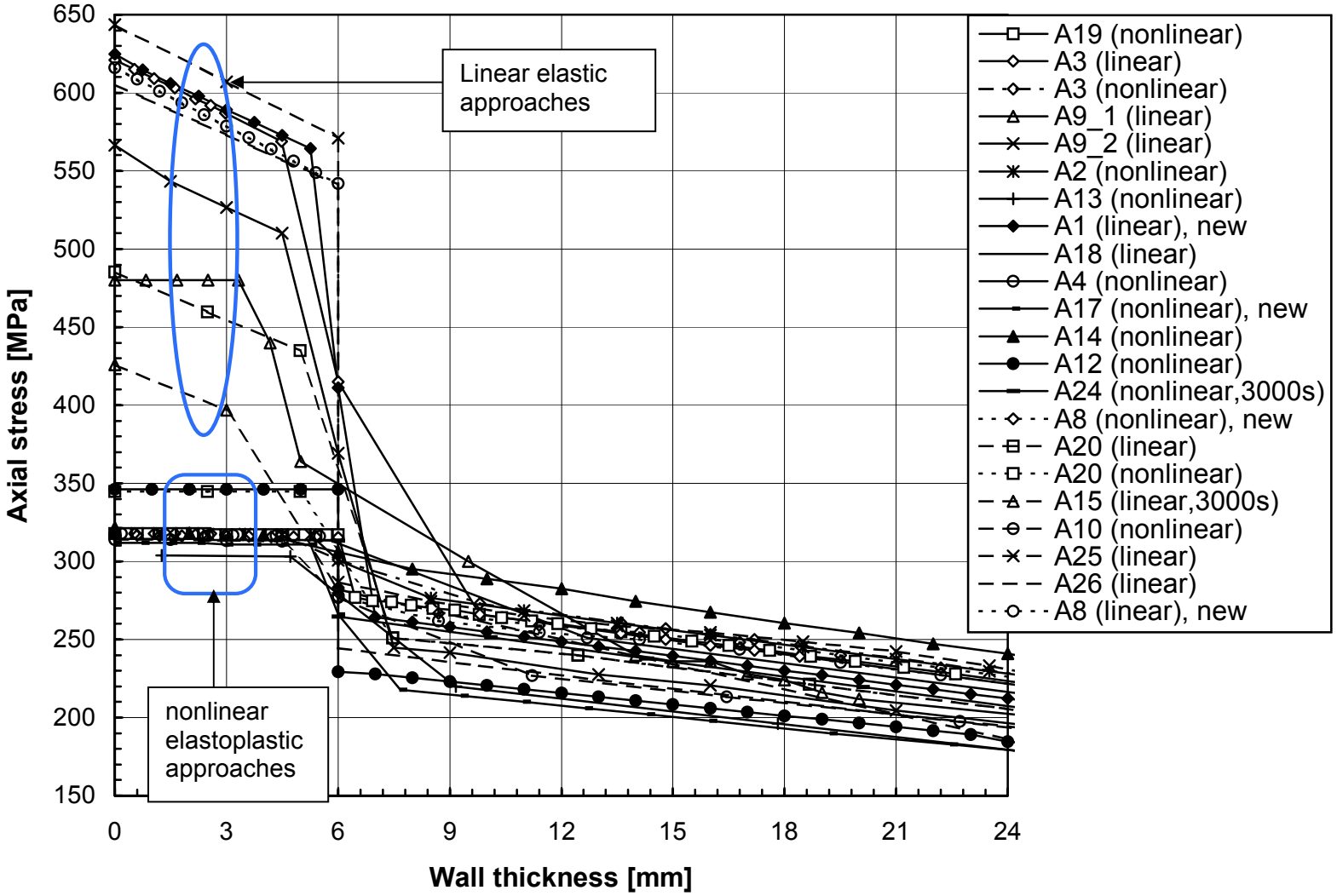

Figure 5.1.6 Task T1: Axial stress across the wall without cracks at time 3600 s (region near the inner surface).

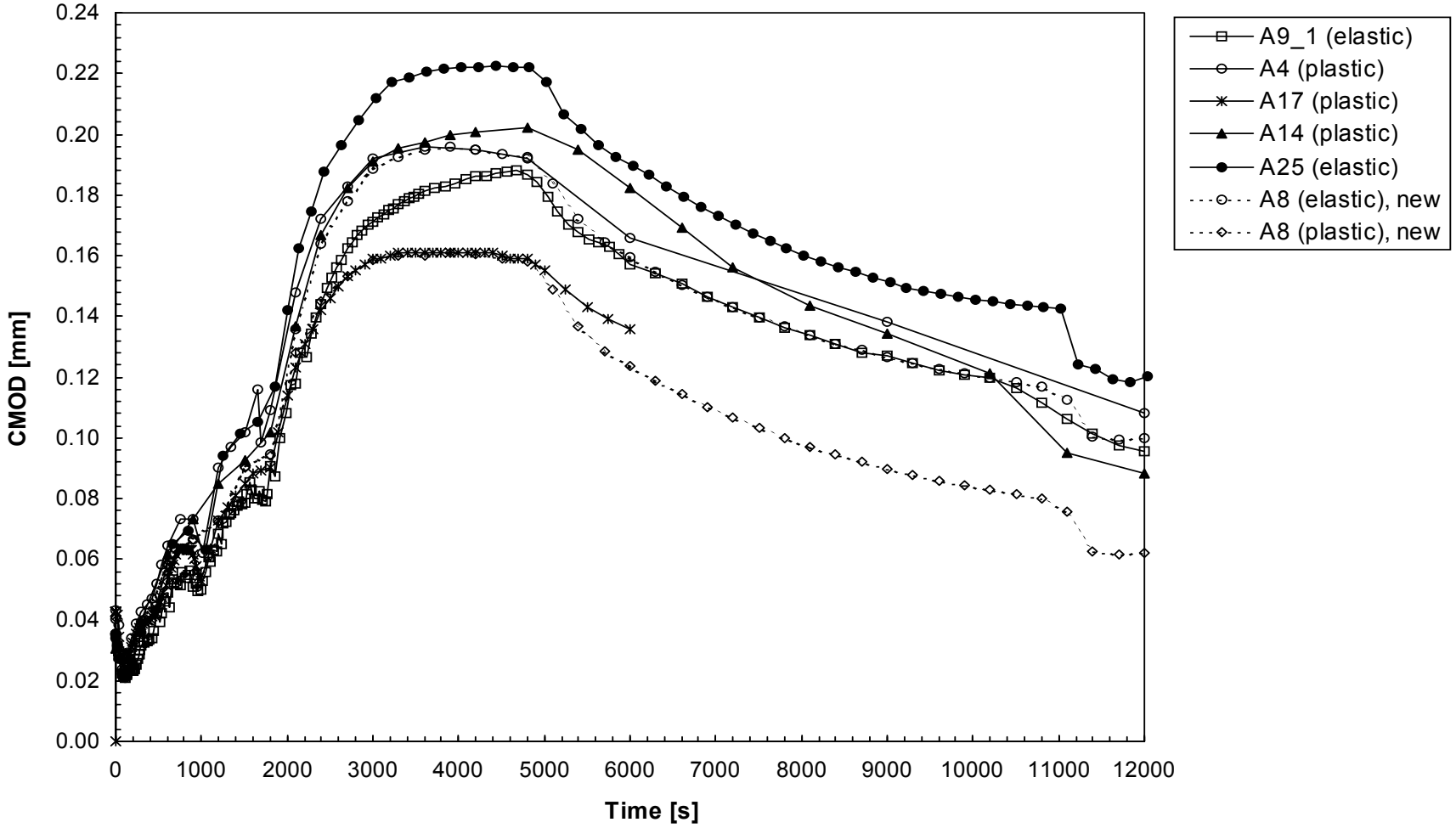

Figure 5.1.7 Task T1C1: Time history of crack mouth opening displacement (CMOD)

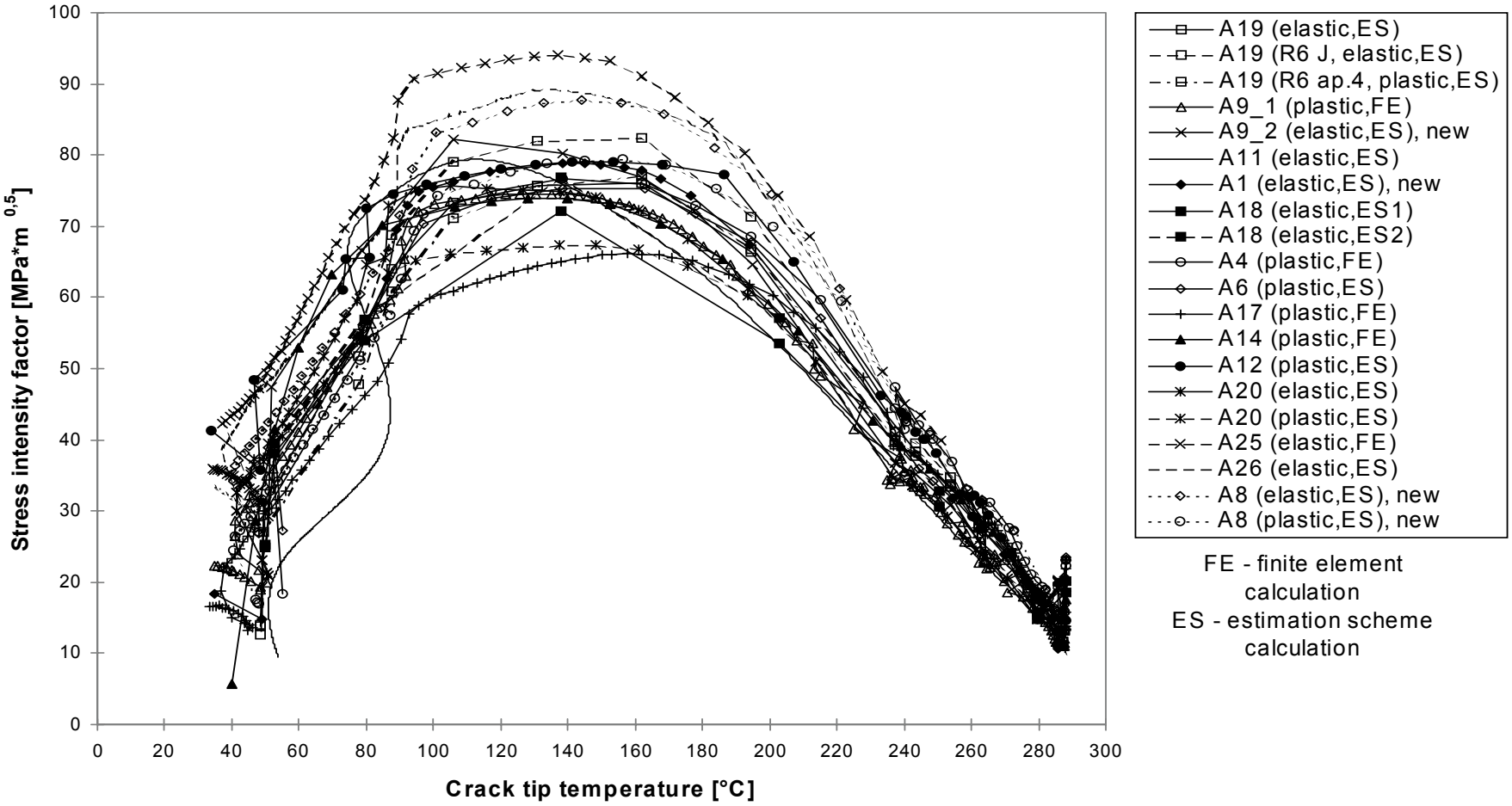

Figure 5.1.8 Task T1C1: Stress intensity factor versus crack-tip temperature (elastic and plastic calculation).

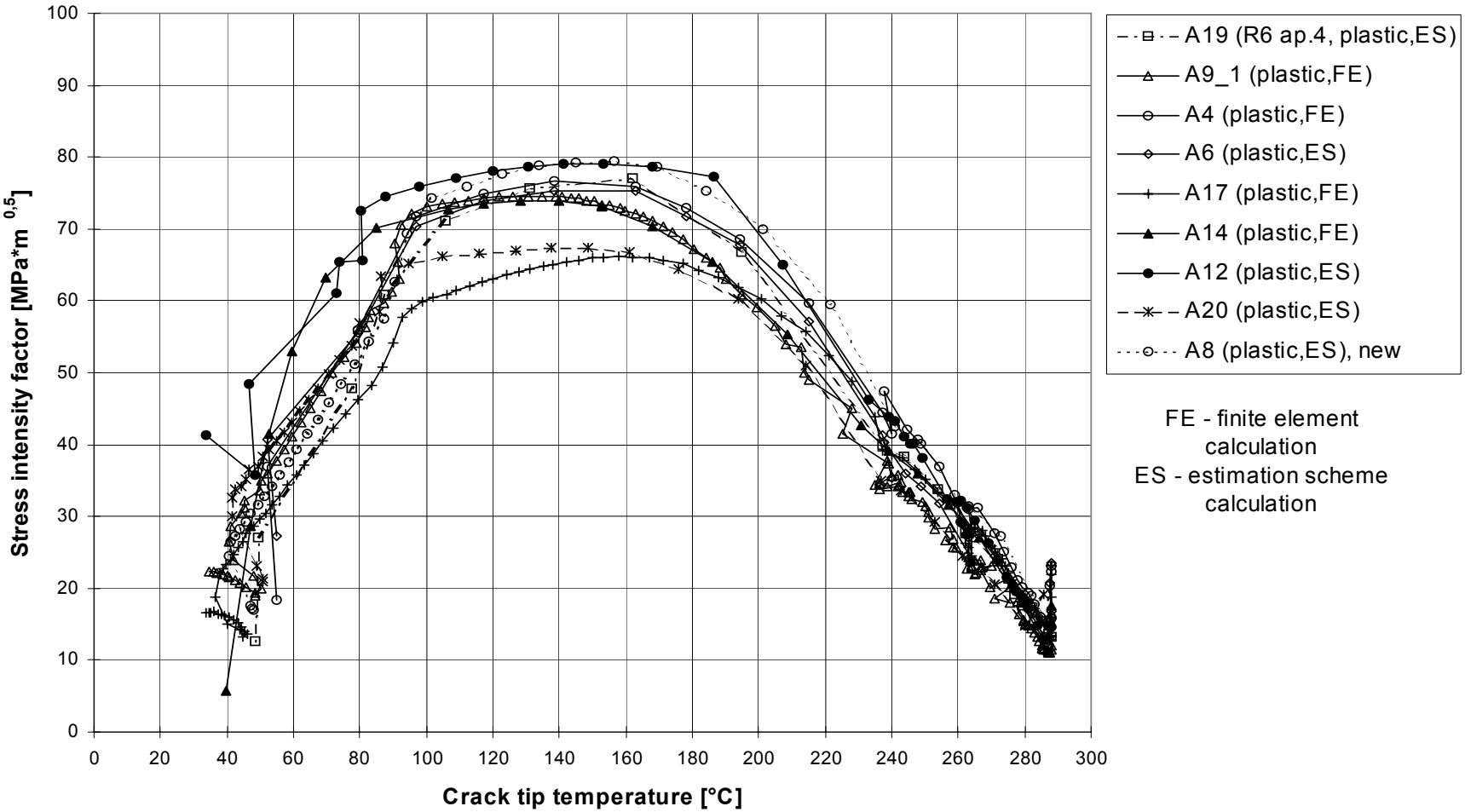

Figure 5.1.9 Task T1C1: Stress intensity factor versus crack-tip temperature (plastic calculations).

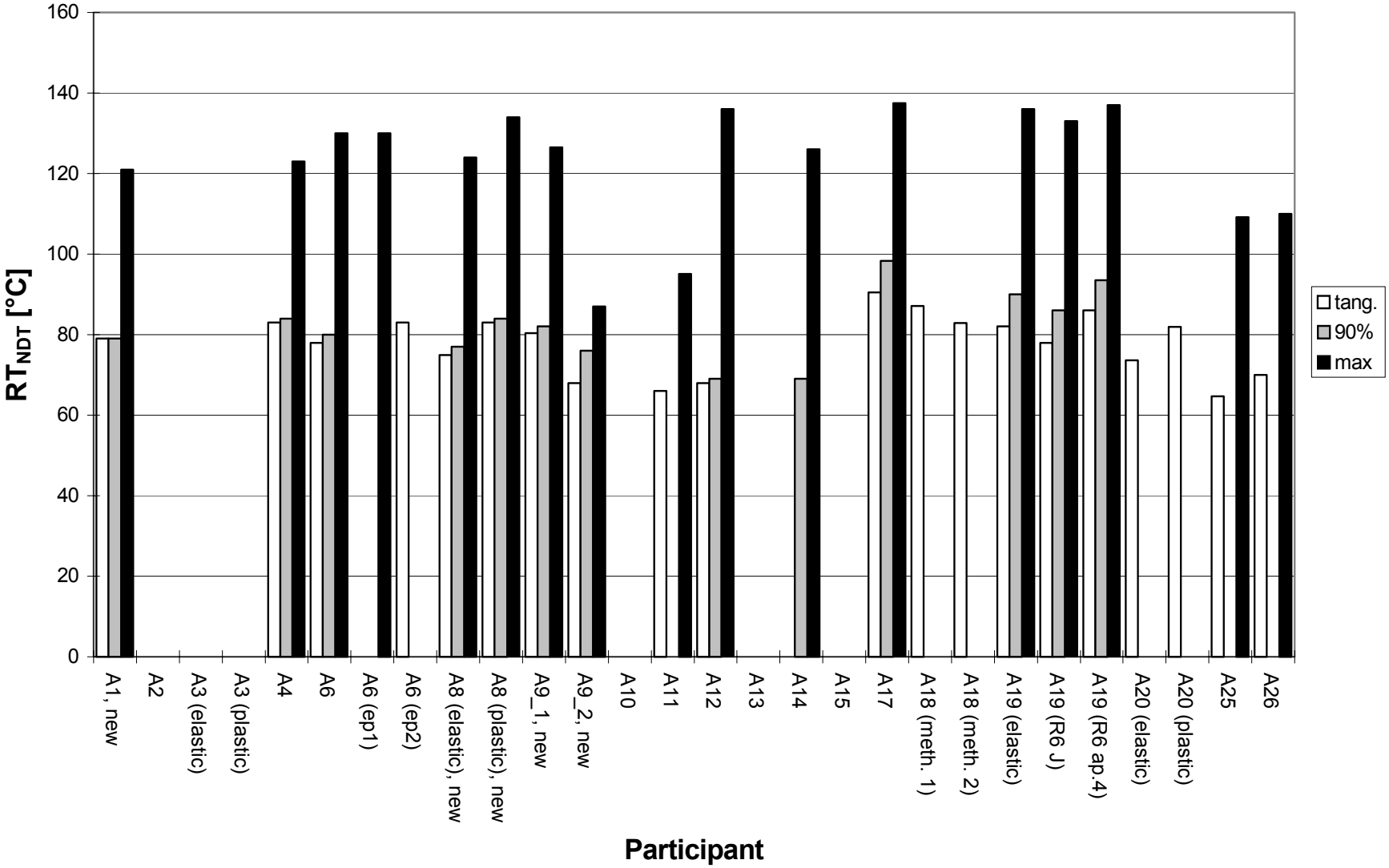

Figure 5.1.10 Task T1C1: Evaluation of the maximum allowable RT_{NDT} based on tangent, ninety-percent, and maximum criteria.

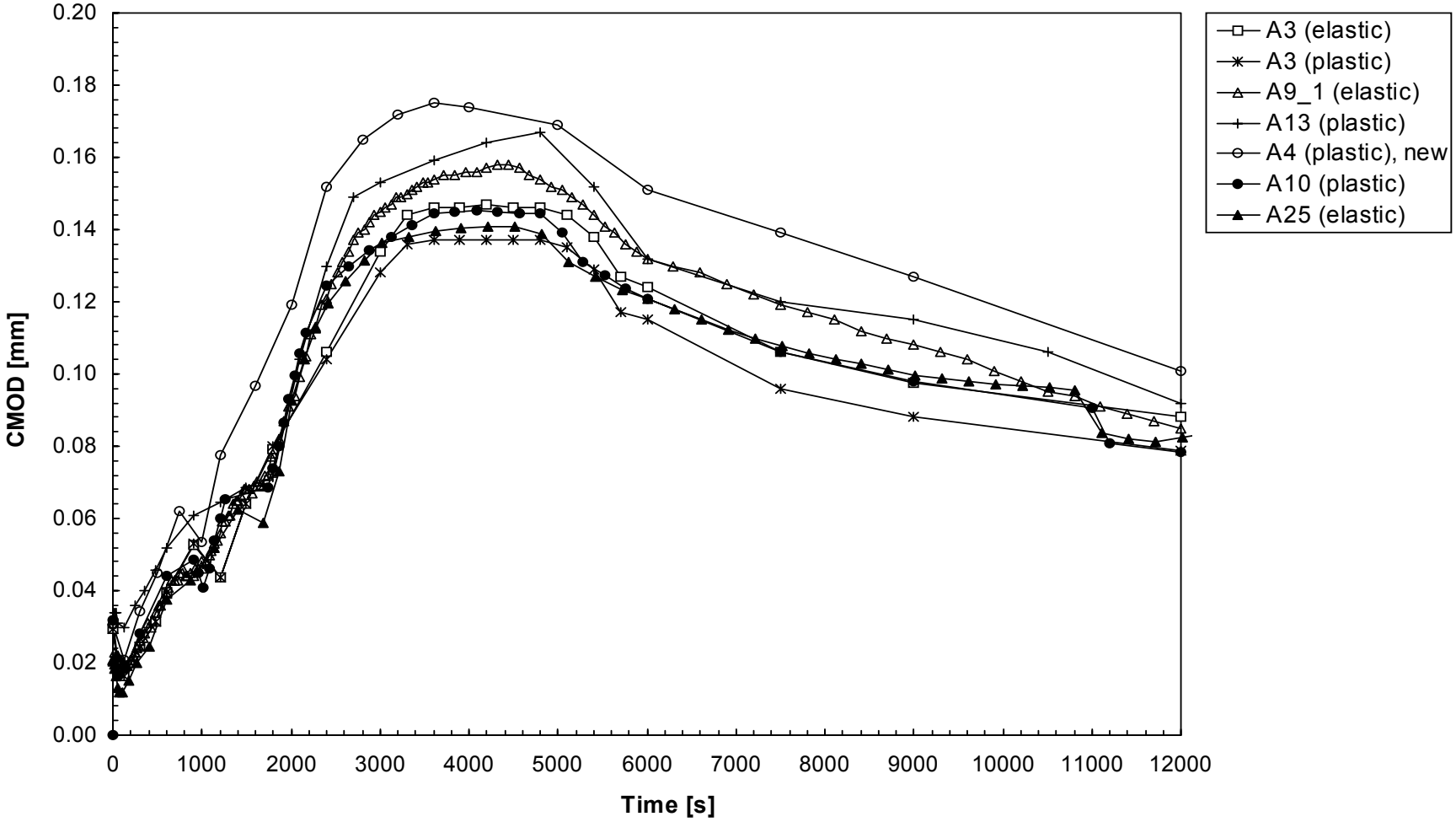

Figure 5.1.11 Task T1C2: Time history of crack mouth opening displacement (CMOD)

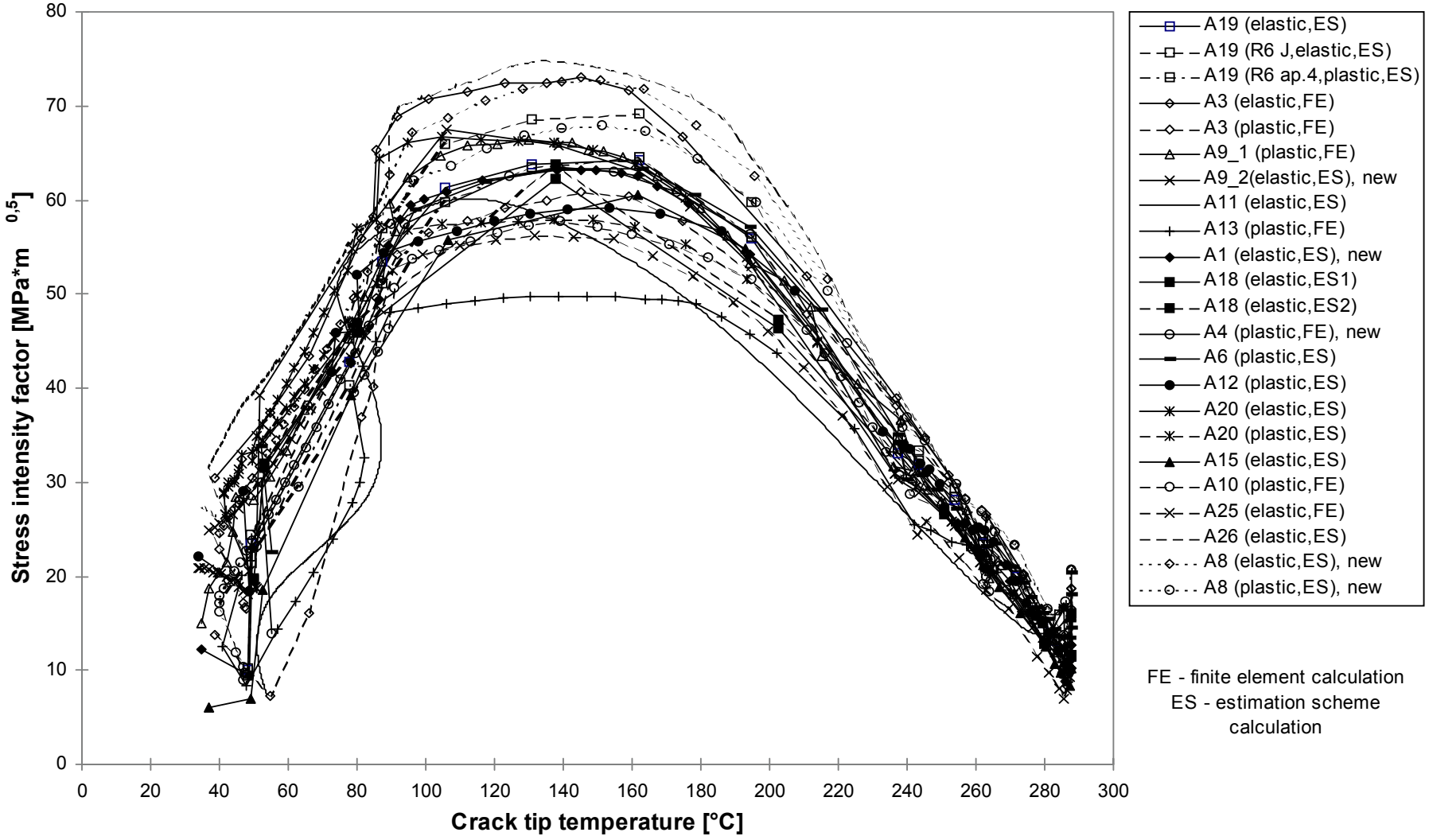

Figure 5.1.12 Task T1C2: Stress intensity factor versus crack-tip temperature (elastic and plastic calculation).

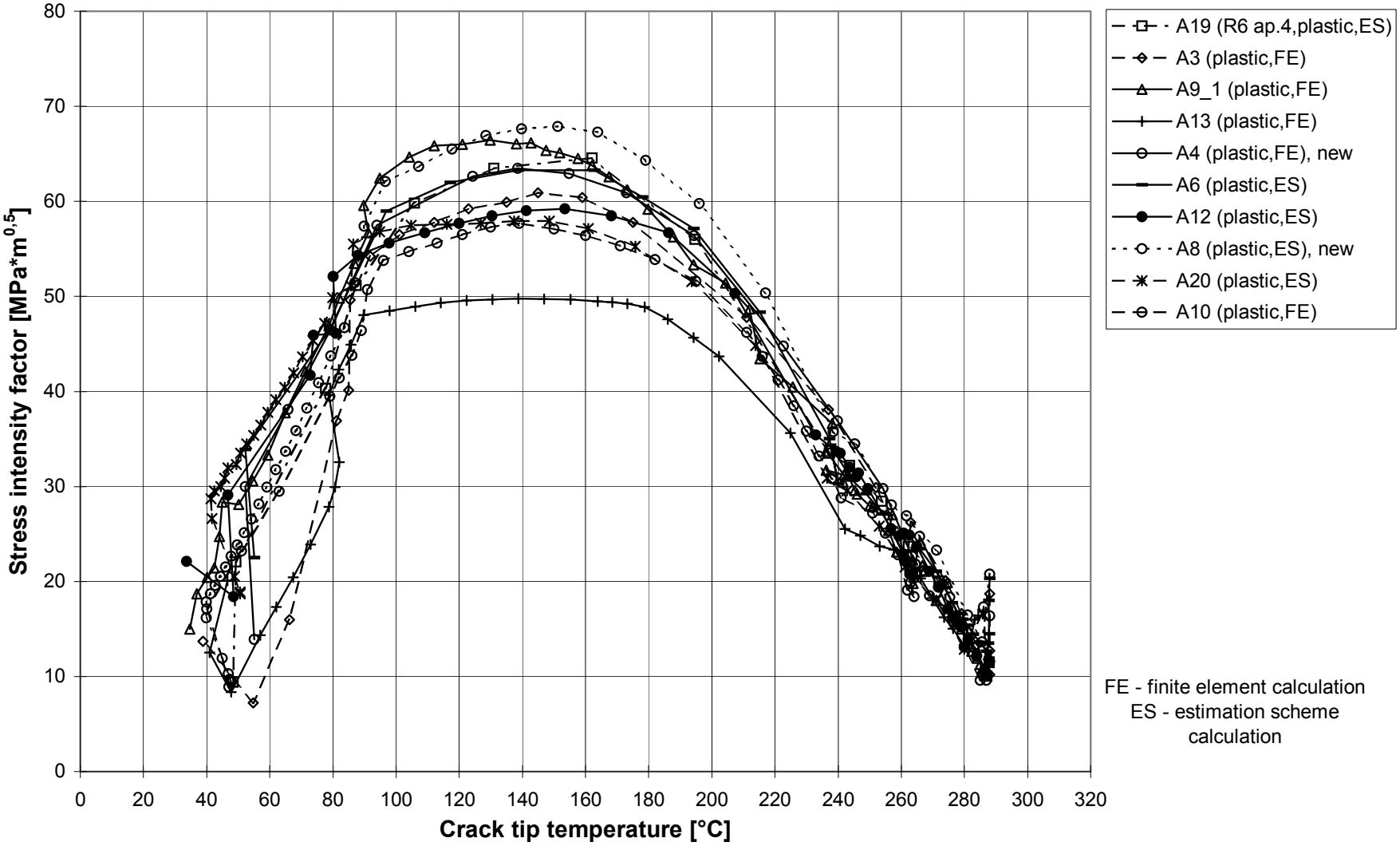

Figure 5.1.13 Task T1C2: Stress intensity factor versus crack-tip temperature (plastic calculations).

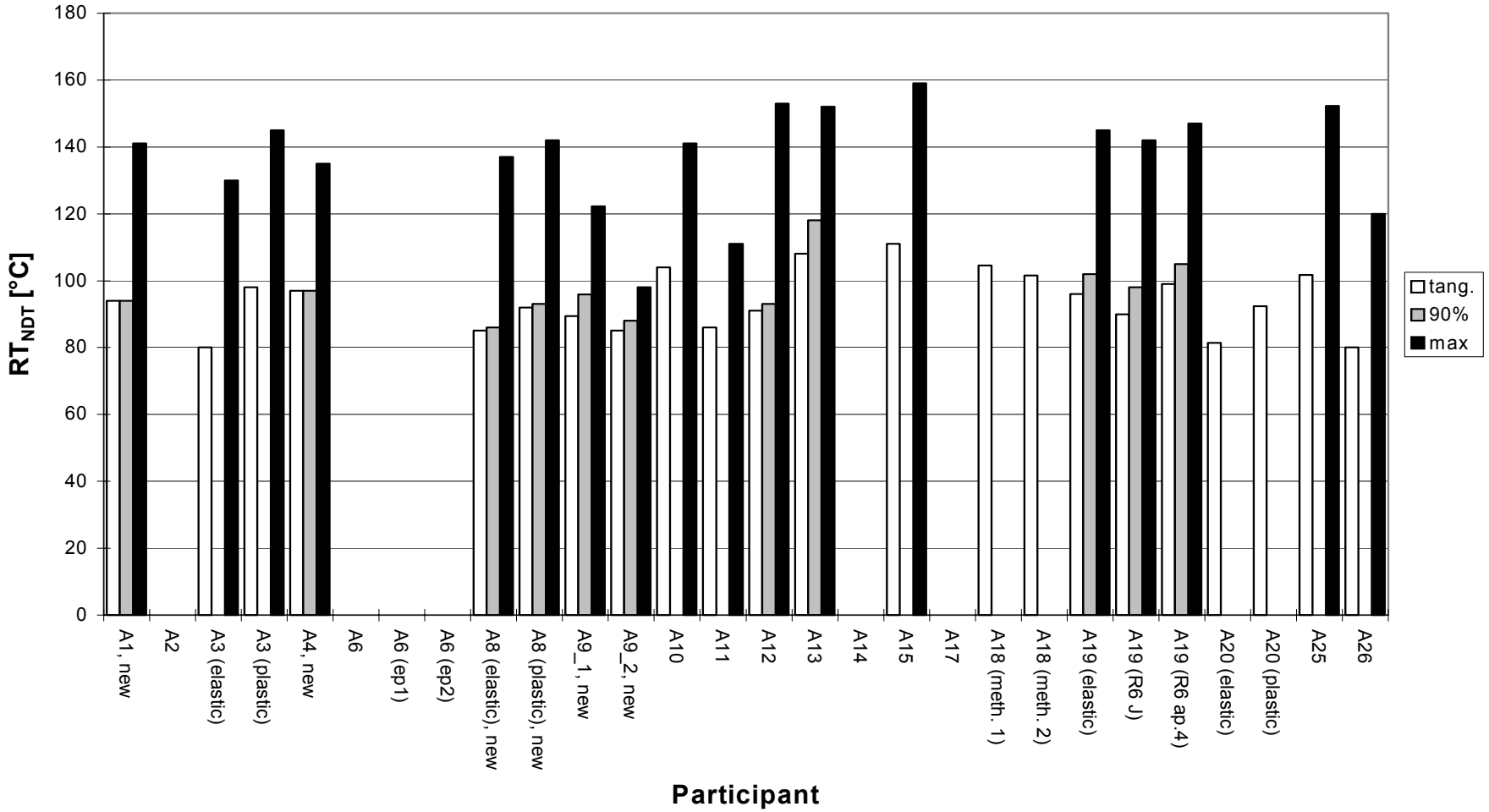

Figure 5.1.14 Task T1C2: Evaluation of the maximum allowable RT_{NDT} (deepest point) based on tangent, ninety-percent, and maximum criteria.

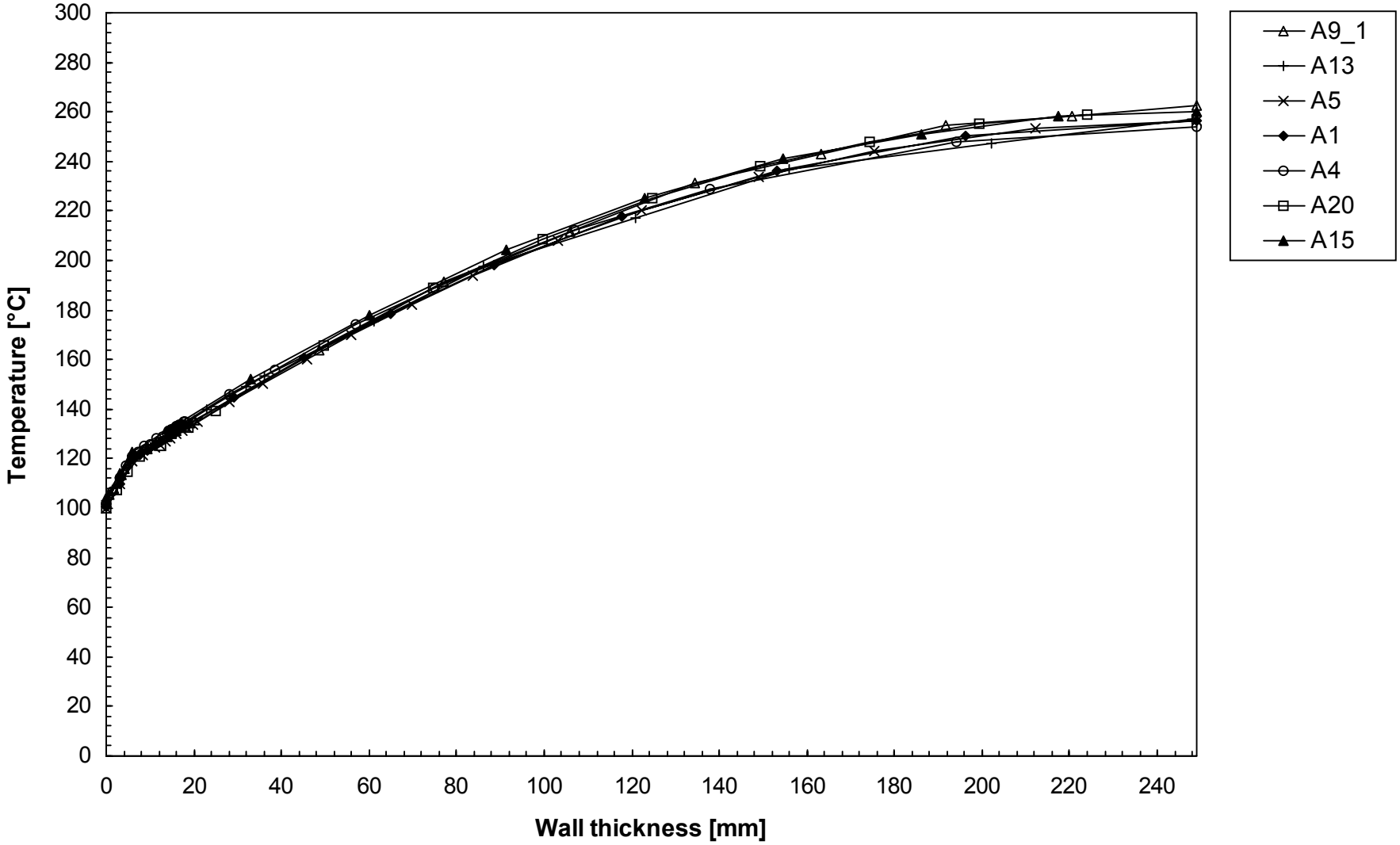

Figure 5.1.15 Task T2: Temperature distribution in the wall inside the cooling region at time 1500 s.

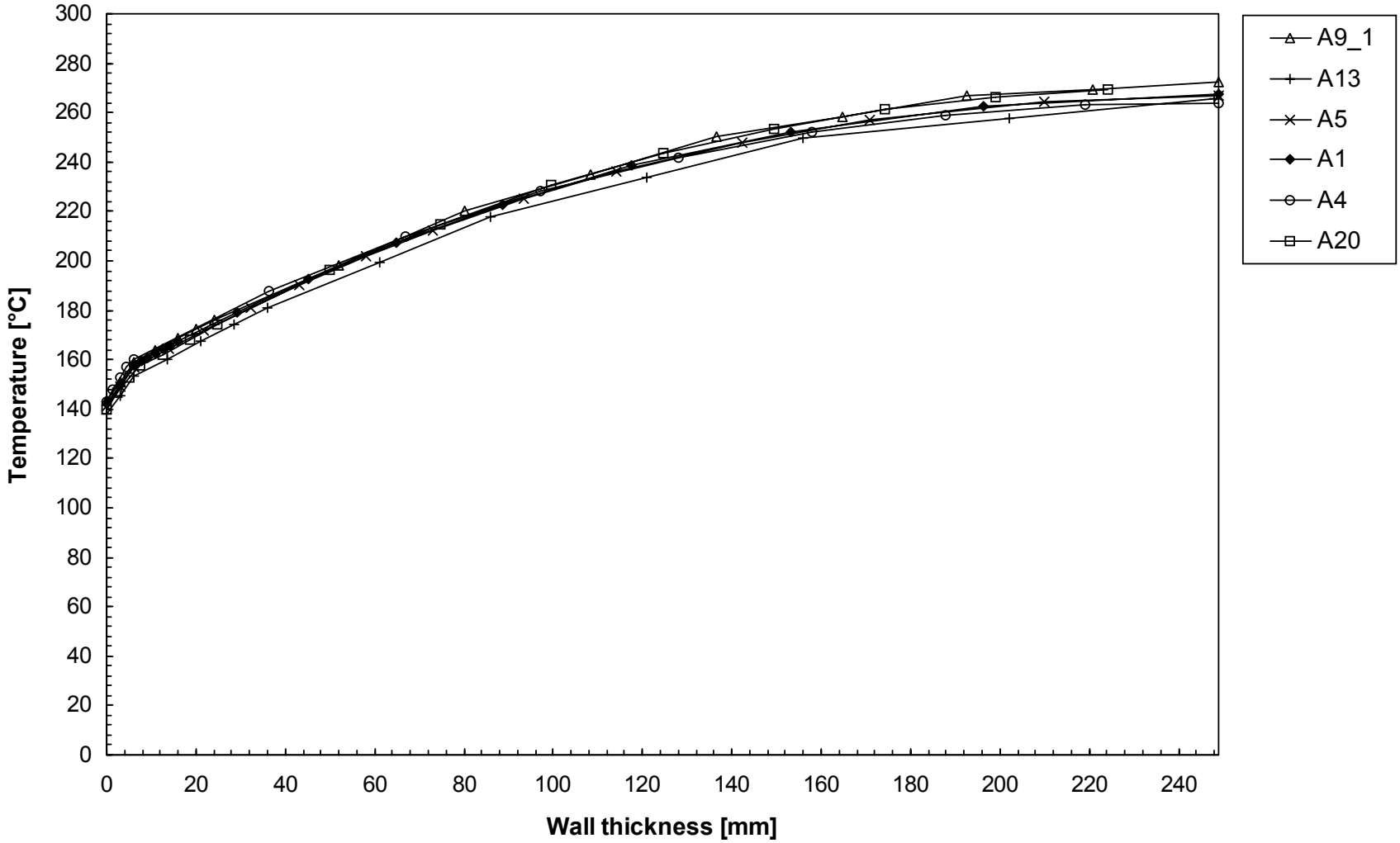

Figure 5.1.16 Task T2: Temperature distribution in the wall outside the cooling region at time 1500 s.

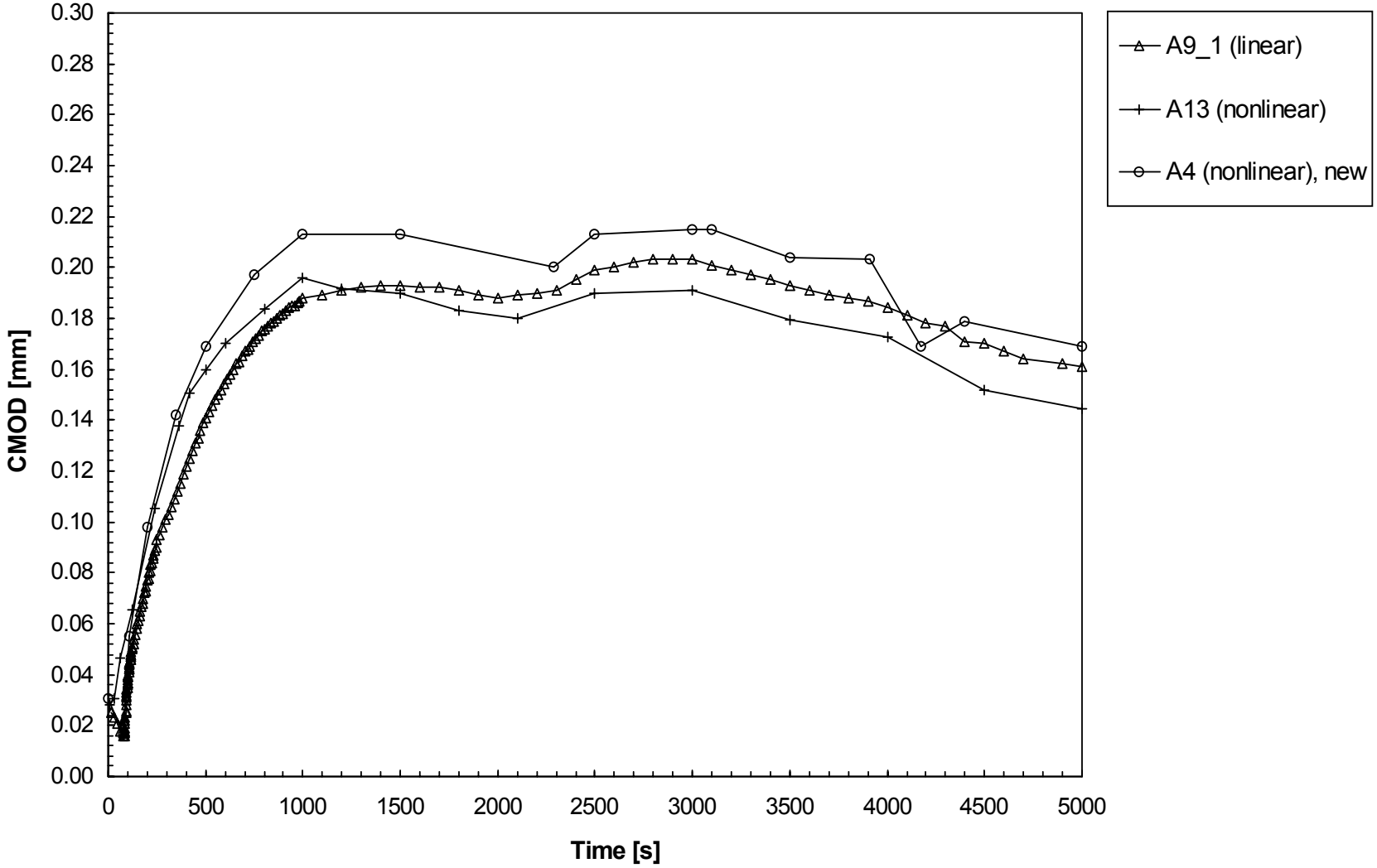

Figure 5.1.17 Task T2C2: Time history of crack mouth opening displacement (CMOD).

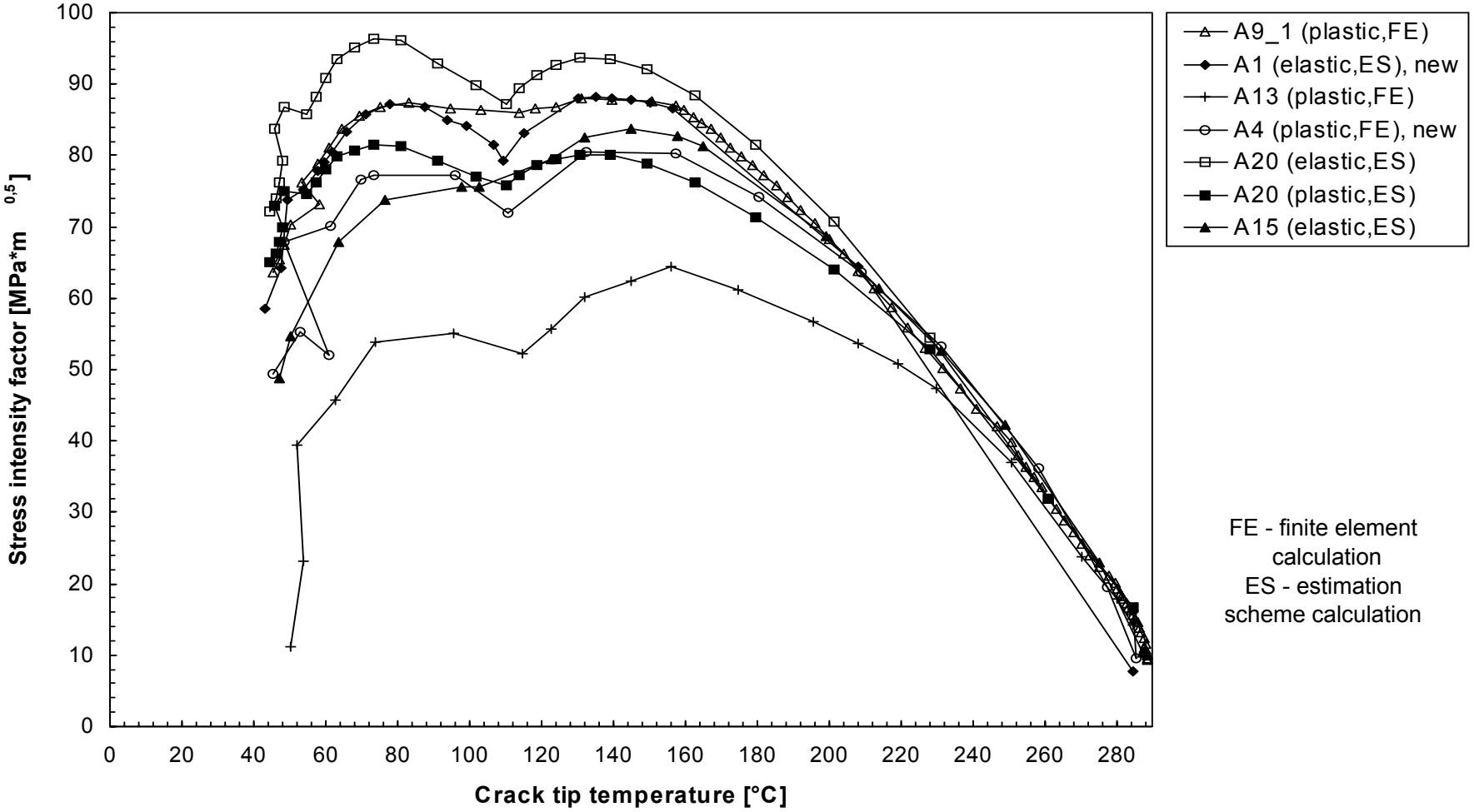

Figure 5.1.18 Task T2C2: Stress intensity factor versus crack-tip temperature at the deepest point of the crack (elastic and plastic calculation).

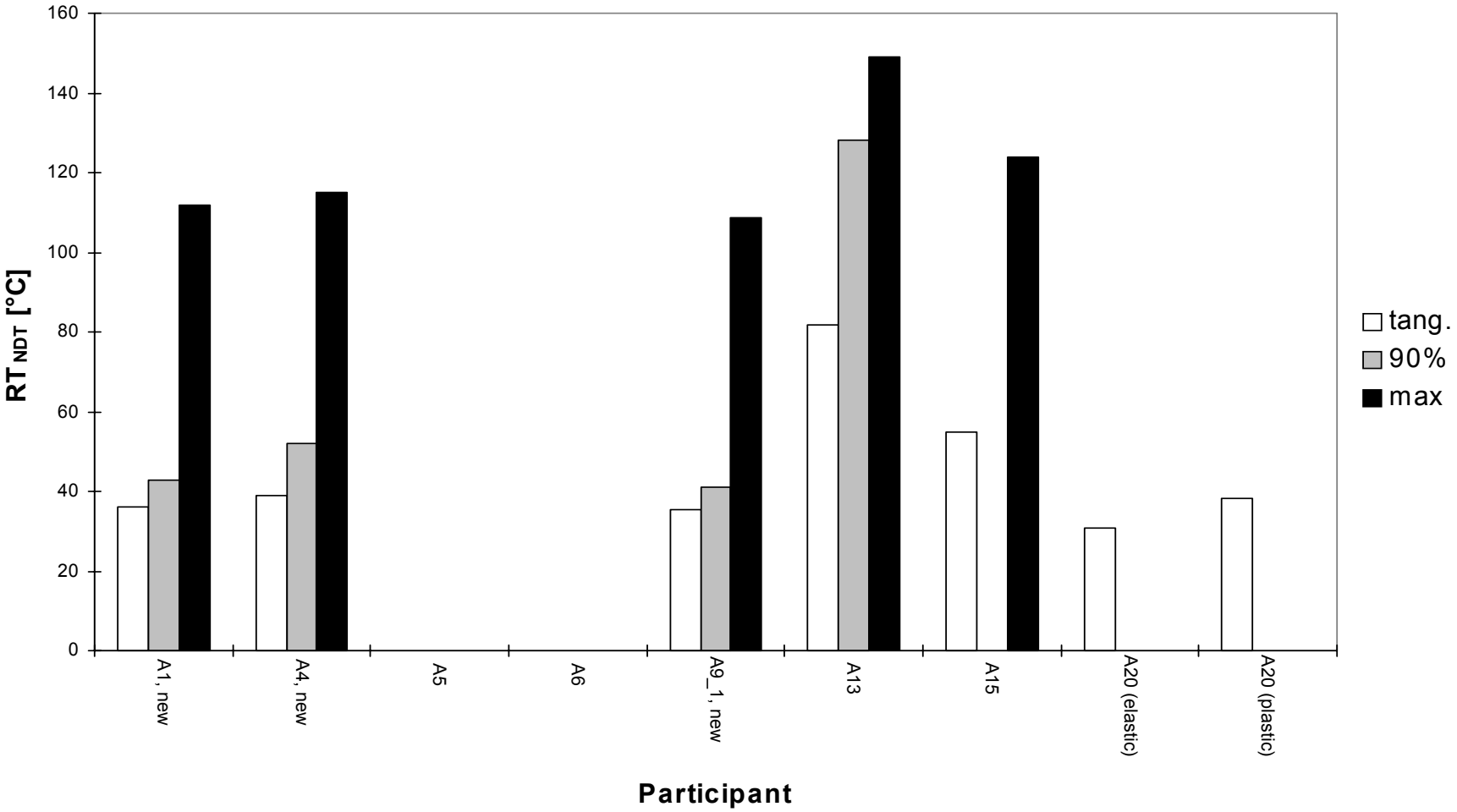

Figure 5.1.19 Task T2C2: Evaluation of the maximum allowable RT_{NDT} (deepest point) based on tangent, ninety-percent, and maximum criteria.

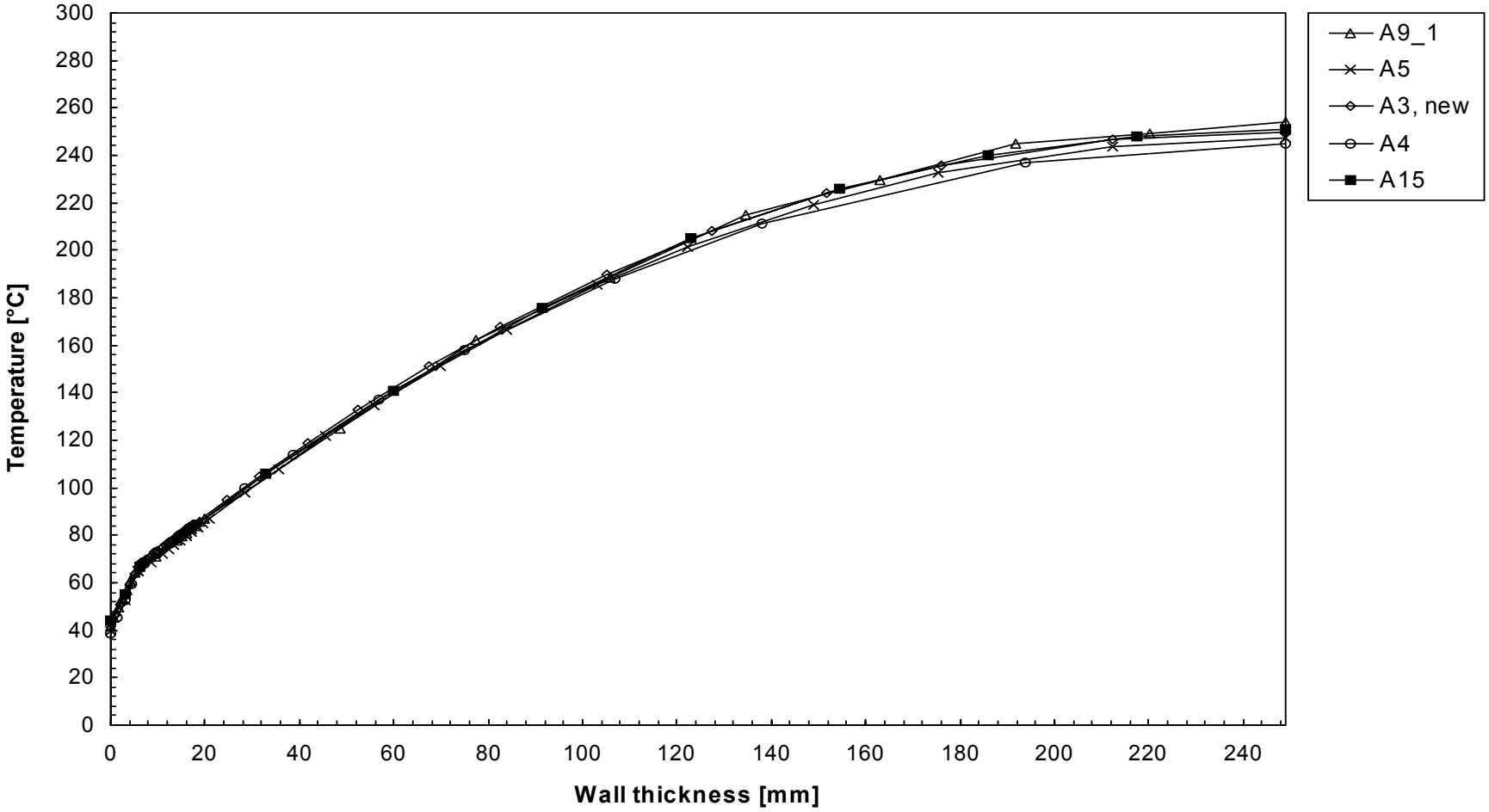

Figure 5.1.20 Task T3: Temperature distribution in the wall inside the cooling region at time 1600 s.

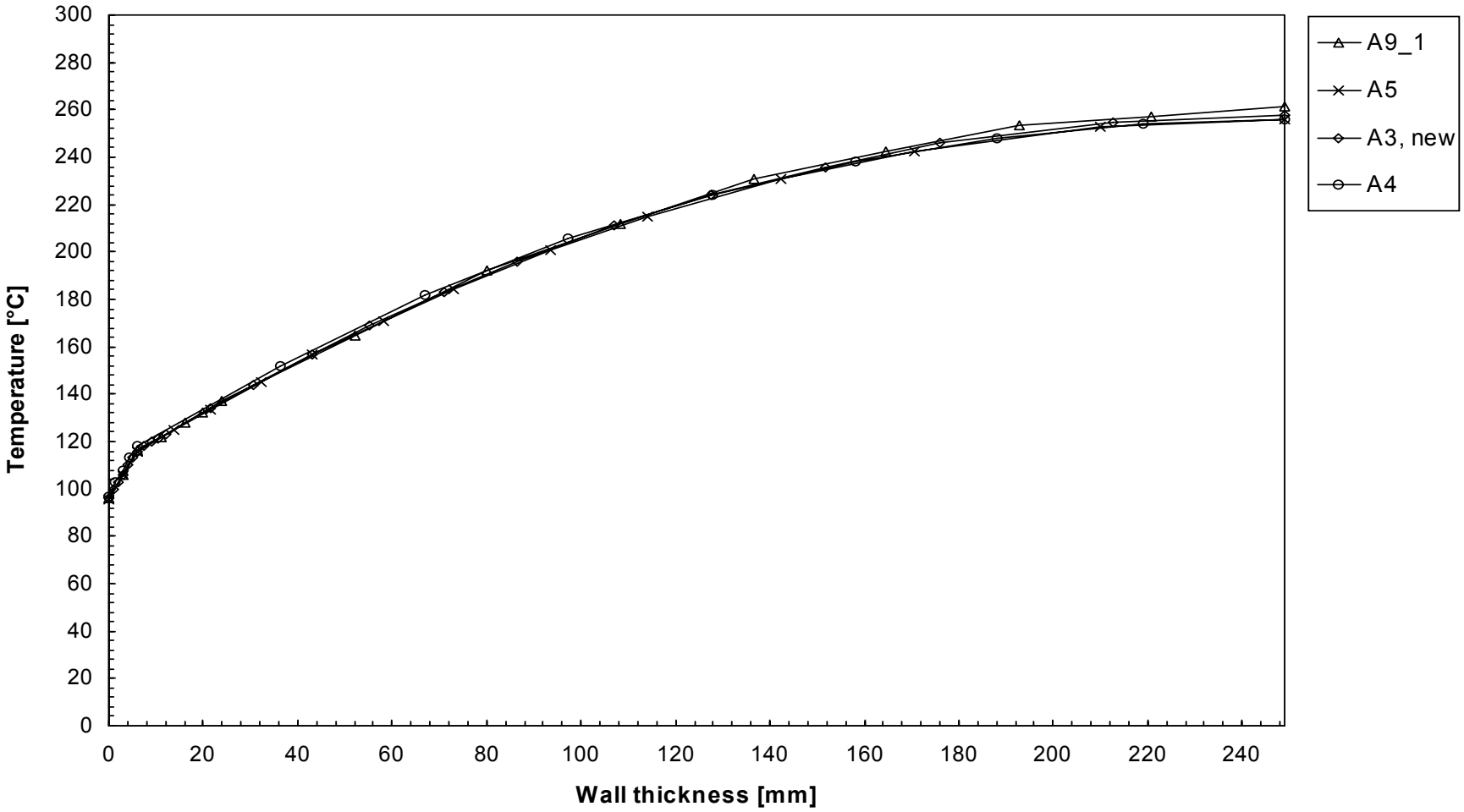

Figure 5.1.21 Task T3: Temperature distribution in the wall outside the cooling region at time 1600 s.

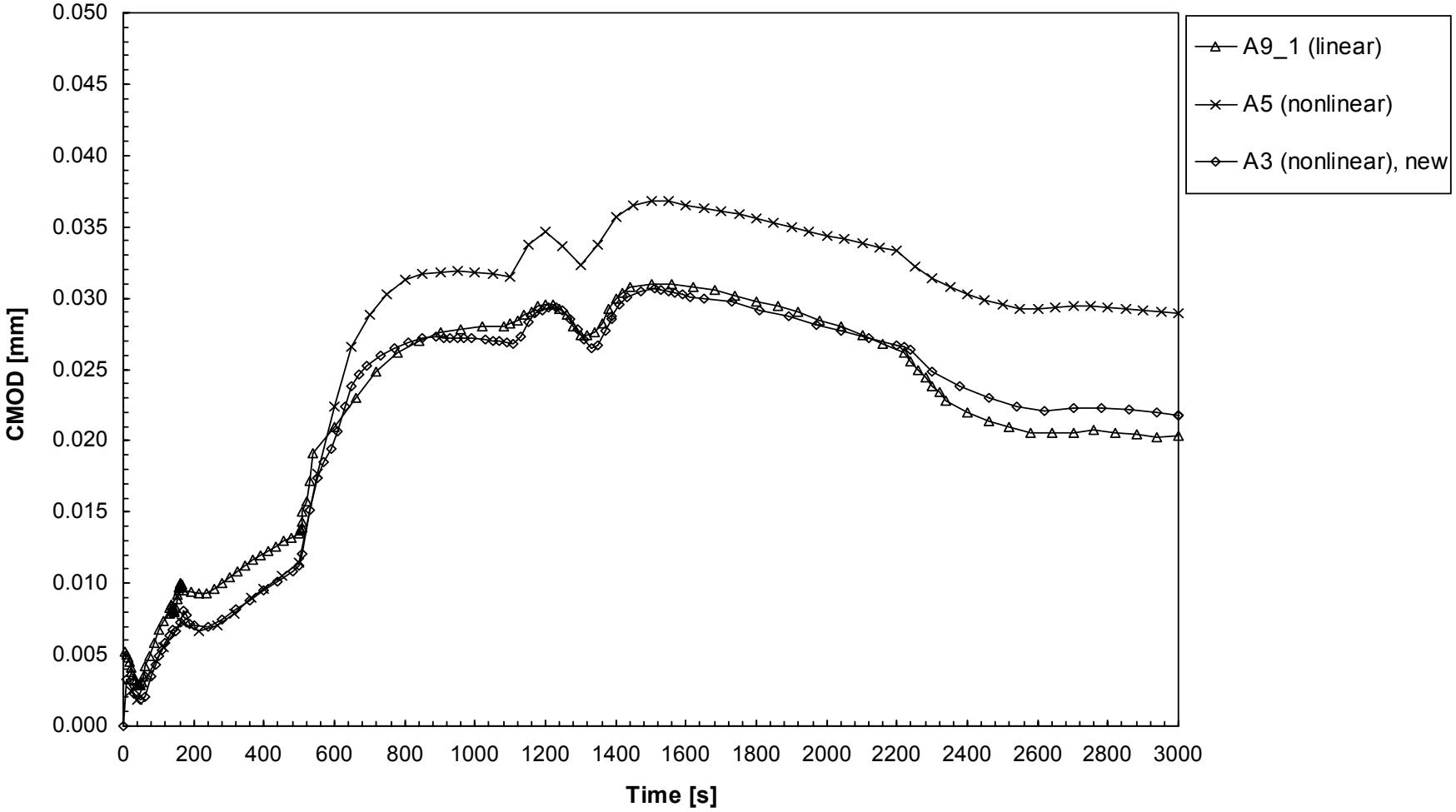

Figure 5.1.22 Task T3C4: Time history of crack mouth opening displacement (CMOD).

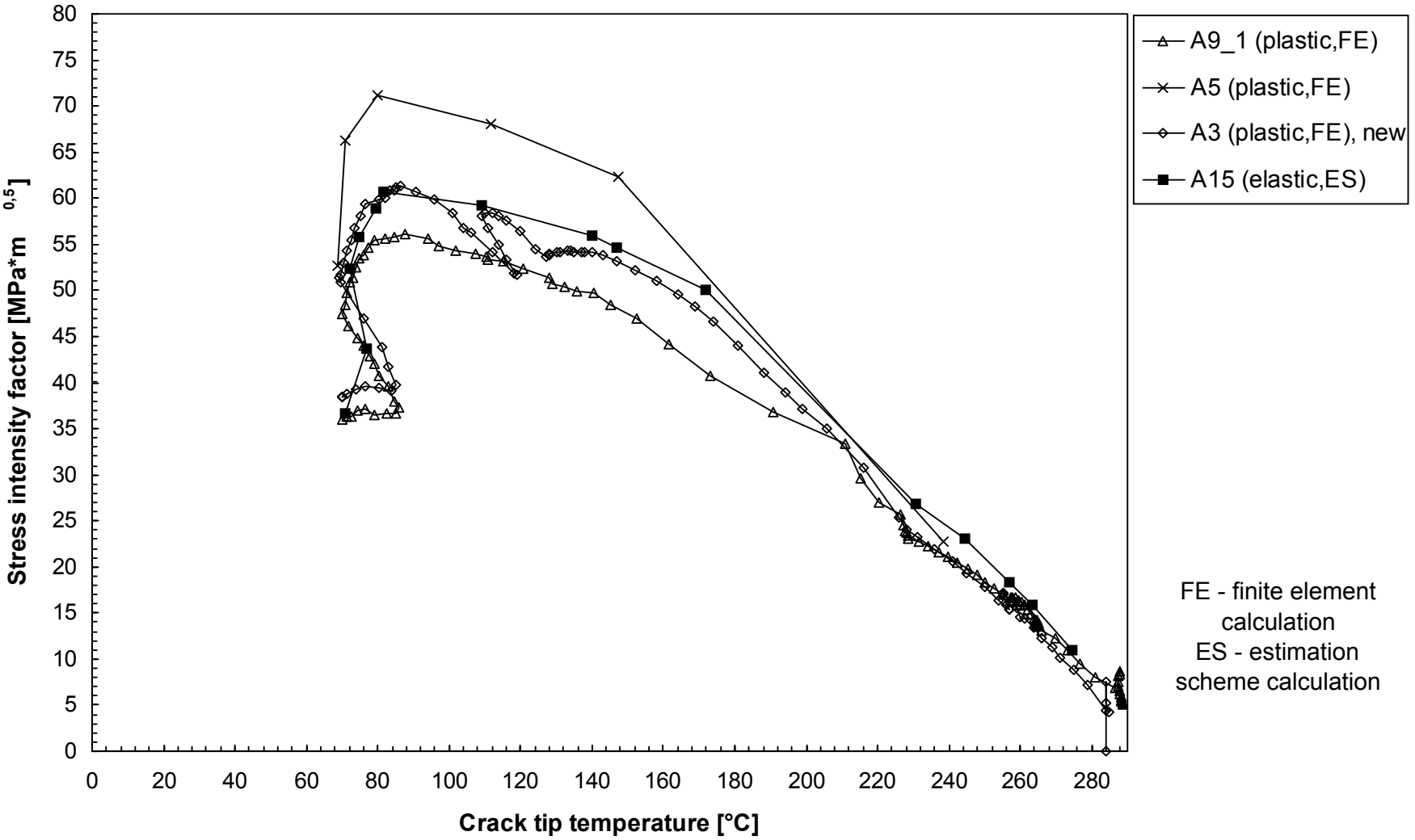

Figure 5.1.23 Task T3C4: Stress intensity factor versus crack-tip temperature at the deepest point of the crack (elastic and plastic calculations).

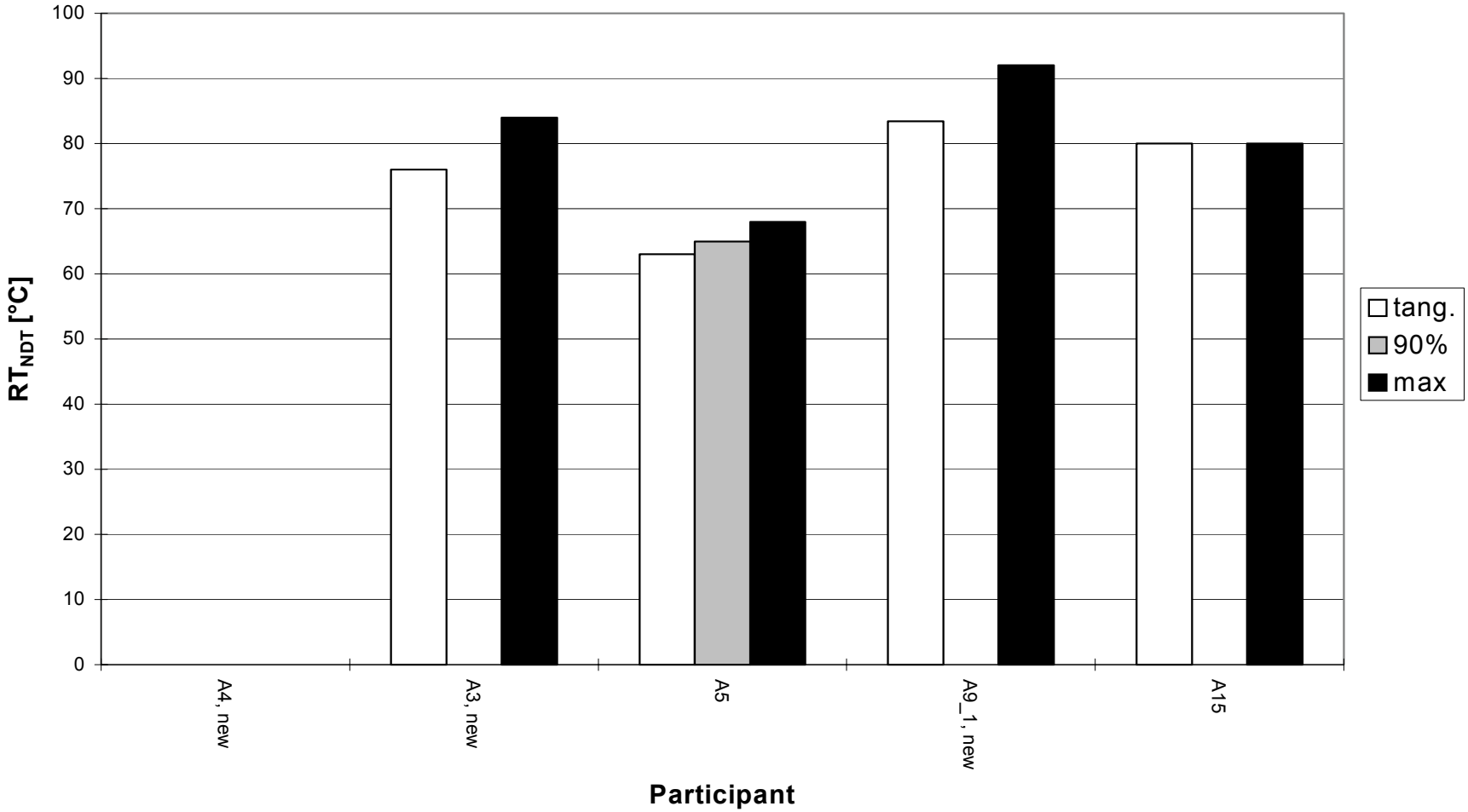

Figure 5.1.24 Task T3C4: Evaluation of the maximum allowable RT_{NDT} (deepest point) based on tangent, ninety-percent, and maximum criteria.

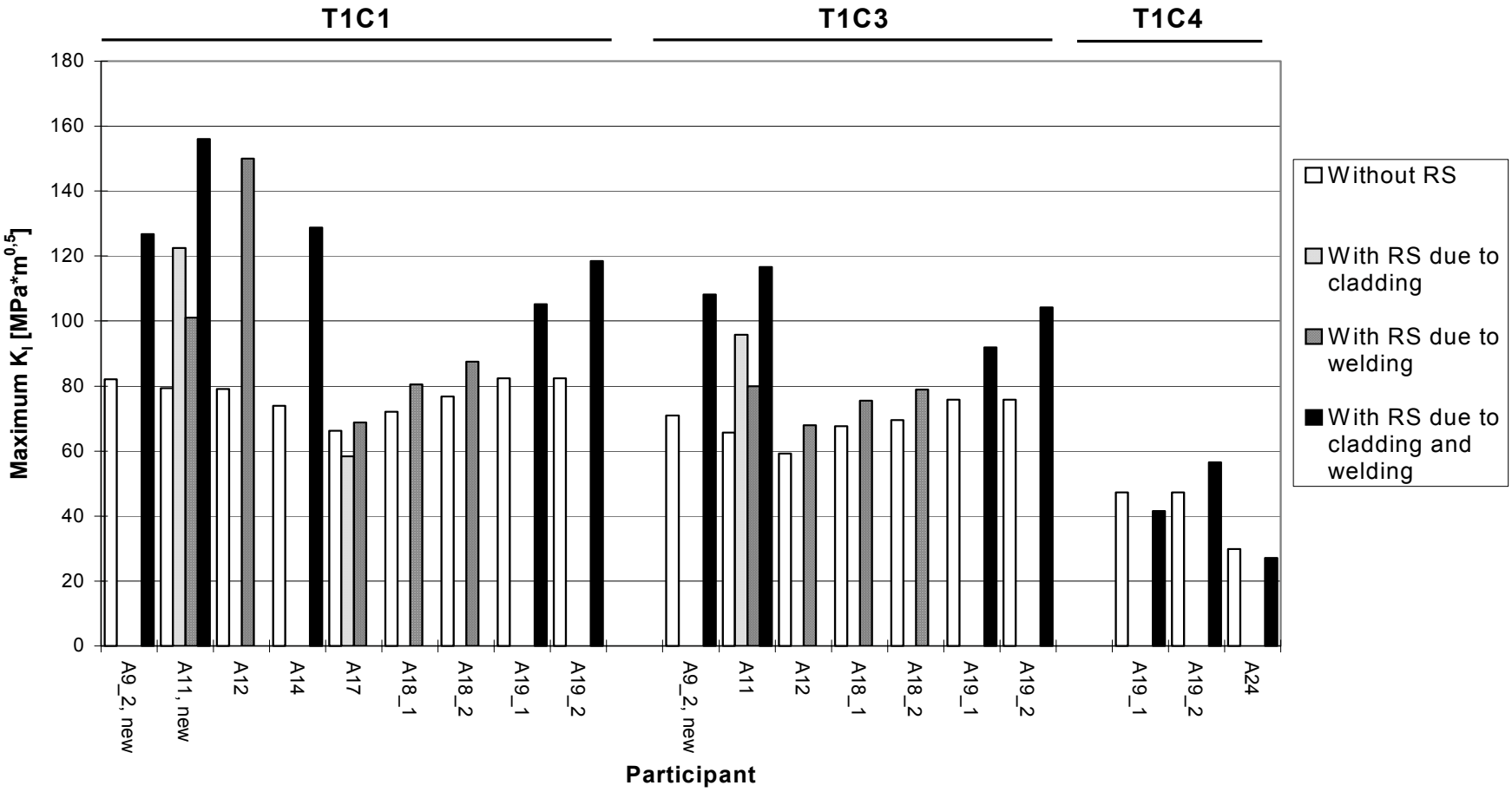

Figure 5.1.25 Task PRS: Influence of residual stresses (RS) on the maximum stress intensity factor at the deepest point of the cracks.

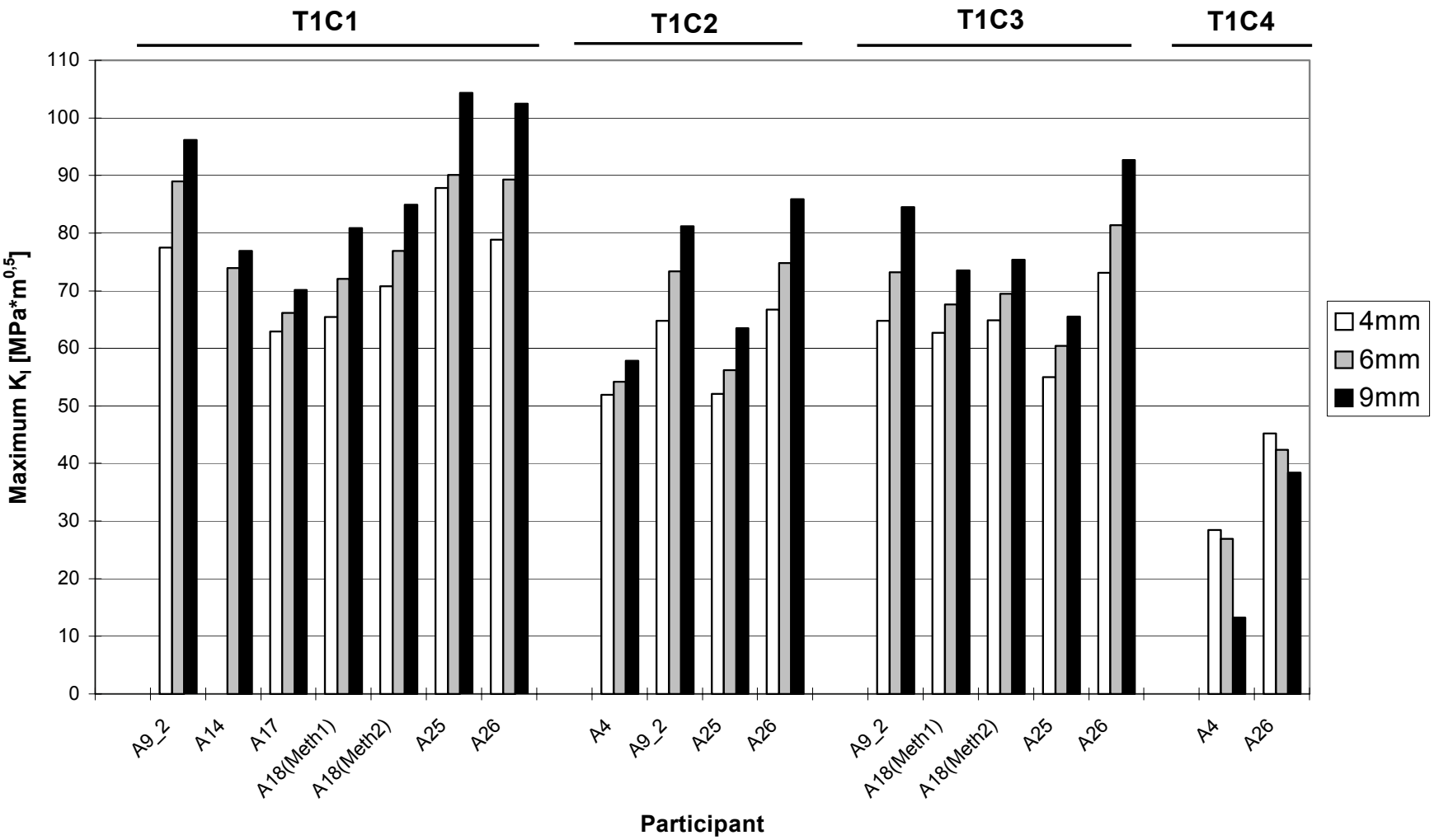

Figure 5.1.26 Task PCT: Influence of the cladding thickness on the maximum stress intensity factor at the deepest point of the cracks.

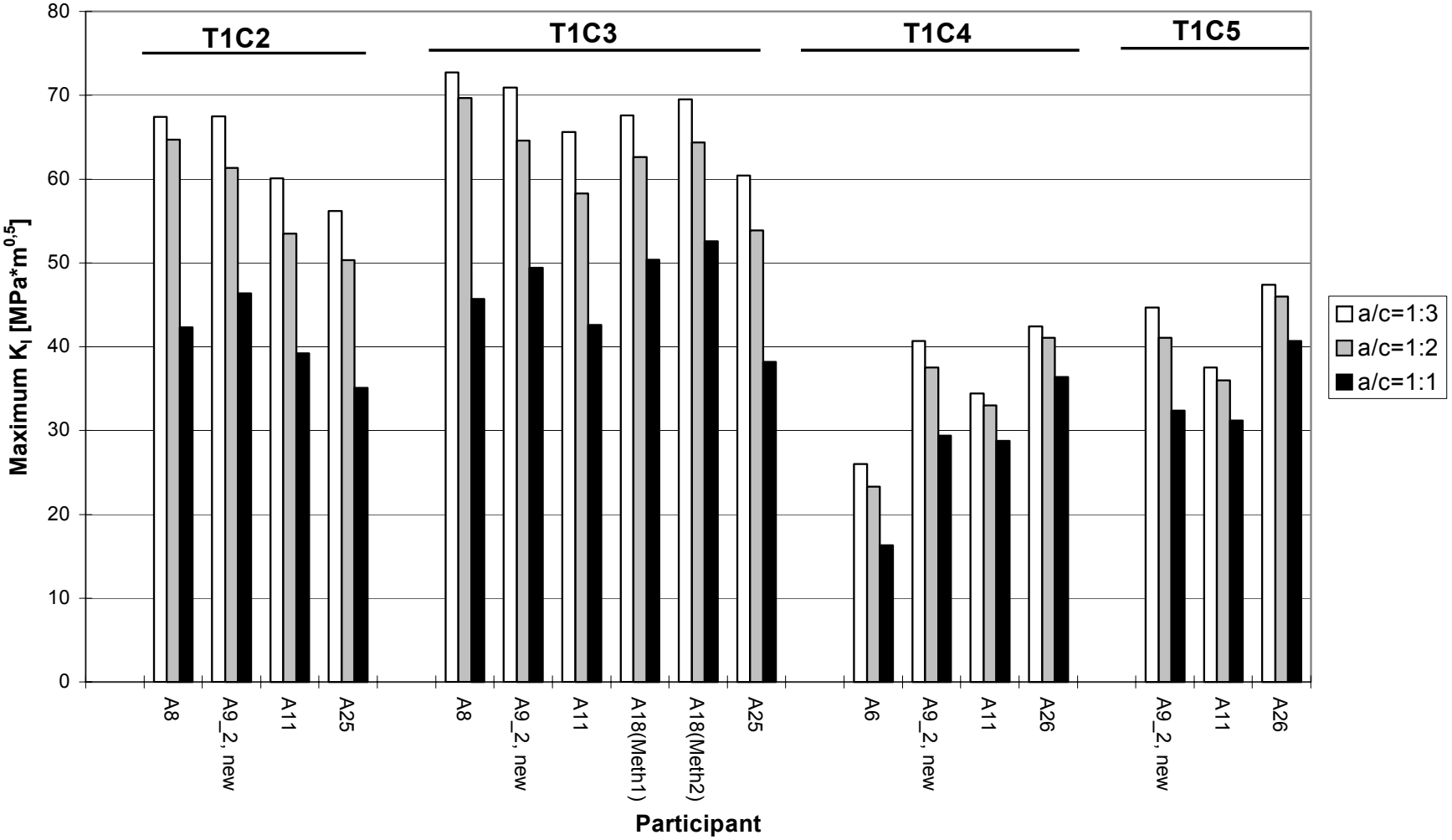

Figure 5.1.27 Task PCAR: Influence of the crack aspect ratio on the maximum stress intensity factor at the deepest point of the cracks

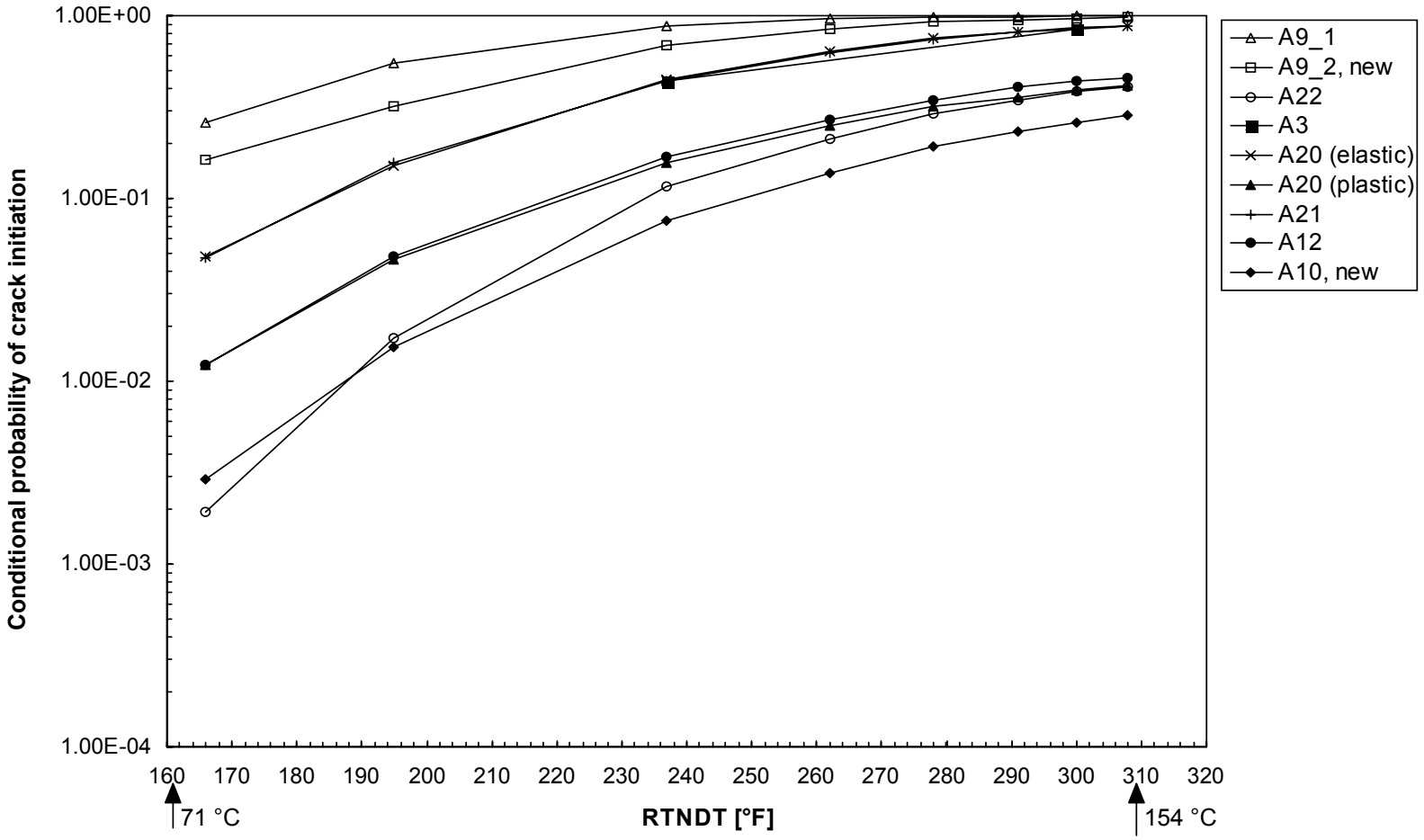

Figure 5.2.1 Task PFM-1: Conditional probability of crack initiation versus mean surface RT_{NDT}

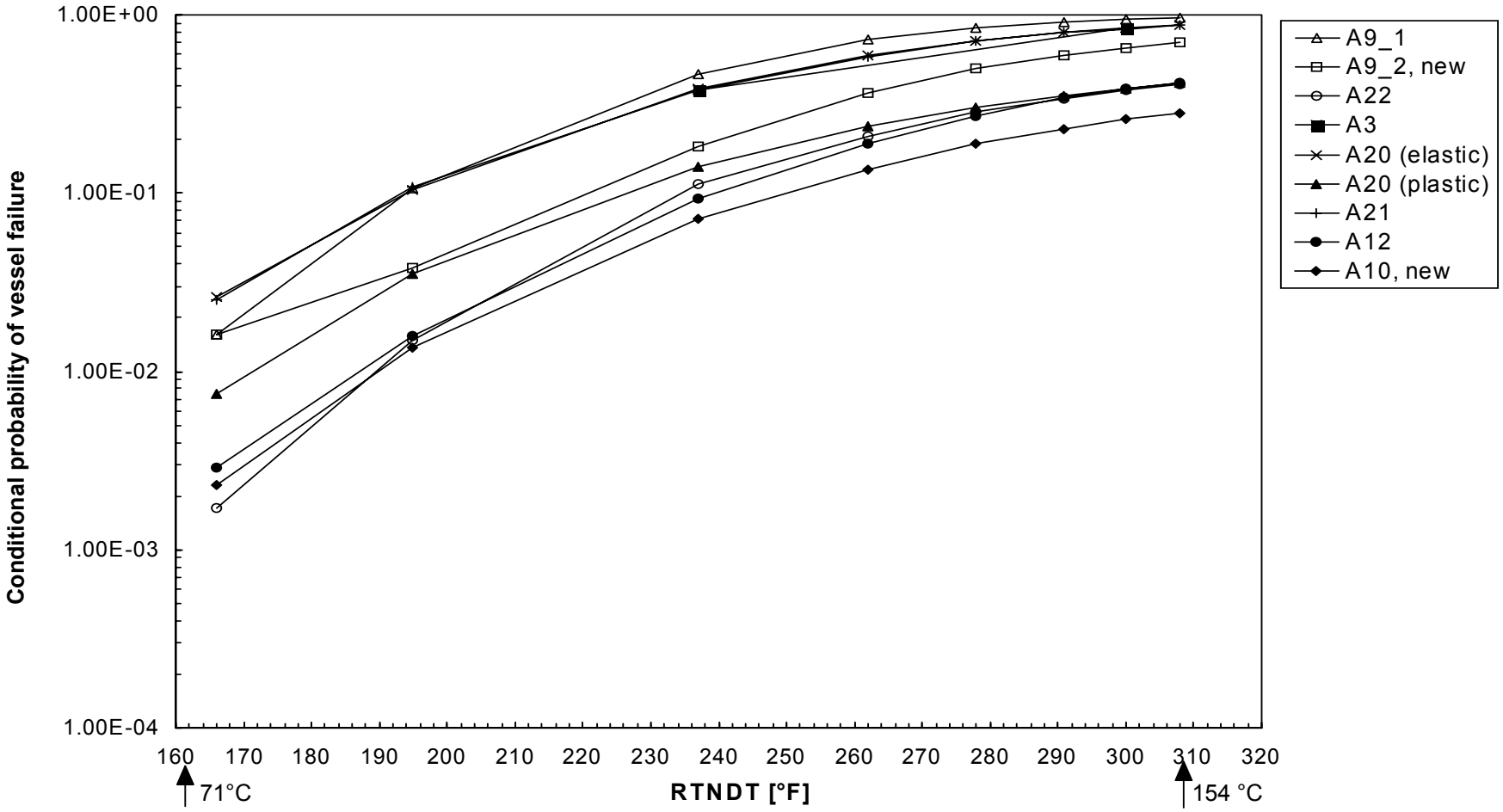

Figure 5.2.2 Task PFM-1: Conditional probability of vessel failure versus mean surface RT_{NDT}

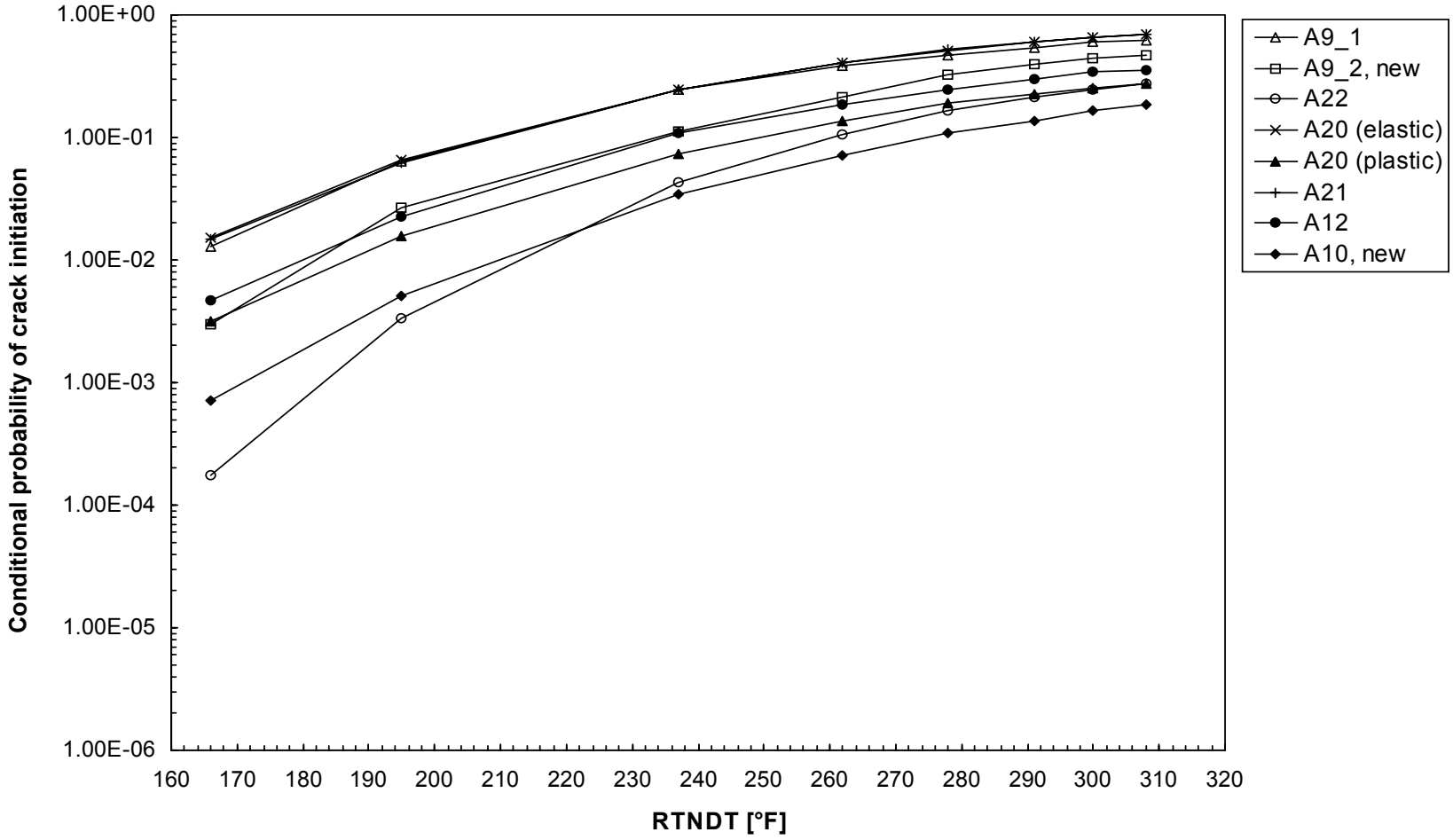

Figure 5.2.3 Task PFM-2: Conditional probability of crack initiation versus mean surface RT_{NDT}

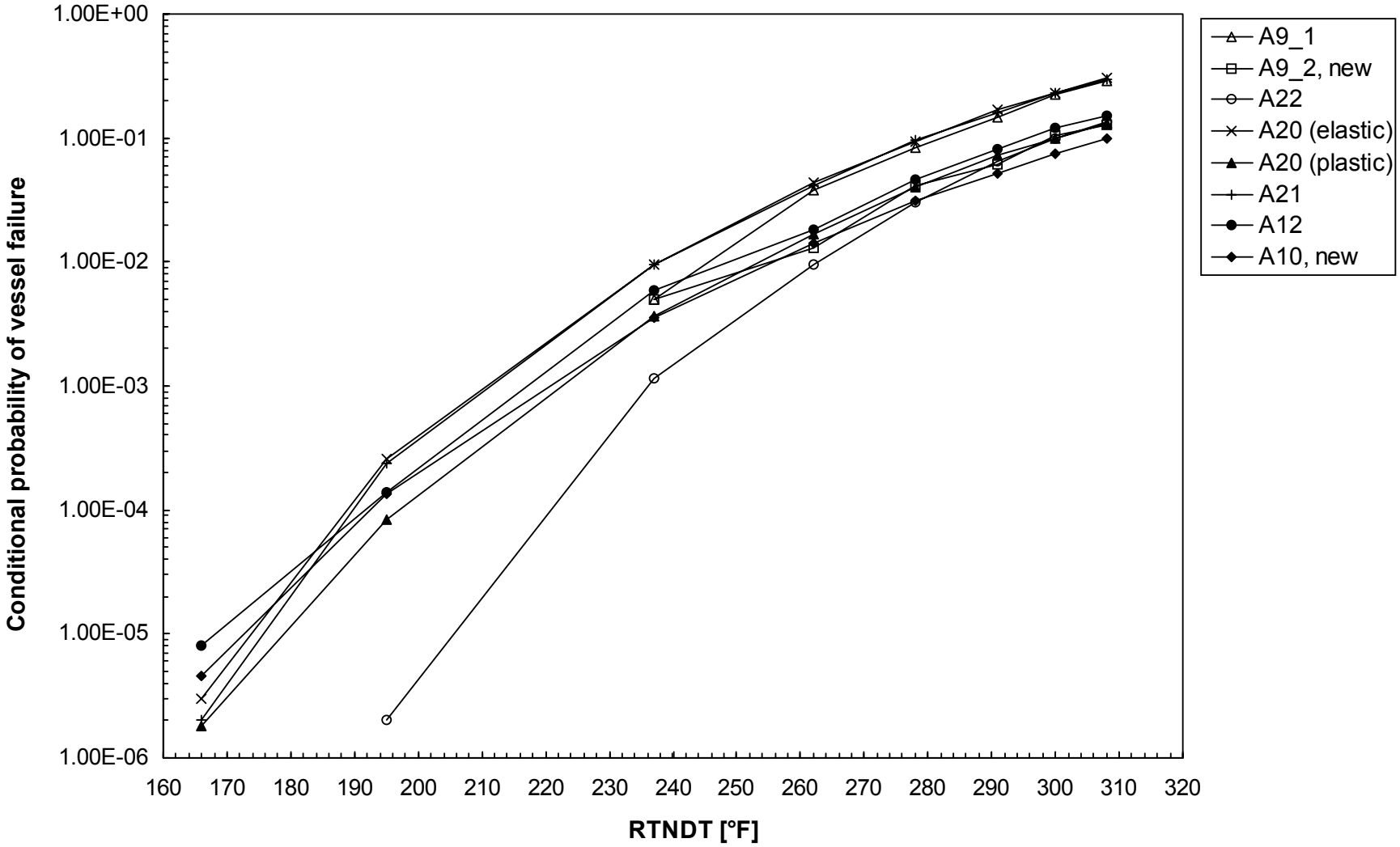

Figure 5.2.4 Task PFM-2: Conditional probability of vessel failure versus mean surface RT_{NDT}

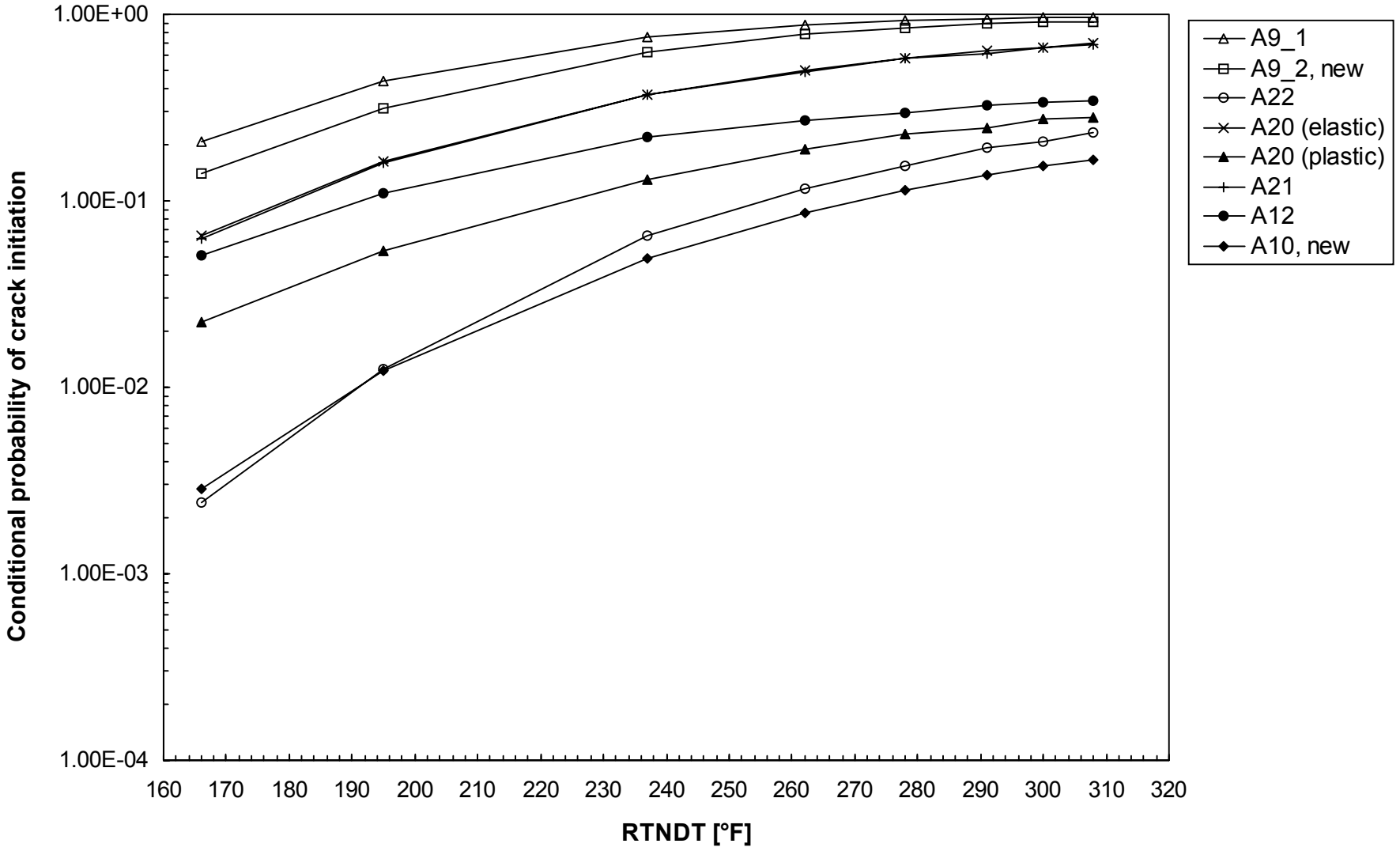

Figure 5.2.5 Task PFM-3: Conditional probability of crack initiation versus mean surface RT_{NDT}

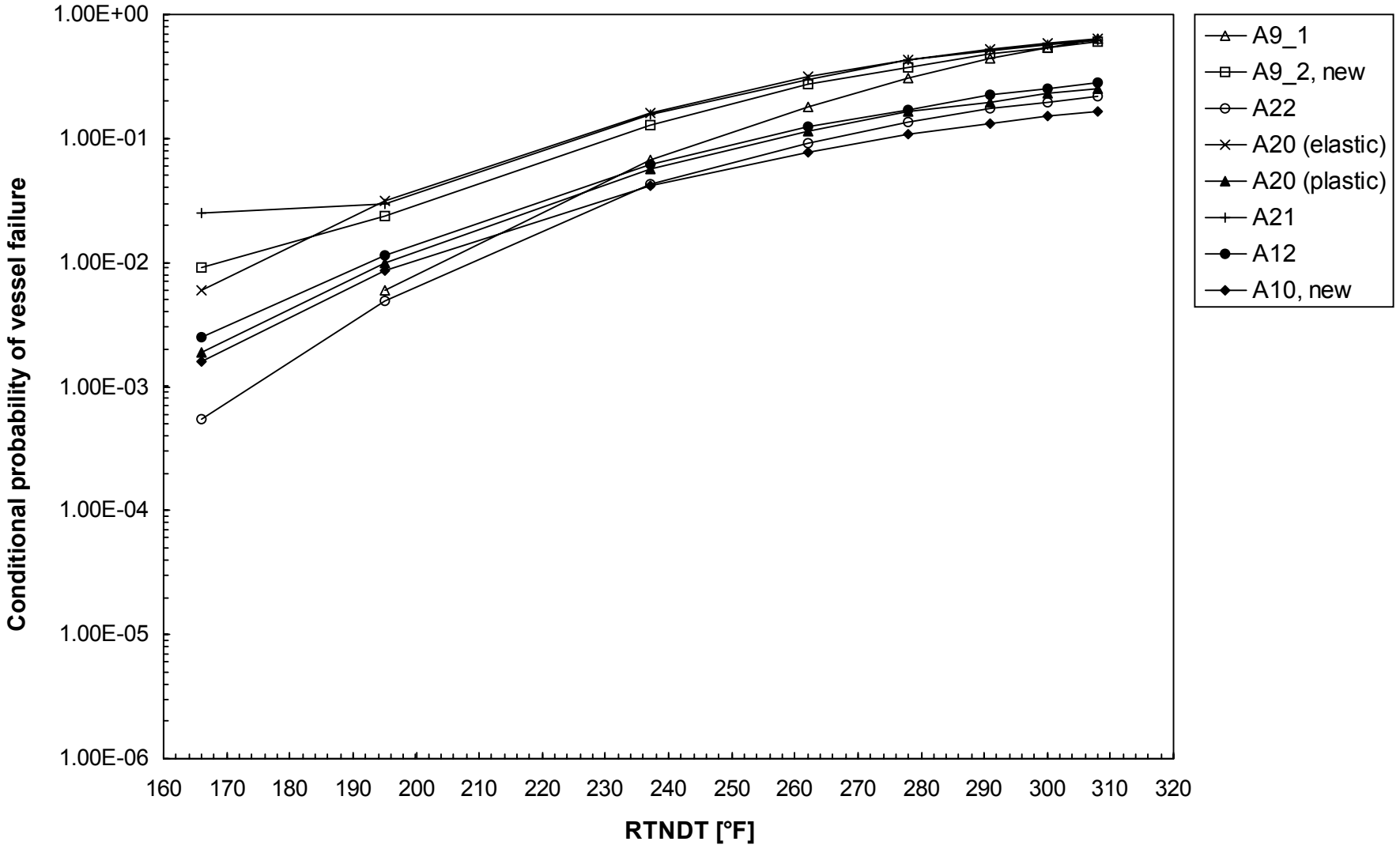

Figure 5.2.6 Task PFM-3: Conditional probability of vessel failure versus mean surface RT_{NDT}

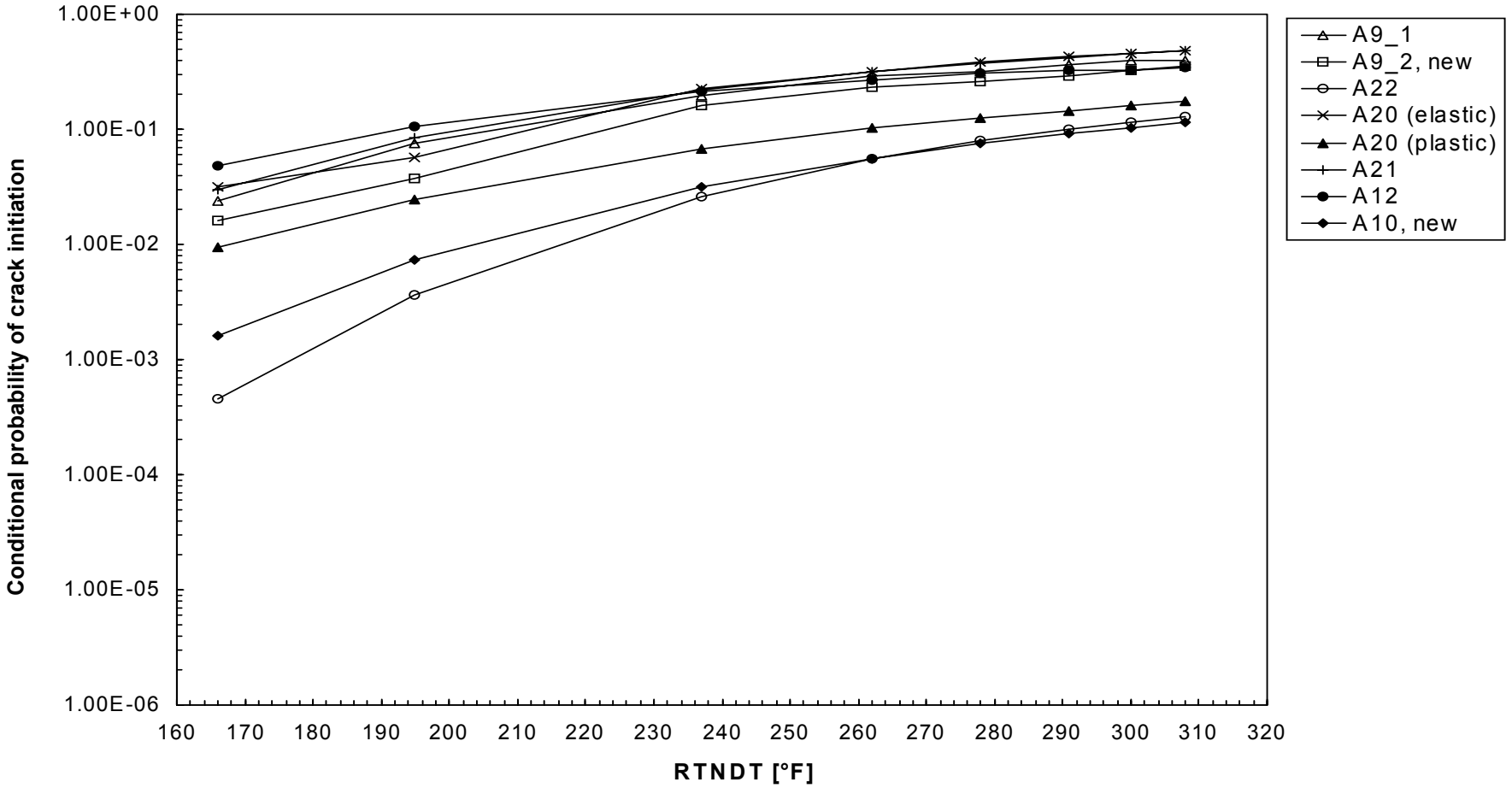

Figure 5.2.7 Task PFM-4: Conditional probability of crack initiation versus mean surface RT_{NDT}

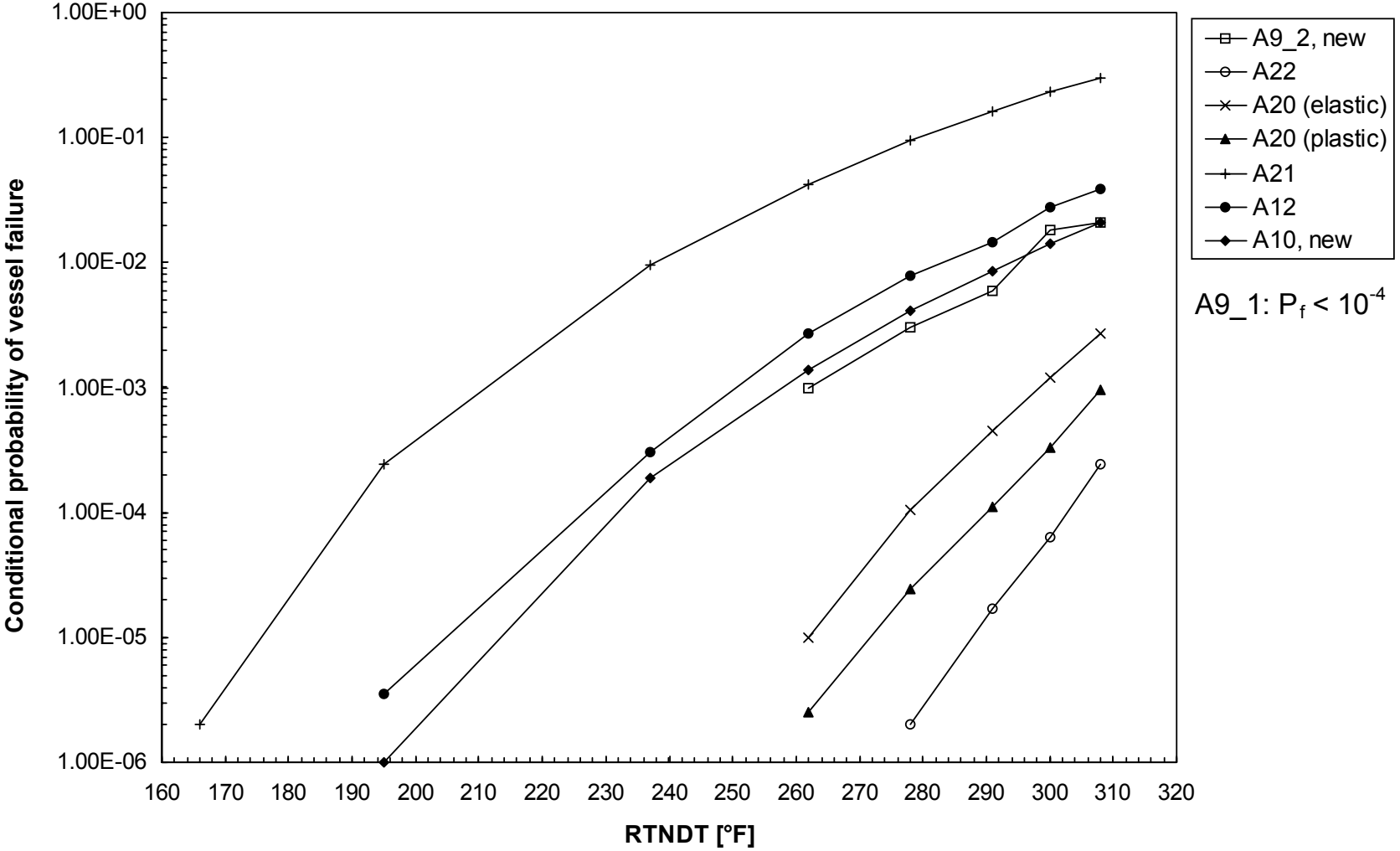

Figure 5.2.8 Task PFM-4: Conditional probability of vessel failure versus mean surface RT_{NDT}

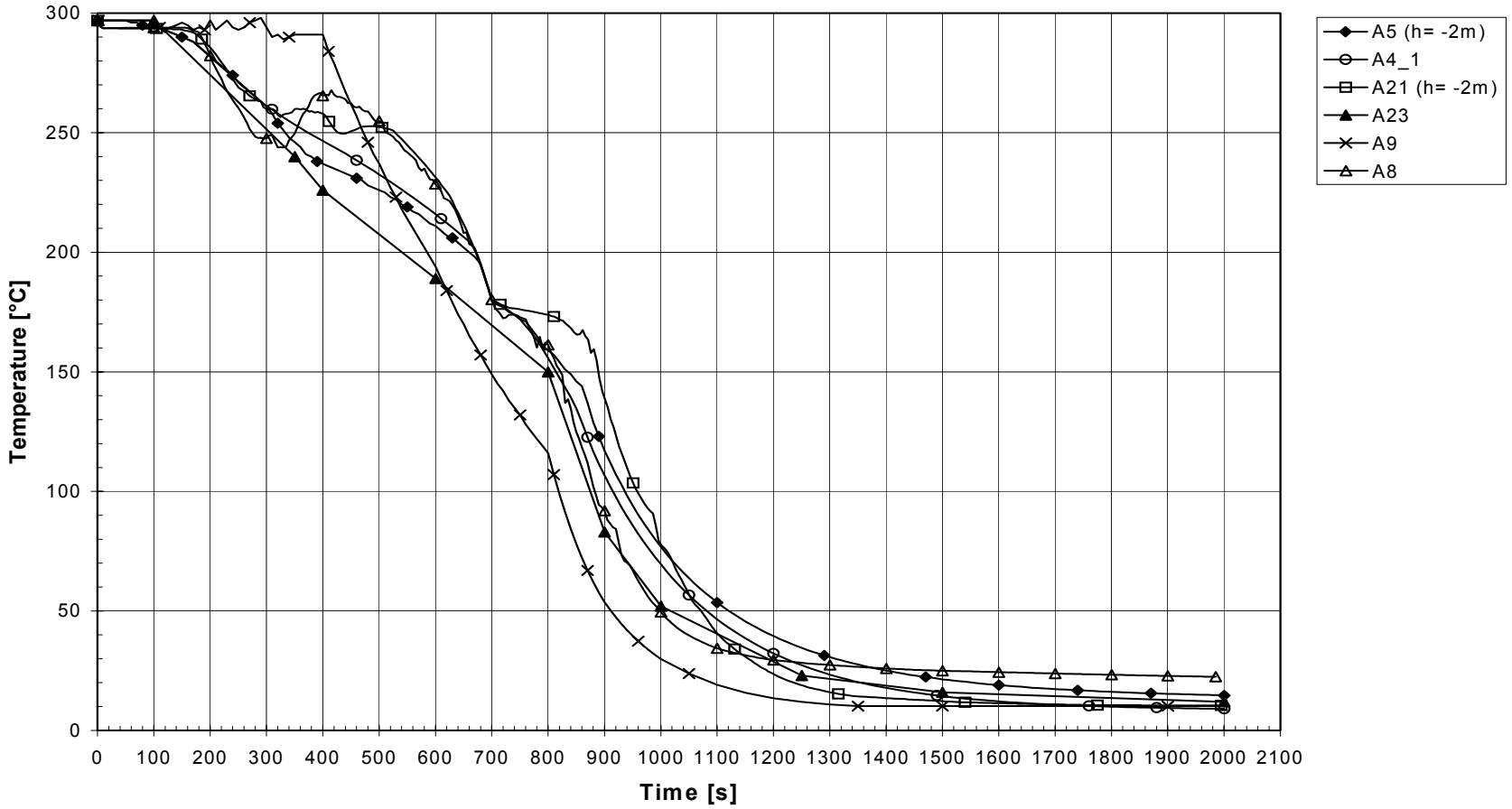

Figure 5.3.1 Task MIX: Global downcomer temperatures outside of the plumes.

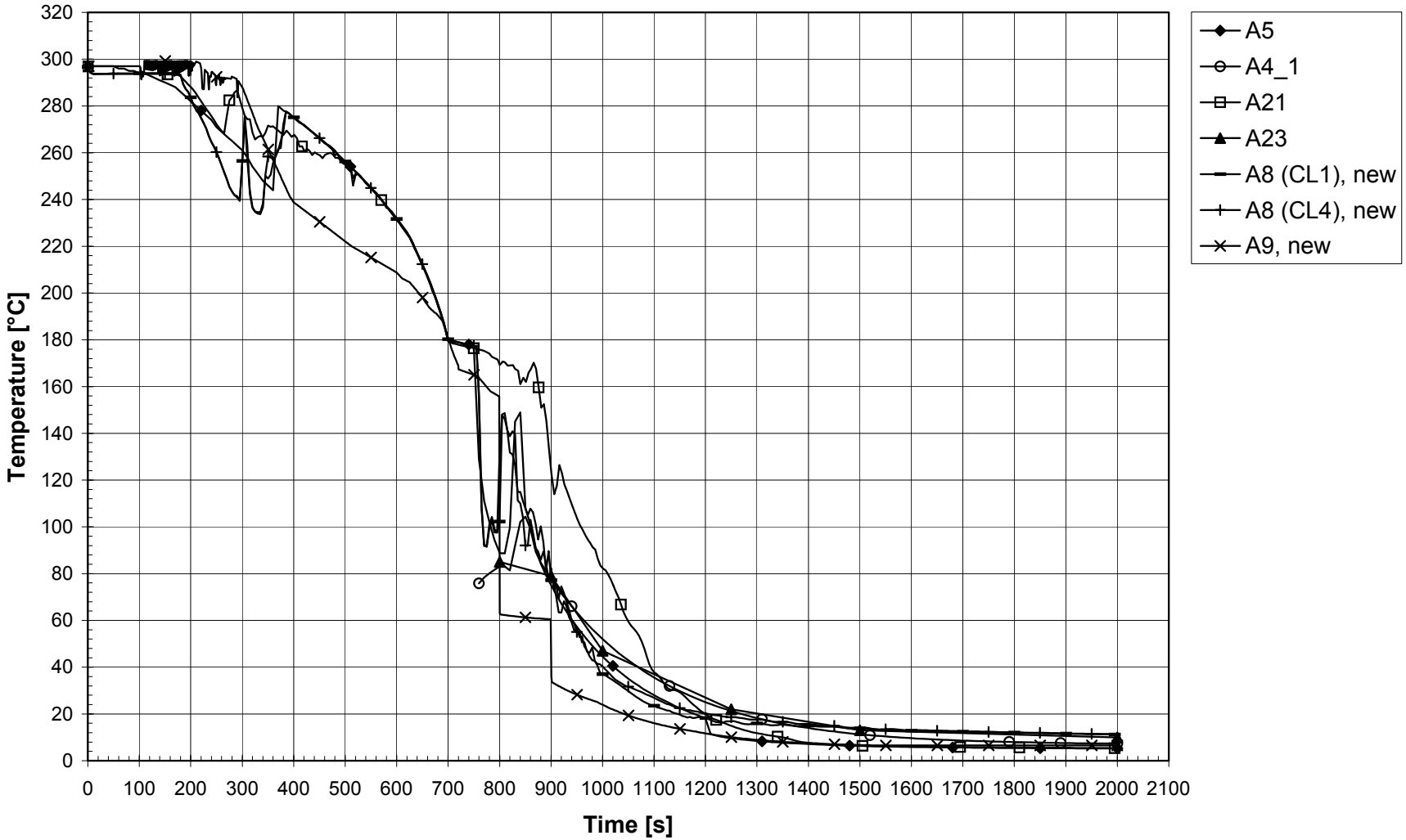

Figure 5.3.2 Task MIX: Downcomer stripe centerline temperatures, cold legs 1 / 4, h = -1 m

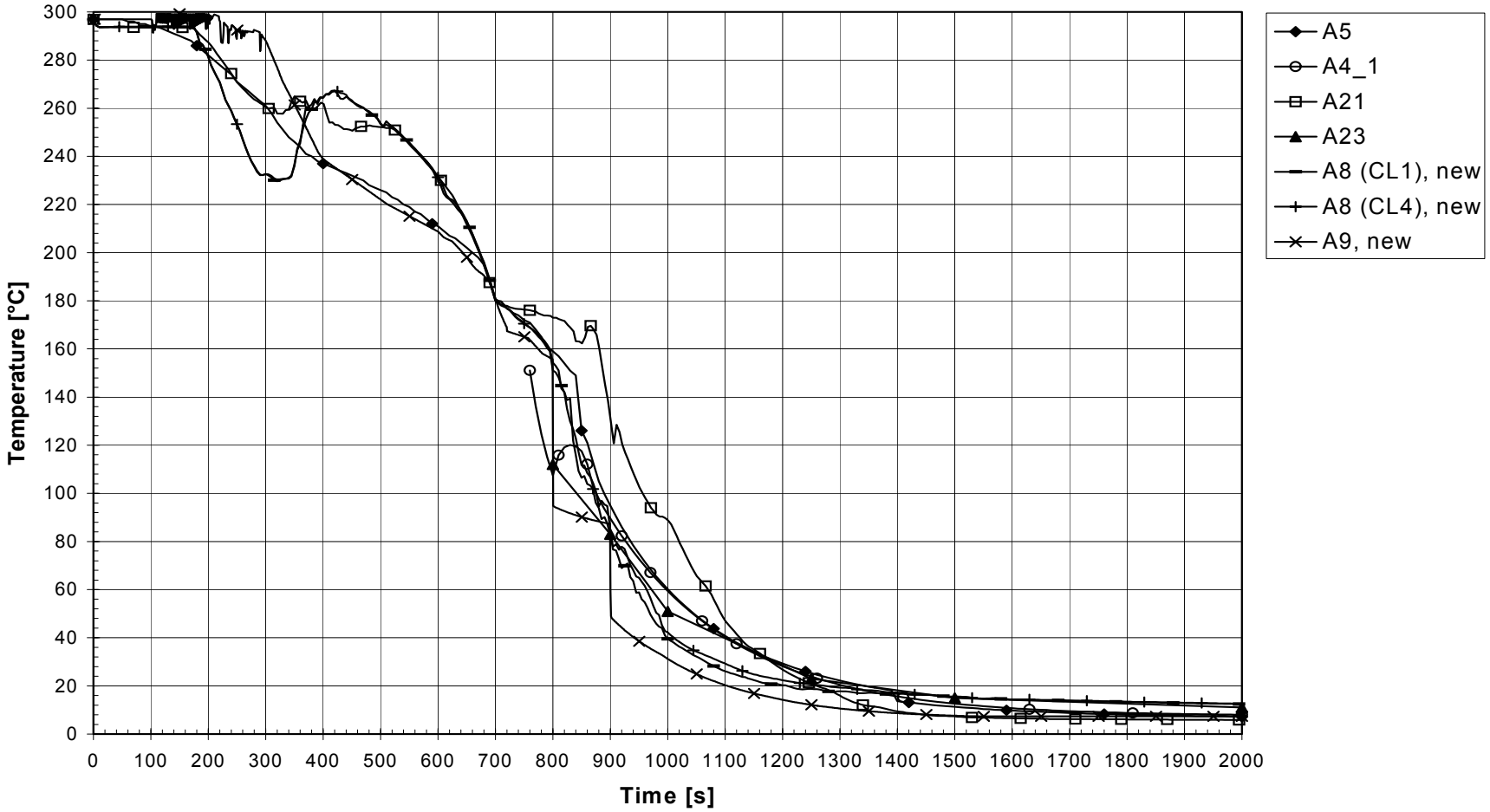

Figure 5.3.3 Task MIX: Downcomer stripe centerline temperatures, cold legs 1 / 4, h = -2 m

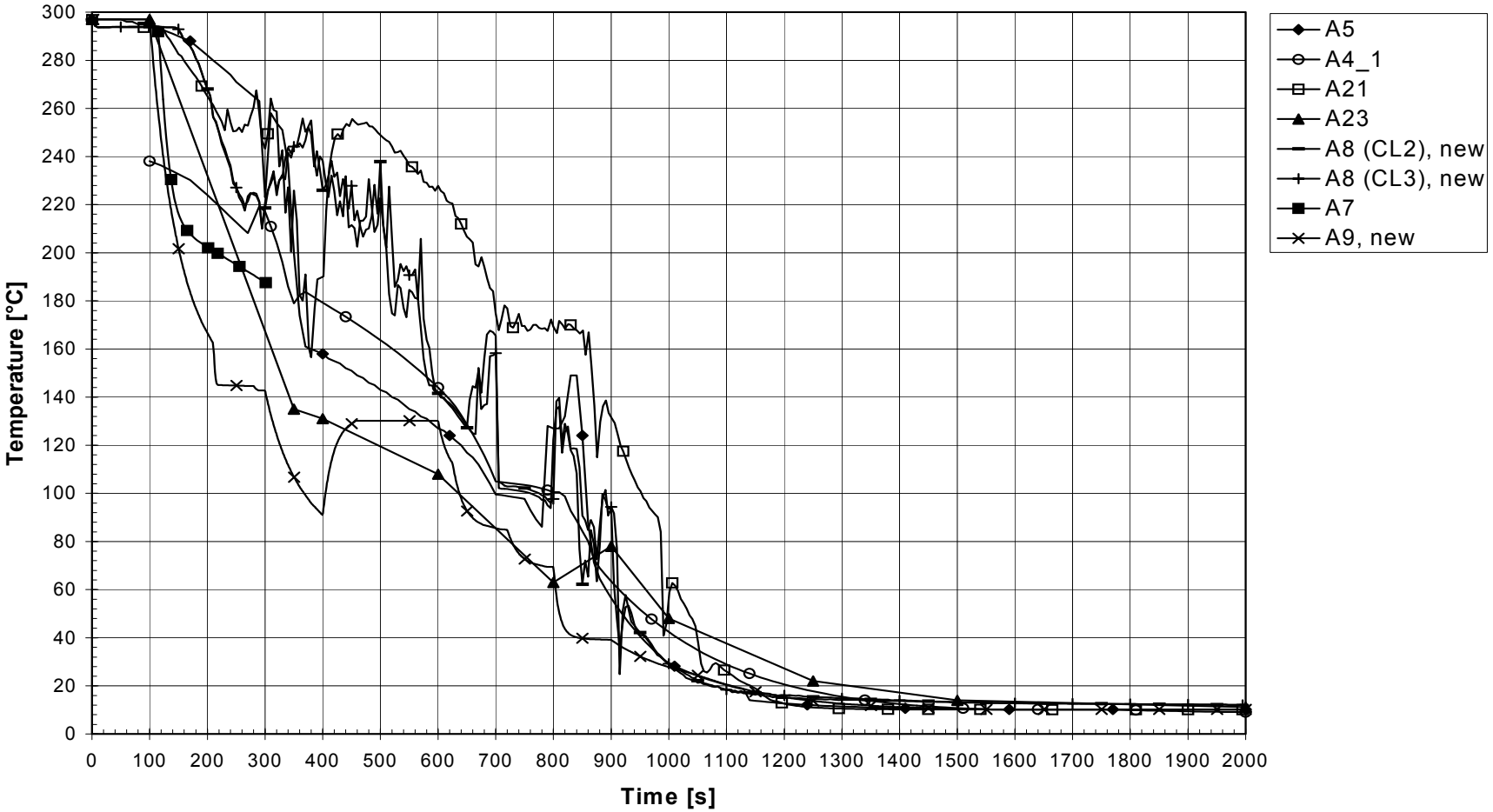

Figure 5.3.4 Task MIX: Downcomer stripe centerline temperatures, cold legs 2 / 3, h = -1 m

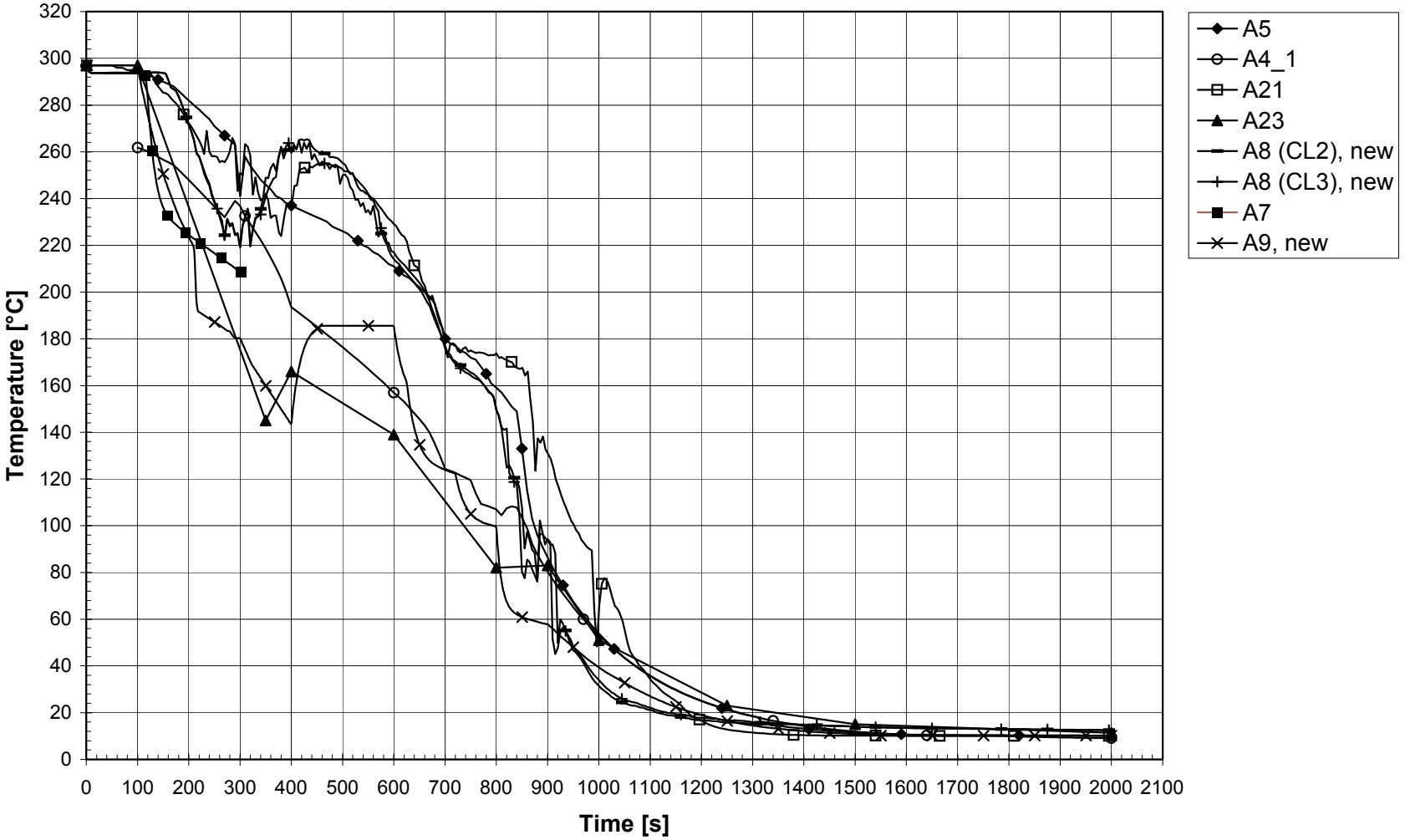

Figure 5.3.5 Task MIX: Downcomer stripe centerline temperatures, cold legs 2 / 3, h = -2 m

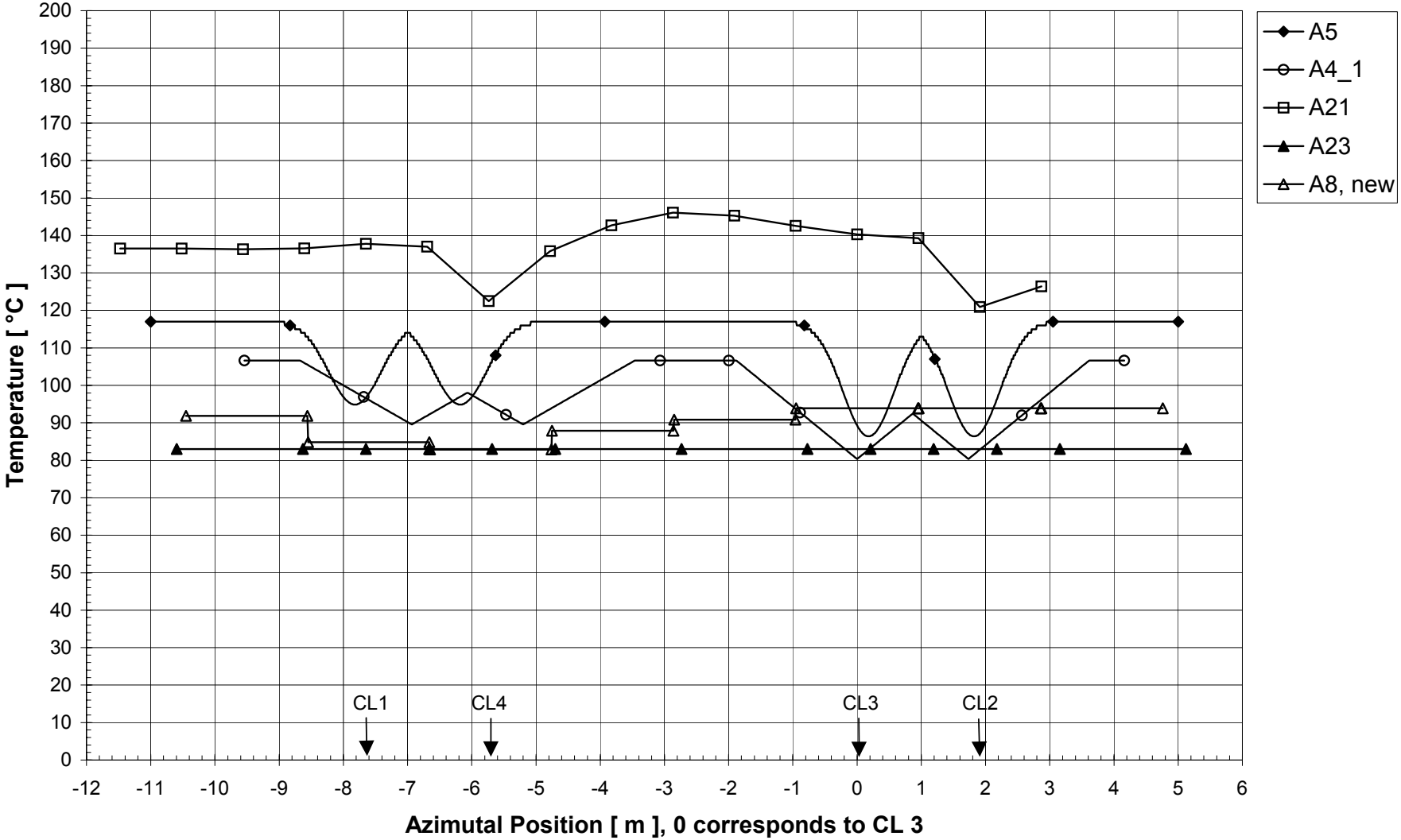

Figure 5.3.6 Task MIX: Azimutal temperature distribution in downcomer, h = -2 m, t = 900 s

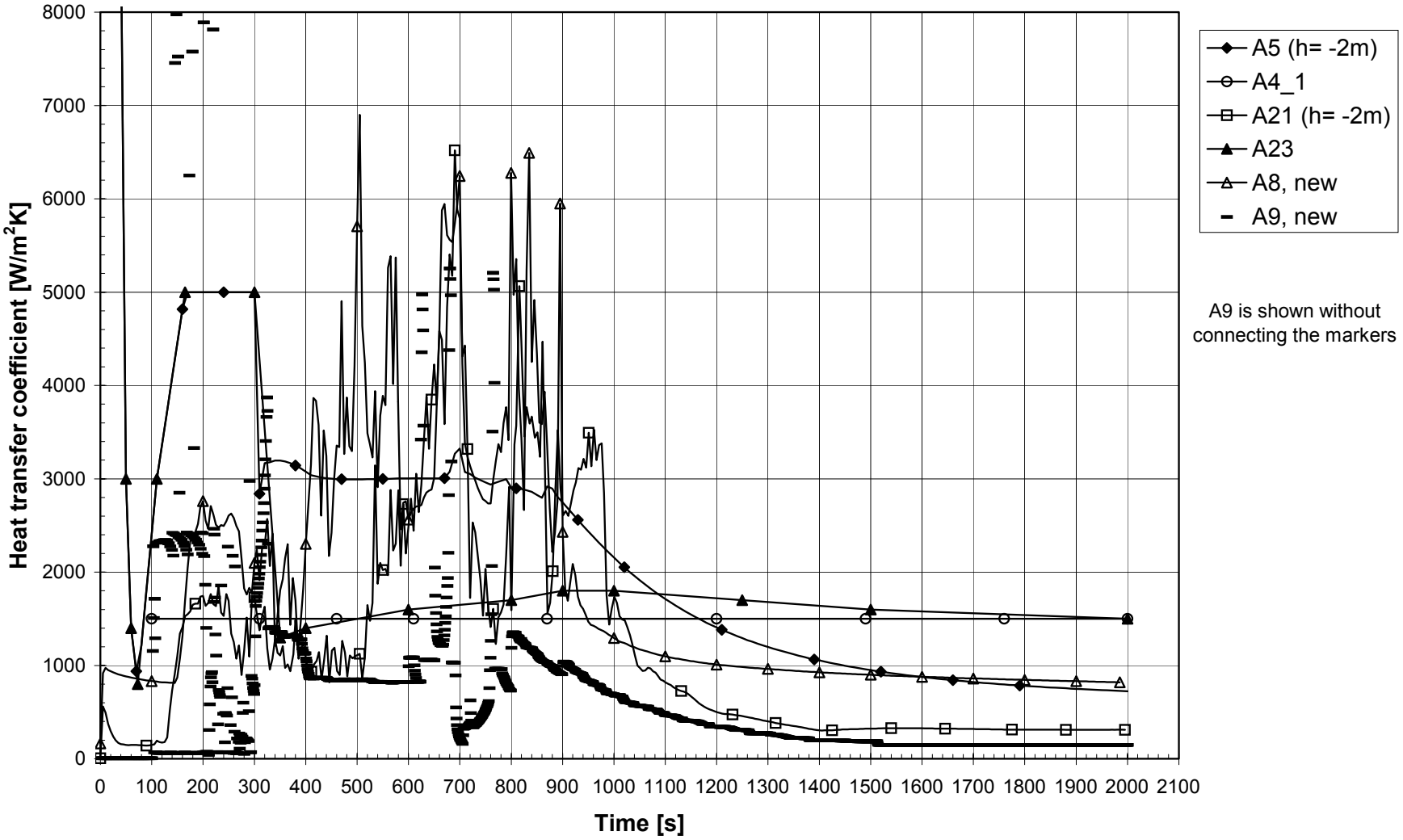

Figure 5.3.7 Task MIX: Global downcomer HTC outside of the plume

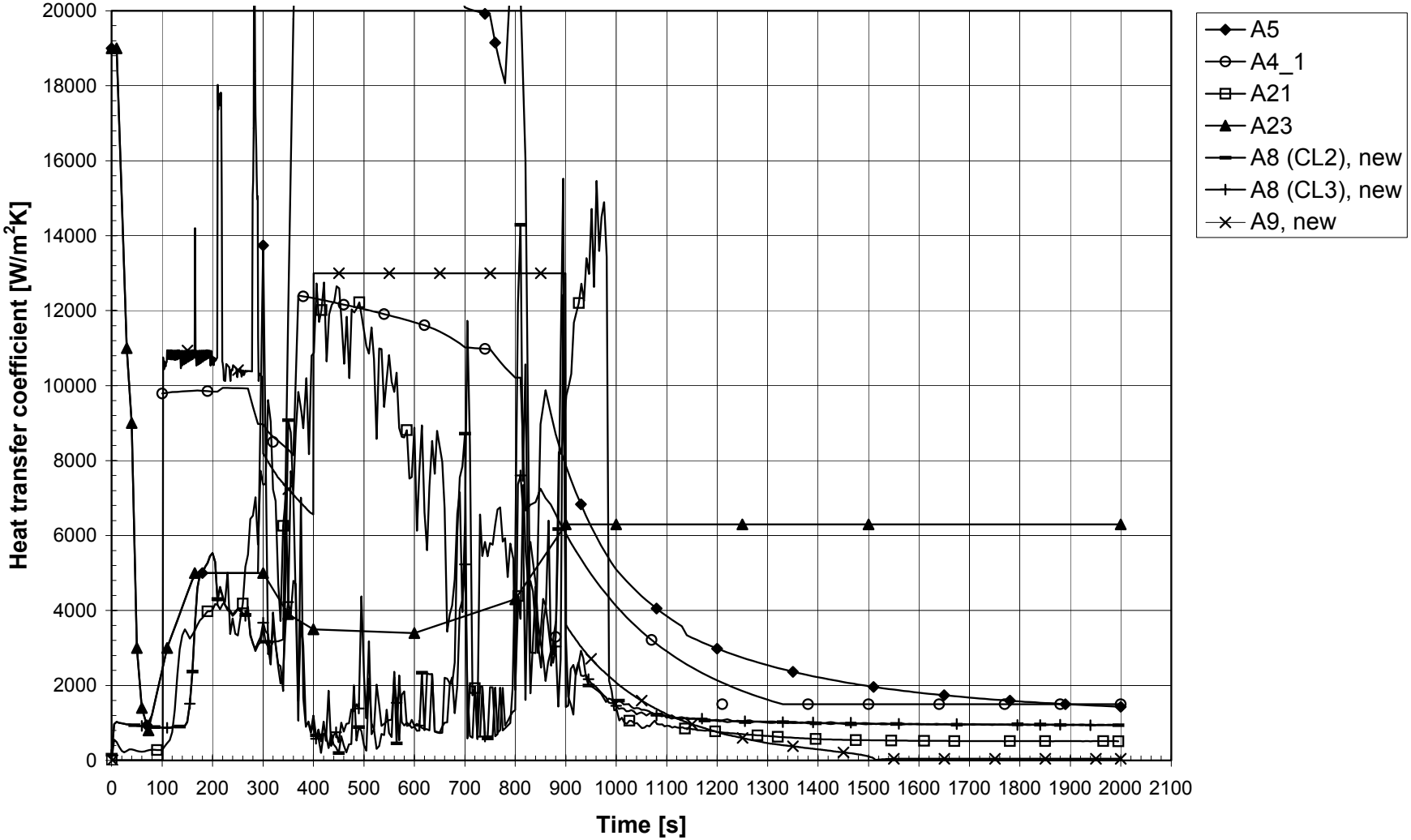

Figure 5.3.8 Task MIX: Downcomer stripe centerline HTC, cold legs 2 / 3, h = -1 m

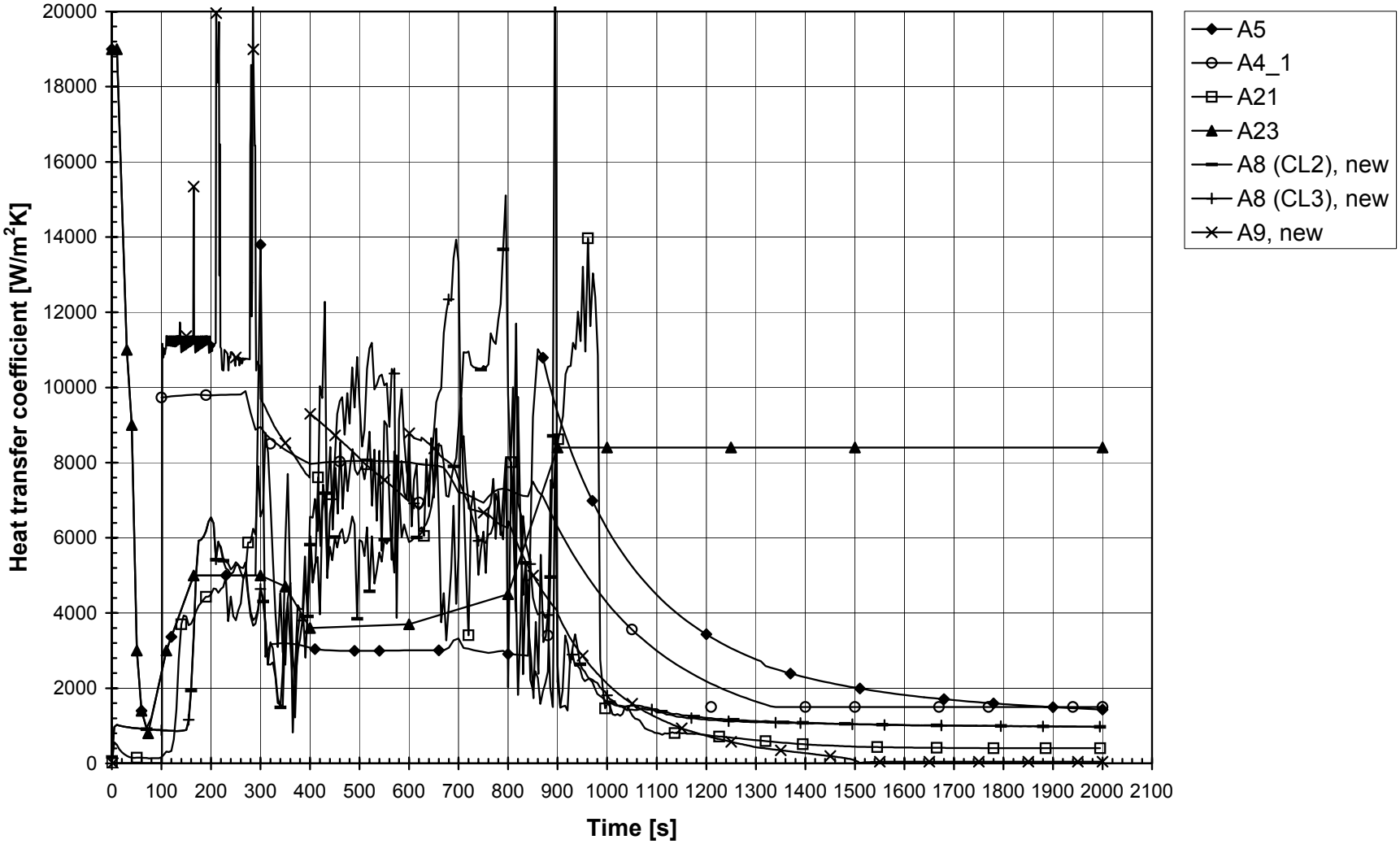

Figure 5.3.9 Task MIX: Downcomer stripe centerline HTC, cold legs 2/3, h = -2 m

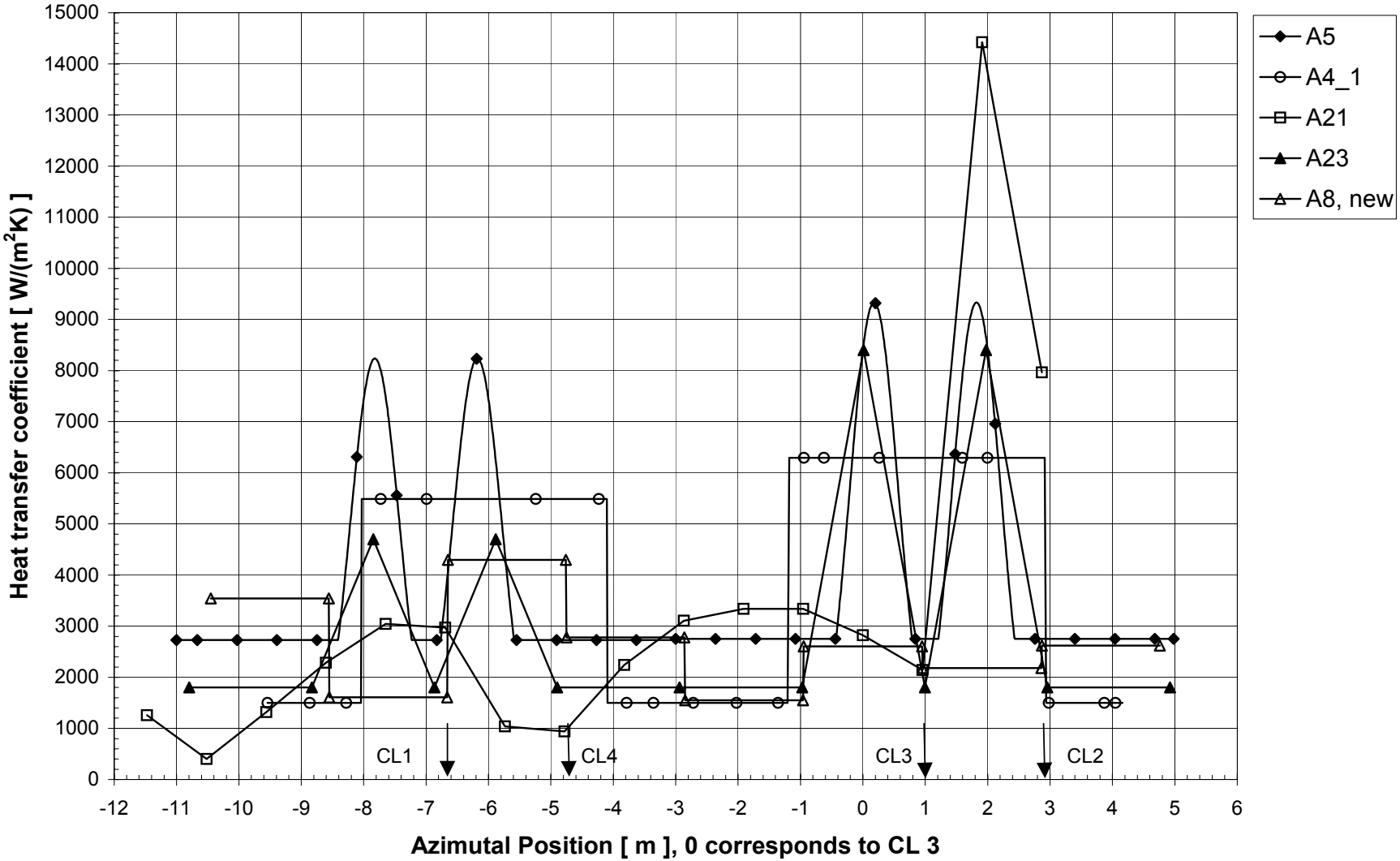

Figure 5.3.10 Task MIX: Azimutal HTC distribution in downcomer, h = -2 m, t = 900 s

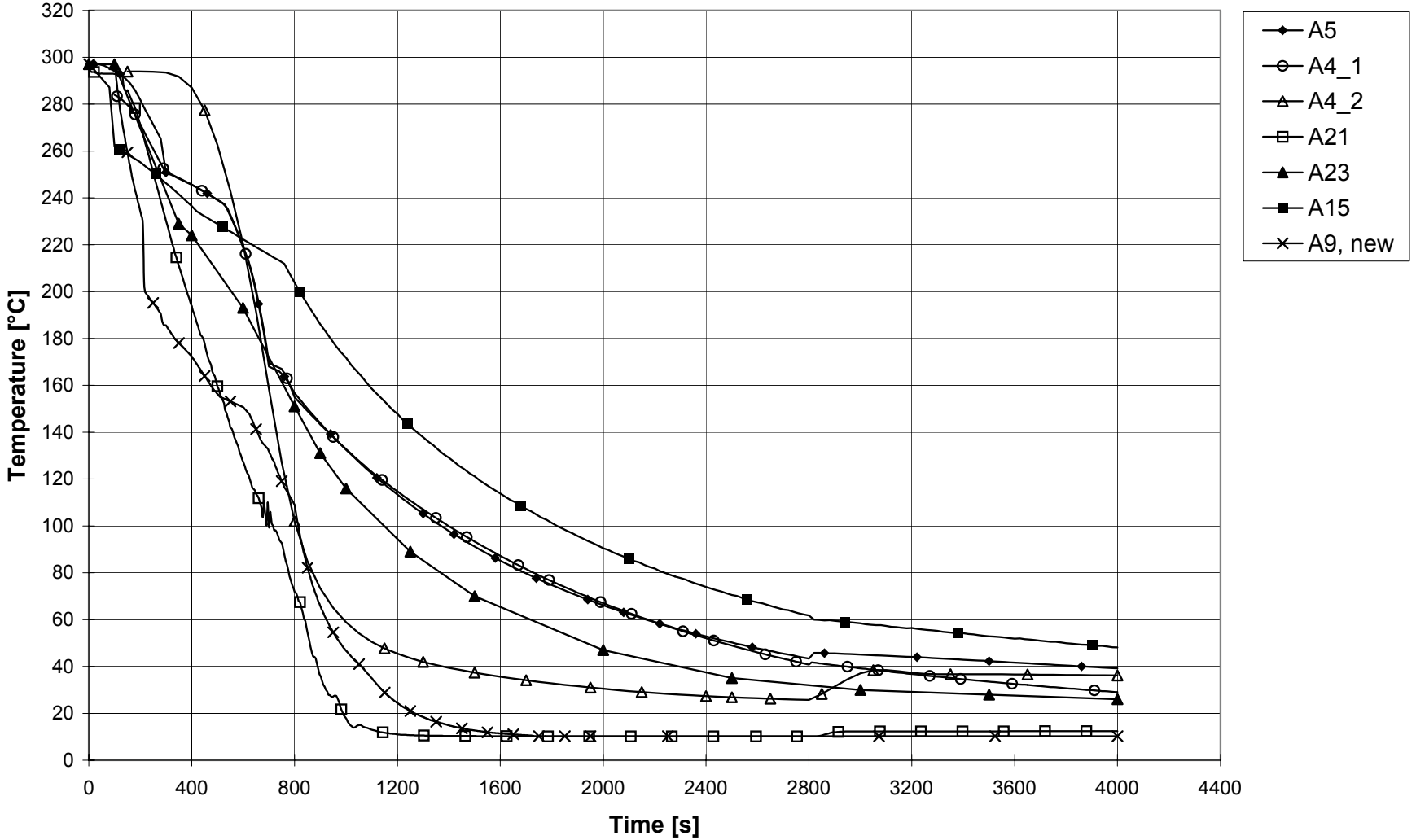

Figure 5.3.11 Task PINJ: Downcomer stripe centerline temperatures, cold legs 2 / 3, h = -2 m

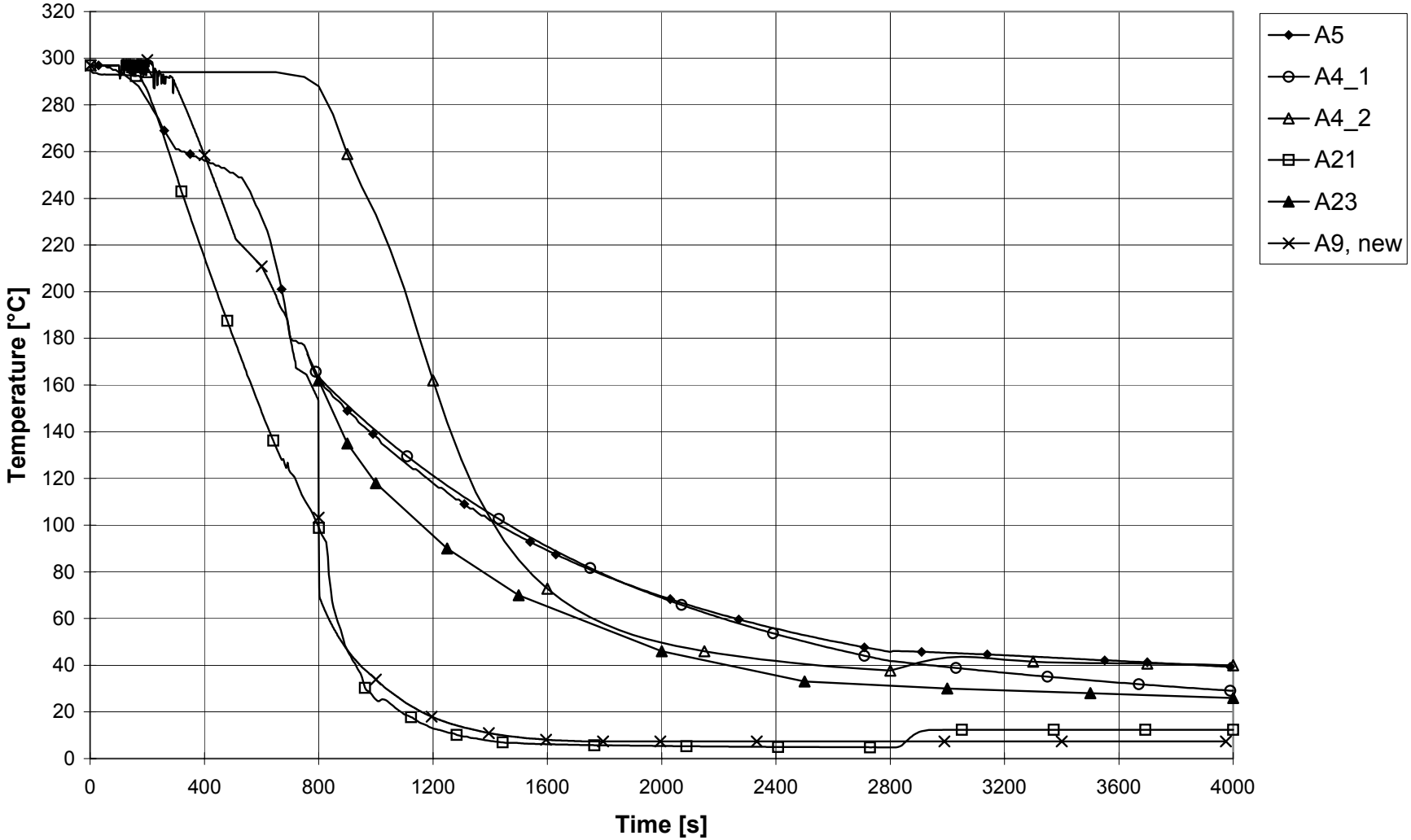

Figure 5.3.12 Task PINJ: Downcomer stripe centerline temperatures, cold legs 1 / 4, h = -2m

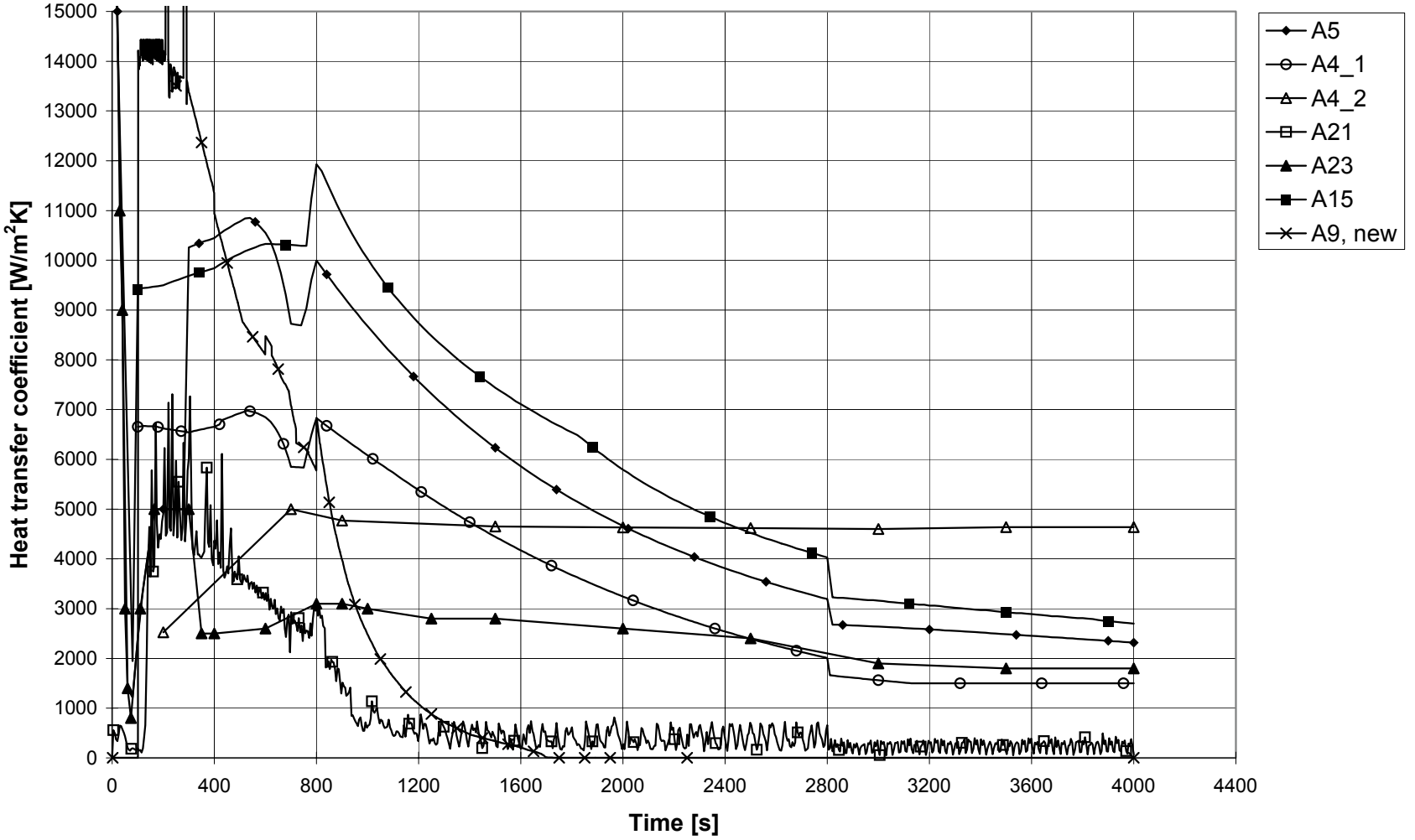

Figure 5.3.13 Task PINJ: Downcomer stripe centerline HTC, cold legs 2 / 3, h = -2 m

Gesellschaft für Anlagen- und Reaktorsicherheit (GRS) mbH

Schwertnergasse 1
50667 Köln
Telefon +49 221 2068-0
Telefax +49 221 2068-888

Forschungsinstitute
85748 Garching b. München
Telefon +49 89 32004-0
Telefax +49 89 32004-300

Kurfürstendamm 200
10719 Berlin
Telefon +49 30 88589-0
Telefax +49 30 88589-111

Theodor-Heuss-Straße 4
38122 Braunschweig
Telefon +49 531 8012-0
Telefax +49 531 8012-200

www.grs.de

ISBN 3-931995-14-3